Light Olefin Oligomerization into Higher Linear and Alpha Olefins over Heterogeneous Cobalt Catalysts

By

Alvin Jonathan

A dissertation submitted in partial fulfillment of

the requirements for the degree of

Doctor of Philosophy

(Chemical Engineering)

at the

UNIVERSITY OF WISCONSIN-MADISON

2021

Date of final oral examination: May 24th, 2021

This dissertation is approved by the following members of the Final Oral Committee:

George W. Huber, Professor, Chemical and Biological Engineering
James A. Dumesic, Professor, Chemical and Biological Engineering
Brian F. Pfleger, Professor, Chemical and Biological Engineering
Ive Hermans, Professor, Chemistry
Shannon S. Stahl, Professor, Chemistry

Light Olefin Oligomerization into Higher Linear and Alpha Olefins over Heterogeneous Cobalt Catalysts

Alvin Jonathan
Under the supervision of Prof. George W. Huber and Prof. James A. Dumesic at the University of Wisconsin-Madison

Abstract

Light olefin oligomerization is an attractive process for synthesis of higher linear and alpha olefins for productions of fuels and chemicals. The advancement of hydraulic fracturing technologies and the discovery of additional natural gas resources have led ethylene, a natural gas-derived product, to be a promising feedstock for this reaction. Light olefin oligomerization reactions into linear alpha olefins (LAOs) are typically performed using homogeneous catalysts, often require extra purification steps, activators, and solvents. The use of heterogeneous catalysts as alternatives is desirable, although low selectivity to linear alpha olefins and poor catalyst stability are often limiting issues. In this dissertation, we investigate heterogeneous cobalt catalysts for ethylene oligomerization into higher linear and alpha olefins.

A carbon-supported cobalt oxide catalyst was studied for ethylene oligomerization in the absence of activators and solvents. This catalyst can selectively oligomerize ethylene into linear and alpha olefins at a reaction temperature of 200 °C. The catalyst was stable during the reaction for 120 h. X-ray diffraction and X-ray photoelectron spectroscopy without exposure to air showed CoO as the cobalt phase after the reaction, suggesting that this is the stable cobalt phase during oligomerization.

Increasing pretreatment temperature of a carbon-supported cobalt catalyst from 230 to 560 °C under inert reduces cobalt oxide to cobalt metal and improves the oligomerization activity. However, cobalt metal supported on carbon is less selective to linear and alpha olefins than cobalt oxide supported on carbon. In addition, cobalt metal supported on carbon deactivated during reaction at 200 °C due to higher rate of polyethylene formation. The oligomerization reaction is first order with respect to ethylene partial pressure, consistent with a mechanism where the rate determining step is the propagation of adsorbed olefins with gaseous ethylene on a highly covered surface with olefins.

The effect of catalyst surface functional groups was also investigated. The oxidized surface functional groups catalyzed the isomerization of linear alpha olefins into internal olefins which have lower rates for oligomerization into higher olefins. To our knowledge, heterogeneous carbon-supported cobalt catalysts are the most selective heterogeneous catalysts for olefin oligomerization into linear and alpha olefins without activators and solvents.

Acknowledgements

First and foremost, I would like to thank both my parents, Sandford Jonathan and Sutini Setiadi for supporting me to pursue both my undergraduate and Ph.D. degrees in the US. Both of them are my biggest supporters and the primary reason why I manage to achieve all of these. I am very grateful to have both parents who love me unconditionally and sacrifice their time for their children.

I am extremely thankful for both my brothers, Christopher Jonathan and Albert Jonathan for their support and guidance during my study in the US. I will always remember the time we spent together in the US to achieve our Ph.D. degrees.

I feel very lucky and thankful for the opportunity to work with both my advisors, Prof. George W. Huber and Prof. James A. Dumesic. They have been very helpful and supportive from the beginning of my Ph.D. career until I complete this dissertation. All the lessons that both my advisors have taught me are very important for my future career.

I am thankful for the friendship and help from my colleagues, David L. Bruns, Joseph P. Chada, Daniel J. McClelland, Nathaniel M. Eagan, Siddarth H. Krishna, Madelyn R. Ball, Peter H. Galebach, Keishla R. Rivera Dones, Theodore W. Walker, Mark J. Lindsay, Jake I. Gold, Anthony D. Anderson, Elise B. Gilcher, Paolo A. Cuello Penaloza, Leida M. Vazquez Ramos, Hochan Chang, Raka G. Dastidar, and Emily G. Tomashek.

I am grateful for the financial support from the ExxonMobil Research and Engineering Company and useful discussions with Michael P. Lanci and Chengrong Wang.

Lastly, I would like to thank Prof. Brian F. Pfleger, Prof. Ive Hermans, and Prof. Shannon S. Stahl for serving as the committee members for my Ph.D. defense.

Table of Contents

List of Figures

List of Tables

Chapter 1. Introduction

1.1 Linear Alpha Olefins: Motivation and Feedstock

Linear alpha olefins (LAOs) are straight chain hydrocarbons with a double bond located at the terminal or primary position of the chain. As of 2020, the global LAOs market was over $9 billion, with a projected compound annual growth rate (CAGR) of more than 4.5% from 2021-2026.[1,2] Commercial reactions involving LAOs include oligomerization, polymerization, hydroformylation, alkylation, bromination, and sulfonation for use in polyethylene comonomers (C_4 - C_8), plasticizers (C_6 - C_{10}), lubricants (C_{10} - C_{12}), and detergents (C_{10} - C_{16}).[3,4] Currently, polyethylene comonomers contribute to more than 40% of the global LAOs market, making the relatively short LAOs, such as 1-butene, 1-hexene, and 1-octene as important LAOs.[1,5] Most commercial productions of LAOs are through the oligomerization of ethylene, one of most manufactured commodity chemicals today.[3,4] Light olefins, such as ethylene and propylene are primarily synthesized through steam cracking of light alkanes (e.g., ethane and propane) from natural gas.[6] Due to the advancement of hydraulic fracturing technologies and the discovery of additional natural gas sources, there has been a considerable increase in the production of natural gas since 2006.[7,8] In the US, the production of dry natural gas in 2006 was 19 trillion cubic feet, increased to 34 trillion cubic feet in 2020, and is projected to reach 42 trillion cubic feet by 2050.[8] Consequently, more steam crackers are currently built to increase the production of ethylene.[9] The development of ethanol as a renewable feedstock is also a promising source to produce ethylene. Braskem, a Brazilian petrochemical company has a commercial plant to produce ethylene from sugarcane-derived ethanol dehydration with a capacity of 200,000 metric tons per year.[10] Therefore, the abundant resources of ethylene from natural gas and ethanol make ethylene a promising feedstock for synthesis of linear alpha olefins (LAOs).

1.2 Light Olefin Oligomerization

Light olefin oligomerization is used commercially to synthesize higher hydrocarbons including linear alpha olefins. The commercial olefin oligomerization technology was first introduced in the 1930s for synthesis of gasoline using acid catalysts.[11,12] The mechanism of acid catalyzed olefin oligomerization begins with the protonation of the carbon-carbon double bond (C=C bond) to make a carbocation. This carbocation can further react with another olefin to make a new carbon-carbon single bond (C-C bond) during the propagation step. The acid catalyzed oligomerization is strongly dependent on the stability of the carbocation intermediates (e.g., a tertiary carbocation is more stable than a secondary and a primary carbocation), which also explains why the resulting olefin products are highly branched. The termination step of this oligomerization is the β-hydride elimination to make an olefin. Many acid catalysts, including solid phosphoric acid (SPA), acid resins, amorphous silica-alumina, and zeolites have been studied for olefin oligomerization.[5] Zeolites, which are well-ordered (crystalline) and microporous silica-alumina have received the most attention over the past few decades. Martens and co-workers reported that H-ZSM-57, a two-dimensional zeolite with 8 and 10-ring channels with a lobate pore structure is selective for 2-butene dimerization (85.7% selectivity) at 89% conversion at 80 °C.[13] The primary products from 2-butene oligomerization over H-ZSM-57 were dimethylhexenes. They also reported that H-ZSM-22, a 1-dimensional zeolite with small 10-ring channels is selective for propylene trimerization where the products were mostly mono-branched.[14]

Our group has studied 1-butene oligomerization over H-FER where a low amount of cracking was observed up to a reaction temperature of 200 °C.[15] FER is a two-dimensional zeolite which has 10-ring channels intersecting with 8-ring channels and has a similar pore size as ZSM-57.[5,15,16] Analysis on the dimers showed that the dimers were mostly dimethylhexenes. Although

acid catalysts have been widely used for olefin oligomerization to synthesize highly branched products, they are not suitable for ethylene oligomerization due to the high temperature requirement (>300 °C) to initiate the reaction where many side reactions occur.[10]

The discovery of the titanium based catalysts and organoaluminum compounds for polymerization of ethylene by Ziegler in 1950s sparked the use of transition metal catalysts to produce linear alpha olefins (LAOs).[17] Other homogeneous transition metal catalysts, such as Hf, Zr, Cr, Co, and Ni complexes have also been shown to be able to produce LAOs.[5,18,19] Several commercial productions of LAOs along with their catalytic systems are shown in Table 1.1.

Table 1.1 Industrial commercial processes for LAO productions.[5,20]

Industrial	**Process Name**	**Catalytic System**	**Product Range**
Chevron Phillips	Gulfene	Trialkylaluminum	C_4-C_{30+}
Ineos	Ethyl	Trialkylaluminum	undisclosed
Shell	SHOP	Ni complex	C_6-C_{30+}
Idemitsu	-	Zr Ziegler catalyst	undisclosed
Sabic	Alpha-Sablin	Zr Ziegler catalyst	C_4-C_{18}

Most transition metal catalyzed olefin oligomerization follows the Cossee-Arlman mechanism.[5] In this mechanism, an olefin first coordinates with the transition metal, then the hydrogen bound to the transition metal is added to the first carbon which has a C=C bond, while the transition metal forms a C-C bond with the second carbon. A new olefin will coordinate with this transition metal and the previous carbon chain will insert in the same manner with a chain growth probability of α. The final step of this mechanism is the β-hydride elimination of the alkyl to make an olefin. In the Cossee-Arlman mechanism, the oxidation state of the metal does not

change during the reaction. When an oligomerization reaction occurs through the Cossee-Arlman mechanism, the oligomers follow a Schulz-Flory distribution, which is given by Equation 1.1,

$$W_n = n\,(1 - \alpha)^2\,\alpha^{n-1} \qquad (1.1)$$

where W_n is the product weight fraction, n is the number of the repeat units, and α is the chain growth probability.[15] Another mechanism for transition metal catalyzed olefin oligomerization is the metallacycle mechanism. In this mechanism, two olefins initially coordinate with the transition metal, then the two olefins form a metallacyclic intermediate with the transition metal where the oxidation state of the transition metal increases by two.[21] Subsequent β-hydride elimination and reductive elimination of this metallacyclic intermediate result in the formation of a new olefin. When an oligomerization reaction occurs through the metallacycle mechanism, the product distribution is shifted towards light olefins (e.g., C_4, C_6, and C_8) because the metallacyclic intermediate is unstable with a hydrocarbon chain longer than C_8.[10]

Although many homogeneous transition metal catalysts are able to produce LAOs, they often require activators or co-catalysts (e.g., methylaluminoxane (MAO) and triethylaluminum (TEA)), complex catalyst recovery, and olefin product purification which make heterogeneous catalysts as desirable alternatives.[22,23] However, many heterogenous catalysts suffer from deactivation and poor selectivity to linear products compared to homogeneous catalysts. There are three commonly studied transition metals for heterogeneous olefin oligomerization, namely Ni, Cr, and Co. Ni has received the most attention in the past few years, primarily due to its high activity and low cost.[24] Although heterogeneous Ni catalysts are active for olefin oligomerization, both the nature of the active site and a rigorous description of the oligomerization mechanism are still the subjects of controversy. Ni^+, $Ni(OH)^+$, and Ni^{2+} are the three most commonly proposed candidates for the active site. Bonneviot et al. reported that Ni^+ is the active site for olefin

dimerization over silica supported or X-type zeolite supported Ni, as confirmed by the more active catalysts after the partial reduction of Ni^{2+}.[25] Iglesia and co-workers studied ethylene oligomerization over Ni-MCM-41 and suggested that $Ni(OH)^+$ is the active site as confirmed by titration with CO and 2,6-di-*tert*-Butylpyridine (DTBP).[26] Moussa et al. performed *in situ* time-resolved FTIR for ethylene oligomerization over Ni-Beta catalysts and proposed that the isolated Ni^{2+} grafted on acidic silanols is the active site.[27] They also proposed that the reaction proceeds via the Cossee-Arlman mechanism.[27] The suggestions of the isolated Ni^{2+} as the candidate of the active site and the Cossee-Arlman mechanism are also supported by the DFT calculations of Ni-containing SSZ-24 zeolite by Broogard et al.[28] A recent publication by Gounder and co-workers also suggests that the isolated Ni^{2+} is the active site for ethylene dimerization as confirmed by IR and XAS.[21] In addition to the state of the Ni itself, the support also has a role in terms of the catalyst stability. In a review of nickel-based oligomerization, Hulea and co-workers claimed that mesoporous supports have a higher stability than microporous supports.[24] The use of heterogeneous nickel catalysts for olefin oligomerization outperforms acid-catalyzed oligomerization in two aspects: 1. Ethylene oligomerization can be performed at lower temperature (e.g., 100-200 °C) as opposed to above 300 °C to avoid cracking reactions; 2. Olefin products are more linear (45% linearity was obtained for 1-butene dimerization over LTA zeolite supported Ni while less than 5% linearity was obtained for 1-butene dimerization over H-FER, both at 20% conversion).[15,29] In addition to Ni, heterogeneous Cr supported on SiO_2 (Philips catalyst) is also active for olefin oligomerization.[30-32] Similar to Ni, the nature of the active site of this catalyst remains controversial.[32]

The utilization of heterogeneous cobalt catalysts for olefin oligomerization was first conducted by Schultz and co-workers in the 1960s for ethylene, propylene, 1-butene, and 1-hexene

oligomerization.[33-35] The olefin products from these reactions were mostly linear (>50%). The catalysts were prepared by incipient wetness impregnation of the activated carbon with a cobalt nitrate solution where ammonium hydroxide was added before and after the incipient wetness impregnation. This ammonia treatment was claimed to improve the catalyst activity. The authors hypothesized that the active site is Co(II)-H, because it is usually associated with the active site for homogeneous olefin oligomerization over cobalt catalysts, and the ammonia treatment helped supply the hydrogen source for the Co(II)-H. The catalysts were pretreated by nitrogen at either 225 °C or 275 °C prior to the reactions, and it was found the that the latter pretreatment led to lower activity. The reactions were carried out at either 25 °C or 85 °C and the conversion was higher at lower temperature. No catalyst stability study as a function of reaction time was reported in those reactions.

Due to the high selectivity to linear olefins, our group has been studying olefin oligomerization over carbon-supported cobalt catalysts for the past few years.[22,36-39] Xu et al. performed ethylene, propylene, 1-butene, and 1-hexene oligomerization reactions over 12 wt% cobalt oxide on ammoniated carbon catalysts (CoO_x/N-C) in fixed-bed reactors at 80 °C, 32 bar (450 psig), and 14.1 h^{-1} weight hourly space velocity (WHSV) where the dimer linearity for each of these species was 100.0%, 53.0%, 82.9%, and 72.5%, respectively.[36] WHSV is defined as the feed mass flow rate divided by the mass of catalyst. The reaction mechanism was found to be Cossee-Arlman because the product distribution follows the Schulz-Flory distribution. The most active isomer for the oligomerization was reported to be the terminal olefin as confirmed from experiments using mixtures of 1-hexene and 2-hexenes as feeds.[36] From the ethylene oligomerization experiments, the highest ethylene conversion was 32.1% where the linearity of the C_6 and C_8 products was 97.5% and 86.1% with 1-hexene and 1-octene being 3.4% and 0.6%

respectively.[38] The only selective LAO product of this experiment was 1-butene which corresponded to 68.4% of all butenes. The linear selectivity was found to decrease as conversion increased. Increasing the catalyst pretreatment temperature (e.g., 230, 270, 350, and 550 °C) in helium prior to the reaction at 80 °C was claimed to reduce the oligomerization activity.[22] All catalysts deactivated at the reaction temperature of 80 °C.

Various catalyst characterizations have been performed to elucidate the nature of the active sites of these catalysts. X-ray diffraction (XRD) and X-ray absorption spectroscopy (XAS) experiments were performed on the catalysts after pretreatment at 230, 270, 350, and 550 °C in helium to investigate the cobalt phases at these temperatures.[22] At 230 °C, the XRD experiment showed that bulk phase was only Co_3O_4. At 270 and 350 °C, the intensity of CoO started to increase and became the dominant phase along with Co_3O_4 at the latter temperature. At 550 °C, metallic cobalt became the dominant phase. The X-ray absorption near edge structure (XANES) results from the XAS experiments also showed a similar pattern as the XRD results. At 230 °C, both Co_3O_4 and CoO were present with the compositions of 72.5 and 27.5 wt% respectively. As the temperature increased to 350 °C, the composition of Co_3O_4 decreased to 61.7 wt% while the composition of CoO increased to 38.3 wt%. At 550 °C, the compositions of Co_3O_4, CoO, and metallic cobalt were 23.7, 40.1, and 36.2 wt% respectively. The reduction of CoO_x to metallic cobalt was also verified by a TGA experiment where the weight loss of Co/N-C at 621 °C occurred.[22]

1.3 Overview of the Dissertation

As previously mentioned, heterogeneous carbon-supported cobalt catalysts are promising catalysts to oligomerize ethylene to higher linear olefins. However, it is not clear why the catalysts

deactivated during the reaction at 80 °C and what the active sites are. It is also desirable to improve the selectivity of the catalysts to linear alpha olefins (LAOs). In addition, the role of the catalyst support for oligomerization has not been thoroughly investigated. In this dissertation, we discuss how to improve the catalyst stability and selectivity to LAOs during the oligomerization reaction, determine which the stable and more active cobalt phases are, understand the reaction mechanism for oligomerization, and investigate the role of the catalyst support for oligomerization.

In Chapter 2, we study ethylene oligomerization over carbon-supported cobalt oxide catalysts at higher reaction temperature (e.g., 200 °C). This higher reaction temperature is an important parameter to improve the catalyst stability as well as the selectivity to linear alpha olefins (LAOs). Sequential reactions with the same catalyst bed at the following reaction temperatures: 200-140-180-160-200 °C with 24 h each reaction showed that the catalyst was stable for 120 h. The linear alpha olefin (LAO) isomer distributions up to C_8 olefins were above 60% at <20% ethylene conversion. The product linearities up to C_{12} olefins were above 90%, even at 48% conversion. Catalyst characterization experiments without exposure to air showed CoO as the bulk and surface cobalt phases, suggesting that this is the stable cobalt phase during oligomerization. Polyethylene was also formed during the reaction as confirmed by X-ray diffraction (XRD) and Soxhlet extraction.

In Chapter 3, we study ethylene oligomerization over a carbon-supported cobalt metal catalyst at 200 °C. This cobalt metal catalyst is more active than the cobalt oxide catalyst when performing the reaction at 200 °C, suggesting that cobalt metal is the more active cobalt phase for oligomerization. XRD experiments on the fresh and spent cobalt metal catalysts showed cobalt metal to be the only cobalt phase before and after the reaction. However, the carbon-supported cobalt metal catalyst deactivated due to polyethylene formation (approximately 50% of the spent

catalyst was polyethylene after a 24 h reaction). The ethylene oligomerization reaction is approximately first order with respect to ethylene partial pressure, suggesting a mechanism where the gaseous ethylene reacts with adsorbed olefins on a highly covered surface.

In Chapter 4, we investigate the role of the catalyst support for ethylene oligomerization over heterogeneous cobalt catalysts. Two different carbon supports, high-temperature-treated carbon (HTTC) and acid-washed carbon (AWC) were used to study the effect of surface functional groups for oligomerization. The high temperature treatment of carbon reduces the oxygen content of the carbon support, whereas the acid wash treatment of carbon increases the oxygen content as well as oxidizes the surface functional group. CoO_x/AWC had lower oligomerization activity, less LAO isomer distributions, and less selectivity to higher olefins (e.g., C_{6+} olefins) than CoO_x/HTTC due to more isomerization of linear alpha olefins into linear internal olefins. We also show that increasing the catalyst support particle size to impose more transport restrictions to the products has a minimal impact towards the product selectivity, the product linearity, and the linear alpha olefin isomer distribution. Finally, we show that the oligomerization activity of a catalyst consisting of cobalt oxide supported on carbon was higher by a factor of six when the cobalt was supported on a carbon which had less impurities (e.g., Al, Ca, Fe, and Mg), suggesting that these impurities likely influenced the activity of the catalyst.

In Chapter 5, we give conclusions and future research directions for olefin oligomerization over heterogeneous cobalt catalysts. The future research directions are primarily targeted towards investigating the role of each cobalt phase (e.g., Co_3O_4, CoO, and Co metal) during reaction. These can be performed with *operando* X-ray characterizations, including X-ray absorption spectroscopy (XAS), X-ray photoelectron spectroscopy (XPS), and X-ray diffraction (XRD), although care must be taken for the set up at high pressure. DFT calculations can also be performed to obtain the

binding energy values of olefins to the desired cobalt phase. The information from the DFT calculations can be used for developing microkinetic modelling on ethylene oligomerization over heterogeneous cobalt catalysts. We also recommend further investigation of the catalyst supports to understand what environment of cobalt influences the activity and the selectivity during the oligomerization reaction. Finally, we recommend regenerating the spent catalyst to remove the liquid oligomers as well as polyethylene which caused deactivation of the cobalt metal supported on carbon catalyst.

1.4 References

1. Expert Market Research, *Global Linear Alpha Olefin Market Report and Forecast 2021-2026*, https://www.expertmarketresearch.com/reports/linear-alpha-olefin-market, (Accessed May 2021).
2. IMARC Group, *Linear Alpha Olefins Market: Global Industry Trends, Share, Size, Growth, Opportunity and Forecast 2021-2026*, https://www.imarcgroup.com/linear-alpha-olefins-market, (Accessed May 2021).
3. E. O. C. Greiner, M. Blagoev and Y. Yamaguchi, *Chemical Economics Handbook: Linear alpha-Olefins*, IHS Chemical, 2013.
4. G. R. Lappin, L. H. Nemec, J. D. Sauer and J. D. Wagner, *Kirk-Othmer Encyclopedia of Chemical Technology*, John Wiley & Sons, Inc., 2000.
5. C. P. Nicholas, Applications of light olefin oligomerization to the production of fuels and chemicals, *Appl. Catal. A*, 2017, **543**, 82-97.
6. N. Rahimi and R. Karimzadeh, Catalytic cracking of hydrocarbons over modified ZSM-5 zeolites to produce light olefins: A review, *Appl. Catal. A*, 2011, **398**, 1-17.
7. T. Ridha, Y. Li, E. Gençer, J. J. Siirola, J. T. Miller, F. H. Ribeiro and R. Agrawal, Valorization of shale gas condensate to liquid hydrocarbons through catalytic dehydrogenation and oligomerization, *Processes*, 2018, **6**, 139.
8. US Energy Information Administration, *Annual energy outlook 2021 with projections to 2050*, https://www.eia.gov/outlooks/aeo/pdf/03%20AEO2021%20Natural%20gas.pdf, (Accessed May 2021).
9. I. Amghizar, L. A. Vandewalle, K. M. Van Geem and G. B. Marin, New trends in olefin production, *Eng.*, 2017, **3**, 171-178.
10. N. M. Eagan, M. D. Kumbhalkar, J. S. Buchanan, J. A. Dumesic and G. W. Huber, Chemistries and processes for the conversion of ethanol into middle-distillate fuels, *Nat. Rev. Chem.*, 2019, **3**, 223-249.
11. V. N. Ipatieff, B. B. Corson and G. Egloff, Polymerization, a new source of gasoline, *Ind. Eng. Chem.*, 1935, **27**, 1077-1081.
12. V. N. Ipatieff and R. E. Schaad, Heptenes and heptanes from propylene and butylenes, *Ind. Eng. Chem.*, 1945, **37**, 362-364.

13. J. A. Martens, R. Ravishankar, I. E. Mishin and P. A. Jacobs, Tailored alkene oligomerization with H-ZSM-57 zeolite, *Angew. Chem. Int. Ed.*, 2000, **39**, 4376-4379.
14. J. A. Martens, W. H. Verrelst, G. M. Mathys, S. H. Brown and P. A. Jacobs, Tailored catalytic propene trimerization over acidic zeolites with tubular pores, *Angew. Chem. Int. Ed.*, 2005, **44**, 5687-5690.
15. Y. T. Kim, J. P. Chada, Z. Xu, Y. J. Pagan-Torres, D. C. Rosenfeld, W. L. Winniford, E. Schmidt and G. W. Huber, Low-temperature oligomerization of 1-butene with H-ferrierite, *J. Catal.*, 2015, **323**, 33-44.
16. A. Kulkarni, A. Kumar, A. S. Goldman and F. E. Celik, Selectivity for dimers in pentene oligomerization over acid zeolites, *Catal. Commun.*, 2016, **75**, 98-102.
17. K. Ziegler, E. Holzkamp, H. Breil and H. Martin, Polymerisation von Äthylen und anderen Olefinen, *Angew. Chem.*, 1955, **67**, 426-426.
18. A. Bollmann, K. Blann, J. T. Dixon, F. M. Hess, E. Killian, H. Maumela, D. S. McGuinness, D. H. Morgan, A. Neveling, S. Otto, M. Overett, A. M. Z. Slawin, P. Wasserscheid and S. Kuhlmann, Ethylene tetramerization: a new route to produce 1-octene in exceptionally high selectivities, *J. Am. Chem. Soc.*, 2004, **126**, 14712-14713.
19. R. D. Broene, M. Brookhart, W. M. Lamanna and A. F. Volpe, Cobalt-catalyzed dimerization of α-olefins to give linear α-olefin products, *J. Am. Chem. Soc.*, 2005, **127**, 17194-17195.
20. A. Forestière, H. Olivier-Bourbigou and L. Saussine, Oligomerization of monoolefins by homogeneous catalysts, *Oil Gas Sci. Technol.,* 2009, **64**, 649-667.
21. R. Joshi, G. Zhang, J. T. Miller and R. Gounder, Evidence for the coordination-insertion mechanism of ethene dimerization at nickel cations exchanged onto beta molecular sieves, *ACS Catal.*, 2018, **8**, 11407-11422.
22. Z. Xu, J. P. Chada, D. Zhao, C. A. Carrero, Y. T. Kim, D. C. Rosenfeld, J. L. Rogers, S. J. Rozeveld, I. Hermans and G. W. Huber, Production of linear octenes from oligomerization of 1-butene over carbon-supported cobalt catalysts, *ACS Catal.*, 2016, **6**, 3815–3825.
23. G. P. Belov and P. E. Matkovsky, Processes for the production of higher linear α-olefins, *Pet. Chem.*, 2010, **50**, 283-289.
24. A. Finiels, F. Fajula and V. Hulea, Nickel-based solid catalysts for ethylene oligomerization - a review, *Catal. Sci. Technol.*, 2014, **4**, 2412-2426.
25. L. Bonneviot, D. Olivier and M. Che, Dimerization of olefins with nickel-surface complexes in X-type zeolite or on silica, *J. Mol. Catal.*, 1983, **21**, 415-430.
26. I. Agirrezabal-Telleria and E. Iglesia, Stabilization of active, selective, and regenerable Ni-based dimerization catalysts by condensation of ethene withinordered mesopores, *J. Catal.*, 2017, **352**, 505-514.
27. S. Moussa, P. Concepción, M. A. Arribas and A. Martínez, Nature of active sites and initiation mechanism for ethylene oligomerization on heterogeneous Ni-beta catalysts, *ACS Catal.*, 2018, **8**, 3903-3912.
28. R. Y. Brogaard and U. Olsbye, Ethene oligomerization in Ni-containing zeolites: theoretical discrimination of reaction mechanisms, *ACS Catal.*, 2016, **6**, 1205-1214.
29. A. Ehrmaier, Y. Liu, S. Peitz, A. Jentys, Y.-H. Chin, M. Sanchez-Sanchez, R. Bermejo-Deval and J. A. Lercher, Dimerization of Linear Butenes on Zeolite-Supported Ni^{2+}, *ACS Catal.*, 2019, **9**, 315-324.
30. D. D. Beck and J. H. Lunsford, The active site for ethylene polymerization over chromium supported on silica, *J. Catal.*, 1981, **68**, 121-131.

31. T. Agapie, Selective ethylene oligomerization: Recent advances in chromium catalysis and mechanistic investigations, *Coord. Chem. Rev.*, 2011, **255**, 861-880.
32. E. Groppo, C. Lamberti, S. Bordiga, G. Spoto and A. Zecchina, The Structure of Active Centers and the Ethylene Polymerization Mechanism on the Cr/SiO_2 Catalyst: A Frontier for the Characterization Methods, *Chem. Rev.*, 2005, **105**, 115-184.
33. R. G. Schultz, J. M. Schuck and B. S. Wildi, Olefin dimerization over cobalt-oxide-on-carbon catalysts: I. Propylene dimerization, *J. Catal.*, 1966, **6**, 385-396.
34. R. G. Schultz, R. M. Engelbrecht, R. N. Moore and L. T. Wolford, Olefin dimerization over cobalt-oxide-on-carbon catalysts: II. Butene and hexene dimerization, *J. Catal.*, 1966, **6**, 419-424.
35. R. G. Schultz, Olefin dimerization over cobalt-oxide-on-carbon catalysts: III. Oligomerization of ethylene, *J. Catal.*, 1967, **7**, 286-290.
36. Z. Xu, D. Zhao, J. P. Chada, D. C. Rosenfeld, J. L. Rogers, I. Hermans and G. W. Huber, Olefin conversion on nitrogen-doped carbon-supported cobalt catalyst: Effect of feedstock, *J. Catal*, 2017, **354**, 213-222.
37. D. Zhao, Z. Xu, J. P. Chada, C. A. Carrero, D. C. Rosenfeld, J. L. Rogers, I. Hermans, and G. W. Huber, Cobalt oxide on N-doped carbon for 1-butene oligomerization to produce linear octenes, *ACS Catal.*, 2017**, 7**, 7479-7489.
38. Z. Xu, J. P. Chada, L. Xu, D. Zhao, D. C. Rosenfeld, J. L. Rogers, I. Hermans, M. Mavrikakis and G. W. Huber, Ethylene dimerization and oligomerization to 1-butene and higher olefins with chromium-promoted cobalt on carbon catalyst, *ACS Catal.*, 2018, **8**, 2488-2497.
39. J. P. Chada, Z. Xu, D. Zhao, R. B. Watson, M. Brammer, M. Bigi, D. C. Rosenfeld, I. Hermans and G. W. Huber, Oligomerization of 1-butene over carbon-supported CoOx and subsequent isomerization/hydroformylation to n-nonanal, *Catal. Commun.,* 2018, **114**, 93-97.

Chapter 2. Ethylene Oligomerization into Linear Olefins over Cobalt Oxide on Carbon Catalyst[1]

2.1 Introduction

The advent of hydraulic fracturing technologies and the discovery of additional natural gas sources have led to considerable increases in natural gas production since 2006.[1,2] Steam cracking of natural gas produces light olefins including ethylene, one of the most manufactured commodity chemicals produced today.[3,4] Ethylene can also be synthesized from dehydration of ethanol which is currently the most widely produced biofuel in the world.[5-7] Light C_2-C_4 olefins are important feedstocks in the production of linear alpha olefins (LAOs) for use in polyethylene comonomers (C_4 - C_8), plasticizers (C_6 - C_{10}), lubricants (C_{10} - C_{12}), and detergents (C_{10} - C_{16}).[8,9] Higher linear olefins (C_{10} - C_{22}) are also valuable as they can be used as precursors for diesel fuels.[3] Current industrial processes for LAO synthesis involve the oligomerization of light olefins, often with homogeneous catalysts.[10-13] Olefin oligomerization has also been classically carried out over solid acids, though this typically produces highly branched products resulting from the underlying carbocation mechanisms.[3,14,15] Various attempts have been made to adapt the former technology to fully heterogeneous systems, most commonly by supporting nickel on aluminosilicates or metal organic frameworks (MOFs).[11,12,16-23] To date, these strategies have only obtained <60% selectivity to C_{8+} linear products at low conversions (e.g., <20%), with decreased linear product selectivity at higher conversion.[22]

Heterogeneous carbon-supported cobalt catalysts, on the other hand, have been reported to yield high selectivities to linear olefins.[24-31] Schultz et al. demonstrated that dimerization of

[1] This chapter is adapted from A. Jonathan, N. M. Eagan, D. L. Bruns, S. S. Stahl, M. P. Lanci, J. A. Dumesic and G. W. Huber, Ethylene oligomerization into linear olefins over cobalt oxide on carbon catalyst, *Catal. Sci. Technol.*, 2021, **11**, 3599-3608.

propylene over a doubly ammoniated cobalt oxide on carbon catalyst (CoO_x/N-C) in a batch reactor at 85 °C yielded 52% selectivity to linear hexenes.[24] This catalyst was prepared by treating the activated carbon in a solution containing NH_4OH, followed by cobalt impregnation, and then a second treatment with NH_4OH. Schultz et al. also reported that dimerization of 1-butene and 1-hexene with this catalyst at 150 °C yielded 65% and 83% selectivities to linear dimers, respectively.[25] However, no catalyst stability study as a function of reaction time was reported in those reactions. Recently, Xu et al. demonstrated that ethylene oligomerization over a doubly ammoniated cobalt oxide on carbon catalyst (CoO_x/N-C) at 80 °C in a continuous flow reactor yielded octenes with 77.6% linearity but only 5.2% 1-octene at 20% conversion.[28] Xu et al. claimed that the addition of Cr to the doubly ammoniated cobalt oxide on carbon catalyst (Cr-CoO_x/N-C) improves the activity and stability of the catalyst.[31] However, these experiments were performed in a reaction condition where the catalyst deactivated losing of over 30% of the catalyst activity in a 12 h period. As we will show in this paper, the hypotheses of implementing ammonia and Cr to the catalyst to improve the activity or stability of the catalyst need to be tested in a regime where the catalyst is stable to prove their validity.

Kiani et al. investigated ethylene oligomerization over both cobalt on carbon and ammoniated cobalt on carbon catalysts at the reaction temperature of 80 °C. They performed *in-situ* DRIFTS, *in-situ* Raman, and *in-situ* UV-Vis to try and elucidate the nature of the active site of these catalysts.[32] Kiani et al. showed that the rate of 1-butene formation with both cobalt on carbon and ammoniated cobalt on carbon catalysts decreased by approximately 80% in an 8 h period at 80 °C. Both catalysts had similar activity for ethylene conversion and deactivation rates at 80 °C. Kiani et al. proposed that the active site is the immobilized pseudo-tetrahedral $[Co(NH_3)_x]^{2+}$, which was unfortunately not present in the cobalt on carbon catalyst (from the

absence of the νNH wavenumber at 3325 cm^{-1} in their *in-situ* DRIFTS spectra).[32] Several fundamental questions need to be elucidated about these cobalt on carbon catalysts including how to reduce the rate of deactivation and what the active site is. It would also be desirable to be able to tune the product selectivity to linear alpha olefins (LAOs) instead of linear internal olefins as well as the selectivity to larger olefins (e.g., C_{8+}) while maintaining high product linearity. In this paper, we elucidate the reactions, the nature of the active site, the causes of catalyst deactivation, and how to tune the product selectivity for ethylene oligomerization over a carbon-supported cobalt catalyst.

2.2 Experimental Methods

2.2.1 Catalyst synthesis

High-temperature-treated carbon (HTTC) was prepared by heating sieved activated carbon (Norit Darco MRX m-2278, 250-600 μm particle size, 600-800 m^2 g^{-1} BET surface area) at 900 °C for 2 h under 100 cm^3 (STP) min^{-1} of He at 10 °C min^{-1} ramp rate. The carbon support used in this paper is the same carbon used by Xu et al., Zhao et al., and Chada et al. (Norit Darco MRX m-1721), except with a different batch.[27-31] This is a different carbon support used by Schultz et al. (Pittsburgh Coke) and Kiani et al. (Alfa Aesar).[24-26,32] After being cooled to room temperature, 2.0 g of the HTTC was impregnated with a solution composed of 1.89 g of $Co(NO_3)_2 \cdot 6H_2O$ (Sigma Aldrich) and 1.22 g of deionized (DI) water while being exposed to air to obtain a Co loading of approximately 12 wt%. This loading was chosen for comparison to results obtained previously by Xu et al.[28,31] The catalyst was dried overnight on a hotplate at 120 °C.

2.2.2 Continuous flow reactions

The ethylene oligomerization experiments were performed in 30 cm in length (1 ft) downflow fixed bed reactors with 1.27 cm (½ in) OD tubing for the reactions at 33.2% and 48.3% conversions, and 0.64 cm (¼ in) OD tubing for all other reactions. A diagram of this system is provided in Figure S2.1. Both ethylene and argon flow rates were varied from 20 to 40 cm^3 (STP) min^{-1} while the amount of catalyst was varied from 0.5 to 13.0 g. The contact time for each experiment is defined as the ratio of the mass of catalyst to the inlet mass flow rate of ethylene (h g_{cat} $g_{ethylene}^{-1}$). Prior to the experiment, the catalyst was pretreated in the reactor at 230 °C (1 °C min^{-1} ramp rate) in 100 cm^3 (STP) min^{-1} of Ar for 2 h. The catalyst was cooled to room temperature, pressurized to 32 bar (450 psig) using a back-pressure regulator (Equilibar), and heated to the desired reaction temperature at 5 °C min^{-1} ramp rate under Ar, followed by a switch in feed. Each reaction was performed with a 50:50 mixture (by volume) of ethylene and argon. After the regulator, the product stream was directed to a 120 mL glass tube submerged in an ice bath to condense out heavier species. The vapor fraction was analyzed by an online gas chromatograph equipped with a flame ionization detector (GC-FID, Shimadzu) approximately every 45 minutes. The liquid product was washed with 10 g of heptane to ensure full collection and analyzed by a two-dimensional gas chromatograph equipped with a flame ionization detector (2D-GC-FID, Agilent) every 3 h. During liquid product collection, the reactor effluent was temporarily directed to a secondary condenser before a new condenser was installed. The details of the GC-FID and the 2D-GC-FID are described elsewhere, except the hold time for the GC-FID was changed to 16 min at 250 °C and the liner for the 2D-GC-FID was not packed with a Pd/C catalyst.[30]

2.2.3 Product quantification

The online GC-FID detected C_2-C_{10} species while the 2D-GC-FID detected C_2-C_{24} species. The online GC-FID was calibrated using a Scotty gas standard (a mixture of 0.1 mol% of each C_2-C_6 LAO and 99.5 mol% of He). For species heavier than C_6, a linear correlation of the inverse calibration constant with the carbon number was approximated, described in detail in the Supplementary Information. For the liquid product quantification, nonane was used as an internal standard, and the quantification was based on the effective carbon number approximation. The C_4 isomer distribution was determined using the online GC-FID while the isomer distributions of heavier species were analyzed by the 2D-GC-FID. LAO standards up to C_{24} and linear internal olefin standards up to C_8 were used to determine retention times. Representative 2D-GC-FID chromatograms for the overall products and the C_8 olefin species are shown in Figures S2.2a and b, respectively. For species heavier than C_8, GC peaks with retention times later than the corresponding LAOs were assumed to be linear internal olefins based on the trends observed with the C_4, C_6, and C_8 olefins. In all cases, GC peaks with retention times earlier than the corresponding LAOs were assumed to be branched olefins. Isomer distributions of species heavier than C_{12} olefins were not analyzed due to extensive GC peak overlap. Oxygenated products were not observed.

Data points before 6 h for experiments with ¼ in tubing and before 48 h for experiments with ½ in tubing were not included due to system transients. Carbon balances were above 97% for all reactions below 30% conversion, above 94% at 33.2% conversion, and above 91% at 48.3% conversion. Because transients have a particularly noticeable impact on isomer distributions, the product selectivity, linearity, and LAO isomer distribution for experiments with ¼ in tubing and

½ in tubing were calculated from the average of 12 to 24 h and 48 to 96 h data points, respectively. Error bars were calculated from the standard deviations of these data points.

Various parameters are defined as follows:

$$\text{Ethylene conversion (C\%)} = \frac{\sum_{i=4}^{n}(i \times F_{\mathrm{C}_{i,\mathrm{out}}})}{2 \times F_{\mathrm{C}_{2,\mathrm{in}}}} \times 100 \quad (2.1)$$

$$\text{LAO isomer distribution of } \mathrm{C}_i \text{ (C\%)} = \frac{F_{\mathrm{C}_{i,\text{linear alpha,out}}}}{F_{\mathrm{C}_i,\mathrm{out}}} \times 100 \quad (2.2)$$

$$\text{Product linearity of } \mathrm{C}_i \text{ (C\%)} = \frac{F_{\mathrm{C}_{i,\text{linear alpha,out}}} + F_{\mathrm{C}_{i,\text{linear internal,out}}}}{F_{\mathrm{C}_{i,\mathrm{out}}}} \times 100 \quad (2.3)$$

$$\text{Product selectivity to } \mathrm{C}_i \text{ (C\%)} = \frac{i \times F_{\mathrm{C}_{i,\mathrm{out}}}}{\sum_{i=4}^{n}(i \times F_{\mathrm{C}_{i,\mathrm{out}}})} \times 100 \quad (2.4)$$

$$\text{Ethylene consumption rate } (\mathrm{mol}_{\text{ethylene}}\ \mathrm{g}_{\text{cat}}^{-1}\ \mathrm{h}^{-1}) = \frac{F_{\mathrm{C}_{2,\mathrm{in}}} \times \text{conversion}}{\text{mass of catalyst}} \quad (2.5)$$

$$\text{Carbon balance (C\%)} = \frac{\sum_{i=2}^{n}(i \times F_{\mathrm{C}_{i,\mathrm{out}}})}{2 \times F_{\mathrm{C}_{2,\mathrm{in}}}} \times 100 \quad (2.6)$$

Here F is the molar flow rate in mol h^{-1} and C_i represents all olefins of a specific structure (linear, linear alpha, or total) containing i carbon atoms.

2.2.4 Soxhlet extraction procedure

In a nitrogen-filled glovebox, the spent catalyst was removed from the sealed reactor tube and placed into a tared 24 mL scintillation vial. A portion of the spent catalyst was placed into a tared oven-dried cellulose thimble, on top of which was placed glass wool (to prevent the catalyst from escaping due to static electricity). The thimble was inserted into a Soxhlet extractor and then attached to a 250 mL round bottom flask with 100 mL of anhydrous toluene and a reflux condenser capped with a ground glass stopper. All ground glass joints were lightly greased with Apiezon H grease. The sealed Soxhlet assembly was removed from the glovebox and moved to a Schlenk line,

placed under a positive pressure of N_2, and refluxed in an oil bath for 24 h. After 24 h, the round bottom flask was replaced with a 25 mL Schlenk flask under a counterflow of N_2. Residual toluene in the Soxhlet assembly was removed *in vacuo* on the Schlenk line before being returned to the glovebox. The hot toluene extract was poured into 500 mL of acetone causing polyethylene to precipitate from solution. The precipitate was collected in a ground glass frit and washed several times with pentane to remove residual waxy pentane-soluble products. Before being transferred to a tared 24 mL scintillation vial, the precipitate was dried under vacuum to remove residual solvent. The filtrate was reduced on a rotary evaporator, and the remaining waxy residue was transferred to a tared 24 mL scintillation vial and dried under vacuum line to remove residual solvent.

2.2.5 X-ray diffraction (XRD) procedure

Powder XRD experiments were performed using a Rigaku Rapid II diffractometer with a Mo K_α source at 50 kV and 50 mA with the 2θ range of 2 to 45° and 30 min exposure time. For the XRD experiments without exposure to air, the catalysts were packed in glass capillaries with one end sealed with glass and the other end sealed by vacuum grease (Apiezon H vacuum grease) inside the glove box. This technique was applied to a highly pyrophoric material (diethylzinc) which did not react after three days outside of the glovebox, thus negligible oxygen entered the capillaries once exposed to air. These catalysts were transferred from the reactor to the glovebox either after pretreatment in argon at 230 °C for 2 h (fresh catalysts) or after reaction (spent catalysts) with both reactor tube ends sealed. For the experiments with exposure to air, the catalysts were packed inside a polyimide tube (American Durafilm) with both ends sealed with a clay. XRD experiments of the spent catalysts were performed prior to Soxhlet extractions. The XRD patterns of standards (e.g., carbon (graphite), polyethylene, and cobalt phases) were obtained from JADE

9 software. The baseline of each XRD pattern was corrected using JADE 9 software. The XRD detection limit of supported nanoparticles is typically 2-2.5 nm.[33]

2.2.6 X-ray photoelectron spectroscopy (XPS) procedure

XPS experiments were performed using a K-alpha spectrometer (Thermo Scientific) with an Al K_α X-ray source. All fresh and spent catalysts were packed into a vessel (Transfer Vessel K-Alpha) and sealed under vacuum inside a glovebox. These catalysts were analyzed without exposure to air. The fresh catalyst was pretreated in argon at 230 °C for 2 h before being transferred to the glovebox. The spent catalysts were treated with Soxhlet extractions without exposure to air to remove the liquid hydrocarbons in order to reach the 10^{-7} mbar vacuum requirement for XPS analyses. The Co_3O_4 and CoO standards (Sigma Aldrich, $\geq$ 99.5% trace metal basis) were analyzed with exposure to air. For the CoO standard, a monoatomic ion gun with 2000 eV was used with 90 s etch time to collect the spectrum. The collected CoO spectrum is consistent with the CoO spectrum from literature.[34] All samples were analyzed with the flood gun on. All binding energy (BE) values were calibrated to the BE of the C 1s peak for graphite at 284.5 eV. The Co 2p spectra were taken over 50 scans with 50 kV pass energy, 50 ms dwell time, and 0.1 eV step size. The C 1s spectra were taken over 20 scans with 50 kV pass energy, 50 ms dwell time, and 0.2 eV step size. The N 1s spectra were taken over 20 scans with 50 kV pass energy, 50 ms dwell time, and 0.2 eV step size. The baseline of each spectrum was corrected using a straight line. Intensities of all Co spectra were normalized to the Co spectrum from the spent 80 °C to have comparable intensities. The XPS detection limit is typically 0.1% to 1%.[35]

2.2.7 Attenuated total reflectance (ATR) procedure

Attenuated total reflectance FTIR (ATR-FTIR) spectra were collected on a Bruker Tensor 27 instrument with a Pike Technologies diamond ATR stage. Approximately 5 mg of precipitate collected in the Soxhlet extraction was used for each measurement. Spectra were collected at 4 cm^{-1} resolution between 600-4000 cm^{-1} with 16 scans and 16 background scans. High density polyethylene (HDPE, ExxonMobil, MW = 7845.30 Da) and low density polyethylene (LDPE, Dow 608A) were used as standards. The baseline of each spectrum was corrected using Origin 2015 software.

2.2.8 Thermogravimetric analysis (TGA) procedure

TGA experiments were performed using a Thermal Analysis Instruments Q500 system. For each measurement, approximately 10 mg of sample was heated at 10 °C min^{-1} under 50 cm^3 (STP) min^{-1} of N_2 to 800 °C.

2.2.9 N_2 physisorption procedure

N_2 physisorption experiments were performed using an ASAP 2020 (Micrometrics) at -196 °C. Approximately 200 mg of sample was used for each measurement. The sample was degassed for 6 h at 120 °C prior to the N_2 physisorption experiment. The Brunauer-Emmett-Teller (BET) surface areas were obtained from the N_2 physisorption data in the relative pressure (P/P_0) range of 0.06 to 0.24. The Barrett-Joyner-Halenda (BJH) pore size distributions (dV/dw where V is the pore volume and w is the pore width as a function of pore width) were obtained from the N_2 desorption isotherm.

2.3 Results and Discussion

2.3.1 Ethylene oligomerization in continuous flow reactor

Supported cobalt oxide on carbon catalysts were synthesized using high-temperature-treated carbon (HTTC) heated at 900 °C in helium prior to incipient wetness impregnation of cobalt nitrate, described in detail in the experimental section. This high temperature treatment has been shown to remove sulfur impurities and oxygen functional groups from activated carbon which could potentially affect the catalytic performance.[36] In addition, we neither incorporated ammonia treatment nor Cr to the catalysts to eliminate the potential contamination of the cobalt oxide on carbon catalysts (CoO_x/HTTC), especially when elucidating the active site. The plots of conversion and ethylene consumption rate of both CoO_x/HTTC and Cr-CoO_x/N-C at similar reaction conditions (i.e., 0.5 g of catalyst, ~40 cm^3 (STP) min^{-1} of ethylene, ~40 cm^3 (STP) min^{-1} of inert, 32 bar (450 psig) total pressure, and 80 °C reaction temperature) are shown in Figure 2.1.[31] Figure 2.1 shows that ethylene oligomerization reaction over CoO_x/HTTC is consistent both in terms of activity and stability with Cr-CoO_x/N-C obtained by Xu et al. at the reaction temperature of 80 °C.[31] For example, the present CoO_x/HTTC catalyst deactivated from 11.2% conversion at 6 h time on stream (TOS) to 7.3% conversion at 12 h TOS (35% activity loss) and subsequently to 3.5% conversion at 24 h TOS (70% activity loss). Xu et al. reported catalyst deactivation from 10% conversion at 6 h TOS to 6% conversion at 12 h TOS (40% activity loss). Data points before 6 h in this study are excluded due to system transients during startup. All ethylene oligomerization reactions in this study were performed with CoO_x/HTTC since this catalyst is simpler to study and analyze than the Cr-CoO_x/N-C.

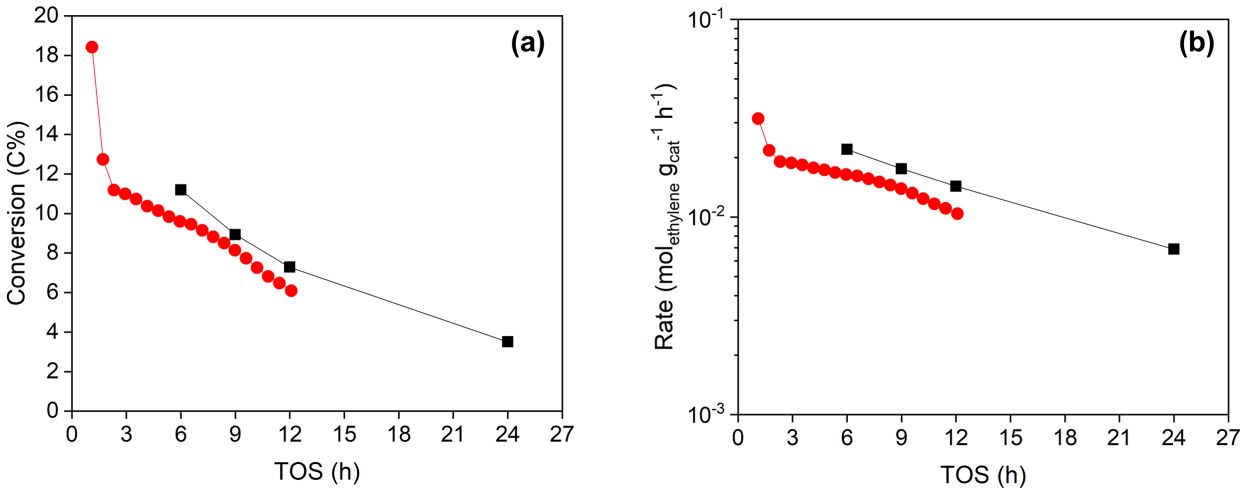

Figure 2.1 Conversions and ethylene consumption rates of CoO_x/HTTC (black square) and Cr-CoO_x/N-C as reported by Xu et al. (red circle) for ethylene oligomerization at 80 °C.[31] (a) Ethylene conversions as a function of time on stream (TOS). (b) Ethylene consumption rates as a function of TOS. Reaction conditions in this study: 32 bar (450 psig) total pressure, 0.5 g of catalyst, 40 cm^3 (STP) min^{-1} of ethylene, 40 cm^3 (STP) min^{-1} of argon, and 0.18 h contact time. Reaction conditions from Xu et al.: 32 bar (450 psig) total pressure, 0.5 g of catalyst, 34.8 cm^3 (STP) min^{-1} of ethylene, and 45.4 cm^3 (STP) min^{-1} of helium.[31] Data points before 6 h in this study are excluded due to system transients.

We hypothesize that CoO_x/HTTC initially deactivates before starting to stabilize, and this initial deactivation occurs faster at higher reaction temperature. To prove this hypothesis, ethylene oligomerization was carried out for 24 h periods at 80 °C and 200 °C with fresh catalysts, and at 80 °C with the catalyst previously used at 200 °C (for 24 h) to assess catalyst stability. Figure 2.2a shows that the fresh catalyst at 80 °C loses 70% of its activity in 24 h. When the reaction was instead performed at 200 °C, the catalyst remained stable (Figure 2.2a). After reaction at 200 °C, the catalyst can also be used at 80 °C without deactivation albeit at a lower rate than with a fresh catalyst at 80 °C. This stability is further shown in Figure 2.2b (rate versus TOS) and Figure S2.3 (conversion versus TOS) for a series of temperatures with a single catalyst bed in the order 200-

140-180-160-200 °C for 24 h each. The conversions from the first and final reactions at 200 °C were 13.7 ± 0.4% and 13.2 ± 0.4%, respectively, thus there is no statistically significant change in catalyst activity after 120 h of reaction. To further support this hypothesis, first order deactivation rate constants (k_d) were calculated for fresh catalysts at reaction temperatures of 80, 140, 160, 180, 200, and 220 °C for data collected over 24 h, shown in Figure S2.4 (see the derivation of k_d in the Supplementary Information). The value of k_d decreased with increasing reaction temperature, consistent with the previous finding that operating at higher temperatures with fresh catalysts during a 24 h period yields more stable performance. A similar trend of increasing catalyst stability at higher reaction temperature was also observed in 1-butene dimerization over nickel zeolitic catalysts in the temperature range of 100-180 °C.[37] An apparent activation energy ($E_{a,app}$) of 25 ± 1 kJ mol^{-1} was obtained using data where stable catalytic activities were observed—fresh catalyst reactions at 180, 200, and 220 °C as well the sequential reactions at 200-140-180-160-200 °C (Figure S2.5).

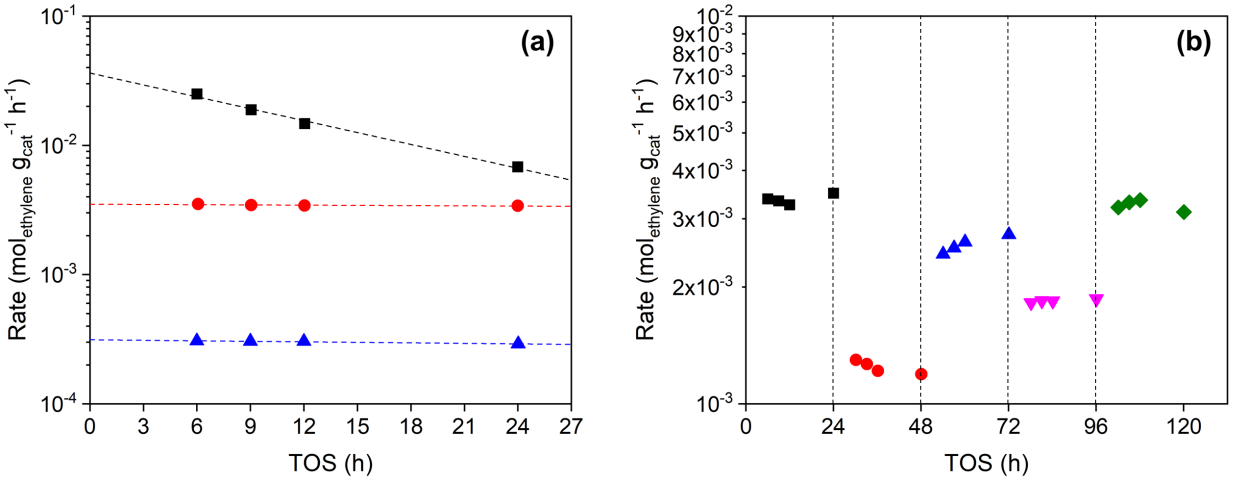

Figure 2.2 Ethylene consumption rates as a function of time on stream (TOS) at different reaction temperatures. (a) Data points represent the following reaction temperatures: fresh 80 °C (black square), fresh 200 °C (red circle), and spent 80 °C after 200 °C (blue triangle). Dashed lines are added to guide the eye. Reaction conditions: 16 bar ethylene, 16 bar argon, 12 wt% CoO_x/HTTC, 0.18 h contact time for fresh 80 °C, and 1.45 h contact time for fresh 200 °C and spent 80 °C after 200 °C. (b) Data points represent the following reaction temperatures: first 200 °C (black square), 140 °C (red circle), 180 °C (blue triangle), 160 °C (magenta upside-down triangle), and last 200 °C (green diamond). Reaction conditions: 16 bar ethylene, 16 bar argon, 12 wt% CoO_x/HTTC, and 1.45 h contact time. Conversions were below 20% in all cases.

The contact time for this catalyst was varied from 0.18 to 9.45 h g_{cat} $g_{ethylene}^{-1}$ at 200 °C and 32 bar (450 psig) total pressure to increase the conversion from 2.8 to 48.3% (Figure S2.6). Figure 2.3a shows the linear alpha olefin (LAO) isomer distributions of C_4, C_6, C_8, C_{10}, and C_{12} olefins versus conversion. C_{14+} olefin distributions are not shown due to substantial peak overlap in the GC. The LAO isomer distributions for all carbon numbers decreased with increasing conversion, likely resulting from more extensive isomerization with higher contact times. Figure 2.3a shows that this catalyst is selective to LAOs among the C_4 to C_8 olefins at low conversions (e.g., <20%). At 14.0% conversion, the LAO isomer distributions of C_4, C_6, and C_8 olefins were 90.2%, 77.6%, and 69.1%, respectively. The product linearities of C_4 to C_{12} olefins, shown in Figure S2.7, were

all above 90% even at 48.3% conversion. To our knowledge this material is the most selective heterogeneous catalyst for ethylene oligomerization to linear olefins in the absence of activators and/or solvents.

Figure 2.3b shows the product selectivities to C_4, C_6, C_8, C_{10}, and C_{12+} olefins versus conversion. The C_4 selectivity decreased from 59.8 to 50.6% as the conversion increased from 2.8 to 48.3%. This result demonstrates that the C_4 olefins can readsorb and further react with either ethylene or themselves to form larger olefins. Selectivities to C_6, C_8, and C_{10} olefins were relatively constant around 22%, 10%, and 5%, respectively, at these conversions. However, the selectivity to C_{12+} olefins increased the most from 4.1% to 10.9% with this increase in conversion.

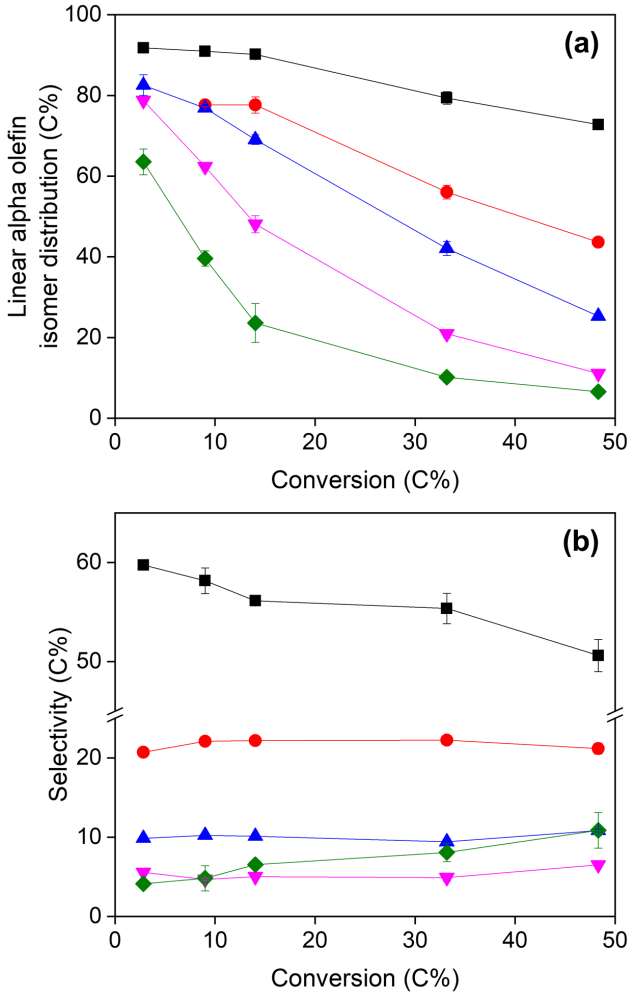

Figure 2.3 Isomer distributions and product selectivities versus conversion. (a) Linear alpha olefin isomer distributions among C_4 (black square), C_6 (red circle), C_8 (blue triangle), C_{10} (magenta upside-down triangle), and C_{12} (green diamond) olefins versus conversion. (b), Selectivities to C_4 (black square), C_6 (red circle), C_8 (blue triangle), C_{10} (magenta upside-down triangle), and C_{12+} (green diamond) olefins versus conversion. Reaction conditions: 200 °C, 16 bar ethylene, 16 bar argon, 12 wt% CoO_x/HTTC, and 0.18 - 9.45 h contact time. Bounds represent standard deviations.

Xu et al. reported that olefin oligomerization over CoO_x/N-C catalysts follows the Cossee-Arlman mechanism which results in a Schulz-Flory type distribution.[28] According to the Cossee-Arlman mechanism, a plot of $\log_{10}$(Carbon selectivity / n) versus n, where n is the number of repeat units, will give a straight line with a slope corresponding to $\log_{10}(\alpha)$ where α is the chain growth

probability. Additional details on the Schulz-Flory distribution are discussed in the Supplementary Information. A representative plot is shown in Figure 2.4. We observed two different slopes for all reactions, one for C_4-C_{10} olefins and one for C_{10+} olefins. This trend was not observed in the prior work on ethylene oligomerization over CoO_x/N-C because the product distribution was only shown up to C_{12} olefins whereas our analysis goes up to C_{16} olefins.[28] Iglesia, Bell, and co-workers also observed similar behavior of two different slopes in Fischer-Tropsch synthesis reactions.[38-40] Iglesia and co-workers proposed that the change in slope is due to intrapellet diffusion limitations for the larger olefins.[39] This result suggests that in the present study, C_{12+} olefins exhibit longer residence times inside the catalyst pores, increasing the probability that they react further before diffusing out. This behavior could explain why the C_{12+} olefin selectivity increased the most with increasing conversion. Figure S2.8 shows the α values (from C_4-C_{10} olefins and C_{10+} olefins) versus conversion. The value of α for C_4-C_{10} olefins was relatively constant around 0.33 while the value of α for C_{10+} olefins increased from 0.44 to 0.57 with increasing conversion from 2.8 to 48.3%.

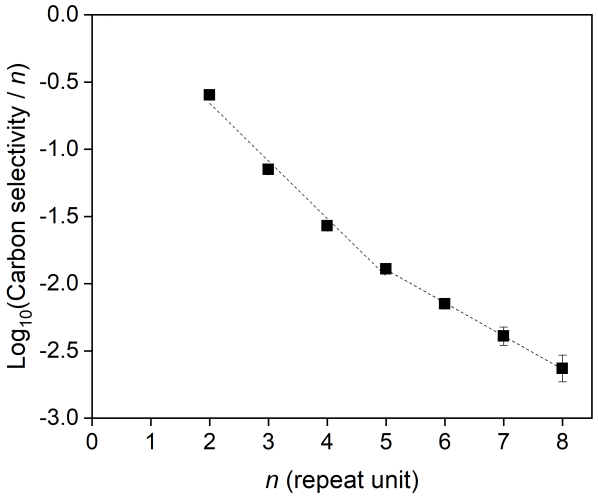

Figure 2.4 A typical product distribution for ethylene oligomerization over CoO_x/HTTC as a function of repeat unit (*n*). Reaction conditions: 200 °C, 16 bar ethylene, 16 bar argon, 12 wt% CoO_x/HTTC, 9.45 h contact time, and 48.3% conversion.

We propose a possible reaction scheme shown in Figure 2.5 for ethylene oligomerization over a heterogeneous cobalt on carbon catalyst. Ethylene is adsorbed onto the catalyst, after which ethylene either desorbs or propagates with other ethylene molecules to extend the olefin chain length. The olefin chains continue to grow or desorb from the catalyst as LAOs. These olefins may also readsorb onto the catalyst after which isomerization may occur to yield linear internal olefins. This hypothesis is consistent with our observation that internal olefin selectivities increase with contact time, allowing each olefin more chances to readsorb and isomerize. Branched olefins are not shown in the reaction scheme as they represent less than 10% of the products. Coupling reactions between C_{4+} olefins to yield larger linear internal olefins may also occur and have only been omitted from this diagram for simplicity.[28]

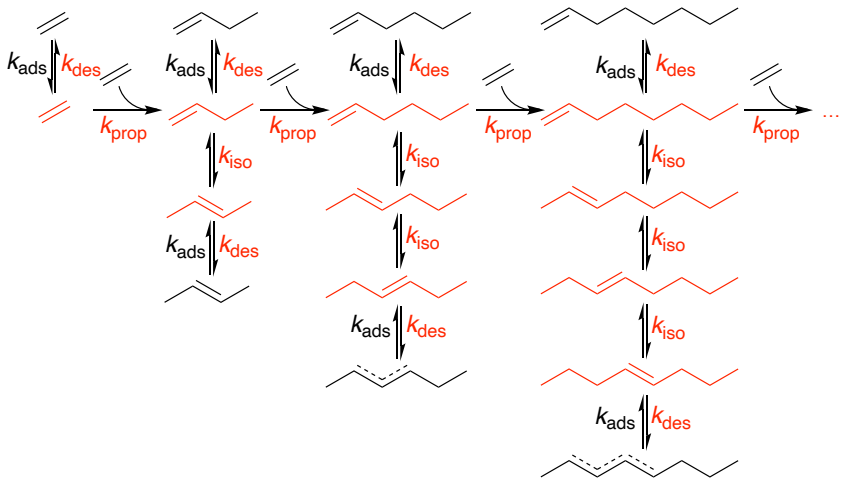

Figure 2.5 Reaction scheme for ethylene oligomerization over a cobalt oxide on carbon catalyst. Higher olefins may also react with C_{4+} alkyl chains forming internal olefins (not depicted). Species and reactions on the catalyst surface are labelled with red color.

2.3.2 Characterizations of fresh and spent catalysts

We investigated both the bulk and surface cobalt phases of the fresh catalyst after pretreatment in argon at 230 °C, the spent catalyst after a 24 h reaction at 80 °C, and the spent catalyst after a 24 h reaction at 200 °C. The X-ray diffraction (XRD) patterns of these catalysts were collected without exposure to air and are shown in Figure 2.6a. Both the fresh and spent 80 °C catalysts showed clear Co_3O_4 reflections, consistent with the work by Xu et al.[28] The XRD pattern of the spent 200 °C catalyst, on the other hand, showed reflection characteristic of CoO, suggesting that the Co_3O_4 had been reduced during the reaction and furthermore that CoO is the more stable bulk phase during oligomerization. Peaks attributable to polyethylene were also observed in the spent 80 °C and spent 200 °C catalysts, suggesting the reaction produced polyethylene with relatively high crystallinity. XRD patterns of air-exposed fresh and spent catalysts from different reaction temperatures were also examined (Figure S2.9), which similarly showed CoO being present in all stable catalysts.

X-ray photoelectron spectroscopy (XPS) measurements of the surface cobalt phase for the fresh, spent 80 °C, and spent 200 °C catalysts were collected without exposure to air. Using an air-free glovebox and Schlenk line techniques, the spent catalysts were initially washed with toluene in a Soxhlet extractor to remove volatile hydrocarbons to meet the vacuum requirements of the XPS instrument. The Co 2p XPS region of these three catalysts along with Co_3O_4 and CoO standards are shown in Figure 2.6b. Co_3O_4 and CoO can be distinguished by comparing the satellite peaks in the Co 2p region.[34] Co_3O_4 has a satellite peak near 790 eV, while CoO has satellite peaks around 786 and 802 eV. All catalysts showed predominantly CoO features, although the spent 200 °C catalyst showed more prominent 786 and 802 eV features than did the fresh and spent 80 °C catalysts, suggesting that a higher fraction of its cobalt surface was in the CoO state. Metallic Co with a characteristic peak at 778 eV was not observed on any of these catalysts. Xu et al. reported that the distribution of Co_3O_4 and CoO according to XANES for CoO_x/N-C catalyst after pretreatment at 230 °C in helium without exposure to air was 72.5 and 27.5 wt%, respectively.[27] These results suggest that Co_3O_4 and/or CoO could be the active catalytic site(s) for oligomerization with different catalyst stability. It is unclear why the catalyst deactivated during a 24 h reaction at 80 °C whereas it was stable during a 24 h reaction at 200 °C when CoO was present on both catalysts. We hypothesize that the catalyst stability during the reaction at 200 °C could be related to the formation of bulk and surface CoO. We also investigated the N 1s XPS region of the fresh catalyst after pretreatment in argon at 230 °C without exposure to air to determine whether nitrogen was present in the catalyst before the oligomerization reaction. Figure S2.10 shows that the N 1s XPS signal is within the noise level of the instrument, thus the active catalytic site of this catalyst is not related to nitrogen.

Thermogravimetric analysis (TGA) under N_2 was performed on the spent 80 °C and spent 200 °C catalysts before and after Soxhlet extractions to probe the presence of polyethylene and to determine whether the catalysts were free from oligomers after the extraction (Figure S2.11). Before the Soxhlet extractions (Figures S2.11a-b), both the spent 80 °C and spent 200 °C catalysts exhibited a peak near 430 °C, in agreement with the traces obtained by Zhao et al. for polyethylene TGA under N_2.[41] After the extractions, the TGA curves of both spent 80 °C and spent 200 °C catalysts (Figures S2.11c-d) still contained oligomers and polyethylene. These hydrocarbons were likely formed inside the catalyst pores during the reactions and may have been too large to diffuse out during extractions.

N_2 physisorption experiments were performed on the fresh, spent 80 °C, and spent 200 °C catalysts to obtain BET surface areas (Table S2.1) and pore size distributions (Figure S2.12). The spent catalysts were previously treated with Soxhlet extractions due to the vacuum requirements of the adsorption equipment. The BET surface areas of the spent 80 °C and spent 200 °C catalysts were 70 and 105 $m^2\ g^{-1}$, respectively, substantially lower than the BET surface area of the fresh catalyst of 418 $m^2\ g^{-1}$. The loss of BET surface area can be explained by the presence of remnant hydrocarbons including polyethylene which could not be fully removed with the extractions. The pore size distributions of these catalysts were similar, suggesting that polyethylene formation impacts all pores equally.

To provide further evidence for the presence of polyethylene, the hot toluene extracts from both spent catalysts were diluted with acetone to promote the precipitation of dissolved solids. The precipitate was collected by filtration and washed with pentane to remove pentane-soluble hydrocarbon fractions before being dried under vacuum. The resulting solids were analyzed by attenuated total reflectance FTIR (ATR-FTIR) along with high density (HDPE) and low density

polyethylene (LDPE) standards, shown in Figure 2.6c. All samples (spent 200 °C and spent 80 °C extracts along with the HDPE and LDPE standards) showed the same characteristic peaks near 719, 1462, 2848, and 2915 cm^{-1}, suggesting polyethylene was present in both spent catalysts. Schultz et al. also reported that the extract from the spent CoO_x/N-C after propylene dimerization had a molecular weight of 2000-3000 Da which they hypothesized to cause catalyst deactivation.[24]

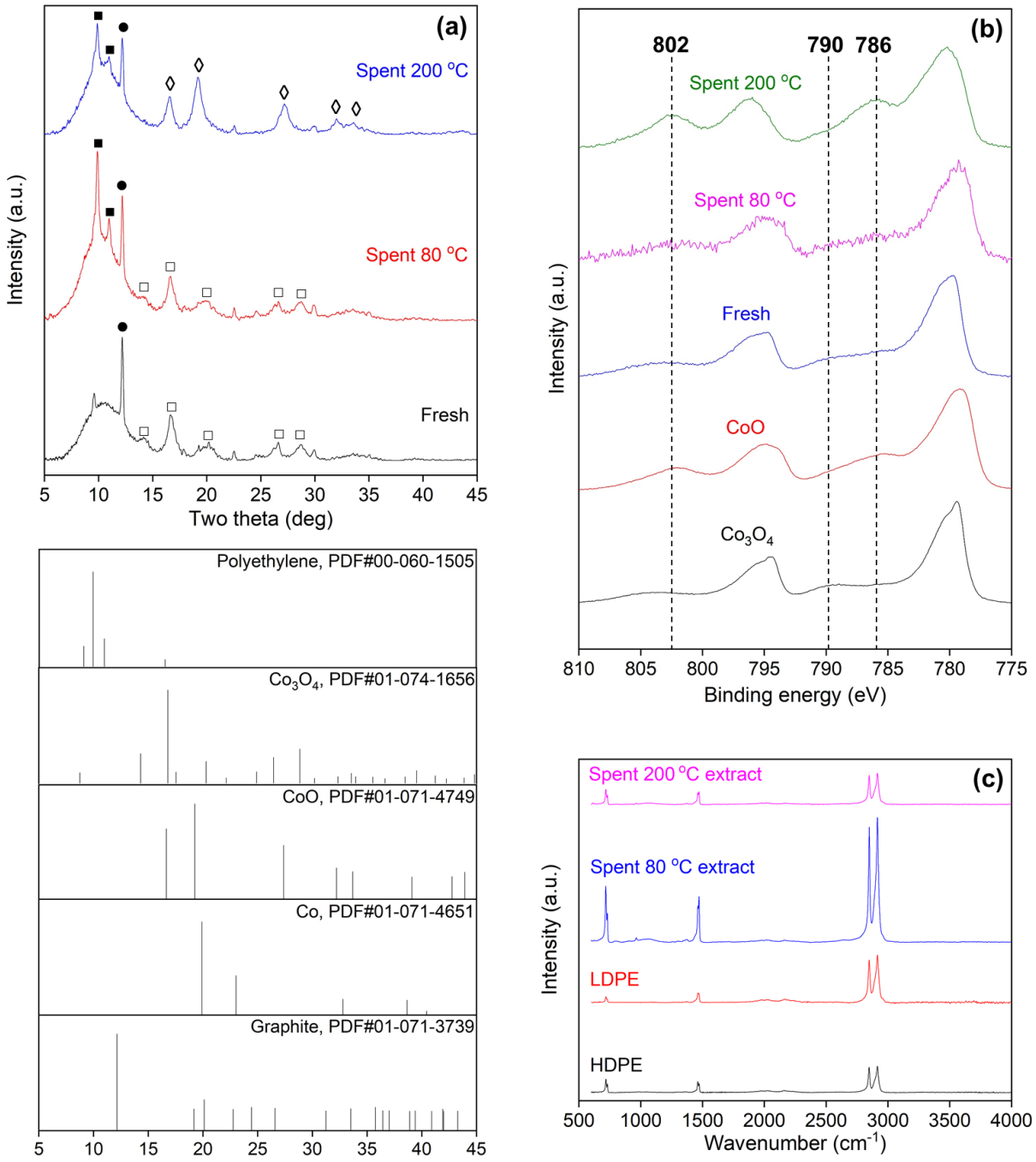

Figure 2.6 XRD patterns and XPS spectra of fresh and spent catalysts as well as ATR spectra of the extracts from spent catalysts. (a) Mo-XRD of fresh catalyst after pretreatment in argon at 230 °C, spent catalyst after a 24 h reaction at 80 °C, and spent catalyst after a 24 h reaction at 200 °C before Soxhlet extractions. Characteristic peaks are carbon (graphite) - filled circle, polyethylene - filled square, Co_3O_4 - unfilled square, and CoO - unfilled diamond. (b) Co 2p XPS region of fresh catalyst after pretreatment in argon at 230 °C, spent catalyst after a 24 h reaction at 80 °C, and

spent catalyst after a 24 h reaction at 200 °C after Soxhlet extractions along with Co_3O_4, and CoO standards. (c) ATR of polyethylene standards (HDPE and LDPE) and extracts from spent catalysts after 24 h reactions at 80 °C and 200 °C.

2.4 Conclusions

CoO_x/HTTC can selectively oligomerize ethylene into linear C_4-C_{12} olefins. The presence of CoO in the bulk and the surface cobalt phases suggests that this is the stable cobalt phase for oligomerization. At higher reaction temperatures (~ 200 °C) the catalyst is reduced from Co_3O_4 to the more stable CoO phase leading to improved catalyst stability. However, the presence of both Co_3O_4 and CoO in the fresh and spent catalysts after a 24 h reaction at 80 °C could suggest that both cobalt states are active for oligomerization. Polyethylene is formed in the catalyst pores during the reaction. The product distribution follows two different Schulz-Flory distributions with the first distribution from C_4 to C_{10} olefins and the second distribution above C_{10} olefins. This shift in product distribution indicates that transport restrictions, likely imposed by the oligomers and polyethylene in the pores, influence the product selectivity similar to chain growth during the Fischer-Tropsch synthesis reaction. We propose a reaction scheme for this reaction, in which ethylene is adsorbed onto the catalyst, after which it either desorbs or propagates with other olefins. At lower conversion (<20%), high selectivity to C_4-C_8 linear alpha olefins (>60% LAO isomer distributions) is obtained while at higher conversion the selectivity to LAOs decreases due to isomerization and chain terminating internal olefin production. In short, these findings show that CoO_x/HTTC is a uniquely stable heterogeneous catalyst that produces highly linear (including linear alpha) olefin products from ethylene without requiring solvents or activators.

2.5 References

1. T. Ridha, Y. Li, E. Gençer, J. J. Siirola, J. T. Miller, F. H. Ribeiro and R. Agrawal, Valorization of shale gas condensate to liquid hydrocarbons through catalytic dehydrogenation and oligomerization, *Processes*, 2018, **6**, 139.
2. US Energy Information Administration, *Annual energy outlook 2019 with projections to 2050*, https://www.eia.gov/outlooks/aeo/pdf/aeo2019.pdf, (Accessed February 2021).
3. N. M. Eagan, M. D. Kumbhalkar, J. S. Buchanan, J. A. Dumesic and G. W. Huber, Chemistries and processes for the conversion of ethanol into middle-distillate fuels, *Nat. Rev. Chem.*, 2019, **3**, 223-249.
4. N. Rahimi and R. Karimzadeh, Catalytic cracking of hydrocarbons over modified ZSM-5 zeolites to produce light olefins: A review, *Appl. Catal. A*, 2011, **398**, 1-17.
5. M. Balat and H. Balat, Recent trends in global production and utilization of bio-ethanol fuel, *Appl. Energy*, 2009, **86**, 2273-2282.
6. K. Kohse-Höinghaus, P. Oßwald, T. A. Cool, T. Kasper, N. Hansen, F. Qi, C. K. Westbrook and P. R. Westmoreland, Biofuel combustion chemistry: from ethanol to biodiesel, *Angew. Chem. Int. Ed.*, 2010, **49**, 3572-3597.
7. G. Hochman and D. Zilberman, Corn ethanol and US biofuel policy 10 years later: A quantitative assessment, *Am. J. Agric. Econ.*, 2018, **100**, 570-584.
8. E. O. C. Greiner, M. Blagoev and Y. Yamaguchi, *Chemical Economics Handbook: Linear alpha-Olefins*, IHS Chemical, 2013.
9. G. R. Lappin, L. H. Nemec, J. D. Sauer and J. D. Wagner, *Kirk-Othmer Encyclopedia of Chemical Technology*, John Wiley & Sons, Inc., 2000.
10. C. P. Nicholas, Applications of light olefin oligomerization to the production of fuels and chemicals, *Appl. Catal. A*, 2017, **543**, 82-97.
11. R. Y. Brogaard and U. Olsbye, Ethene oligomerization in Ni-containing zeolites: theoretical discrimination of reaction mechanisms, *ACS Catal.*, 2016, **6**, 1205-1214.
12. S. Moussa, P. Concepción, M. A. Arribas and A. Martínez, Nature of active sites and initiation mechanism for ethylene oligomerization on heterogeneous Ni-beta catalysts, *ACS Catal.*, 2018, **8**, 3903-3912.
13. Z. Wang, G. A. Solan, W. Zhang and W.-H. Sun, Carbocyclic-fused N, N, N-pincer ligands as ring-strain adjustable supports for iron and cobalt catalysts in ethylene oligo-/polymerization, *Coord. Chem. Rev.*, 2018, **363**, 92-108.
14. Y. T. Kim, J. P. Chada, Z. Xu, Y. J. Pagan-Torres, D. C. Rosenfeld, W. L. Winniford, E. Schmidt and G. W. Huber, Low-temperature oligomerization of 1-butene with H-ferrierite, *J. Catal.*, 2015, **323**, 33-44.
15. M. L. Sarazen, E. Doskocil and E. Iglesia, Catalysis on solid acids: Mechanism and catalyst descriptors in oligomerization reactions of light alkenes, *J. Catal.*, 2016, **344**, 553-569.
16. M. A. Deimund, J. Labinger and M. E. Davis, Nickel-exchanged zincosilicate catalysts for the oligomerization of propylene, *ACS Catal*, 2014, **4**, 4189-4195.
17. A. N. Mlinar, G. B. Baur, G. G. Bong and A. T. Bell, Propene oligomerization over Ni-exchanged Na-X zeolites, *J. Catal.*, 2012, **296**, 156-164.
18. I. Agirrezabal-Telleria and E. Iglesia, Stabilization of active, selective, and regenerable Ni-based dimerization catalysts by condensation of ethene withinordered mesopores, *J. Catal.*, 2017, **352**, 505-514.

19. E. D. Metzger, R. J. Comito, Z. Wu, G. Zhang, R. C. Dubey, W. Xu, J. T. Miller and M. Dincă, Highly selective heterogeneous ethylene dimerization with a scalable and chemically robust MOF catalyst, *ACS Sustain. Chem. Eng.*, 2019, **7**, 6654-6661.
20. A. Finiels, F. Fajula and V. Hulea, Nickel-based solid catalysts for ethylene oligomerization - a review, *Catal. Sci. Technol.*, 2014, **4**, 2412-2426.
21. R. Joshi, G. Zhang, J. T. Miller and R. Gounder, Evidence for the coordination-insertion mechanism of ethene dimerization at nickel cations exchanged onto beta molecular sieves, *ACS Catal.*, 2018, **8**, 11407-11422.
22. A. Ehrmaier, Y. Liu, S. Peitz, A. Jentys, Y.-H. Chin, M. Sanchez-Sanchez, R. Bermejo-Deval and J. A. Lercher, Dimerization of Linear Butenes on Zeolite-Supported Ni^{2+}, *ACS Catal.*, 2019, **9**, 315-324.
23. H. Olivier-Bourbigou, P. A. R. Breuil, L. Magna, T. Michel, M. F. Espada Pastor and D. Delcroix, Nickel Catalyzed Olefin Oligomerization and Dimerization, *Chem. Rev.*, 2020, **120**, 7919-7983.
24. R. G. Schultz, J. M. Schuck and B. S. Wildi, Olefin dimerization over cobalt-oxide-on-carbon catalysts: I. Propylene dimerization, *J. Catal.*, 1966, **6**, 385-396.
25. R. G. Schultz, R. M. Engelbrecht, R. N. Moore and L. T. Wolford, Olefin dimerization over cobalt-oxide-on-carbon catalysts: II. Butene and hexene dimerization, *J. Catal.*, 1966, **6**, 419-424.
26. R. G. Schultz, Olefin dimerization over cobalt-oxide-on-carbon catalysts: III. Oligomerization of ethylene, *J. Catal.*, 1967, **7**, 286-290.
27. Z. Xu, J. P. Chada, D. Zhao, C. A. Carrero, Y. T. Kim, D. C. Rosenfeld, J. L. Rogers, S. J. Rozeveld, I. Hermans and G. W. Huber, Production of linear octenes from oligomerization of 1-butene over carbon-supported cobalt catalysts, *ACS Catal.*, 2016, **6**, 3815–3825.
28. Z. Xu, D. Zhao, J. P. Chada, D. C. Rosenfeld, J. L. Rogers, I. Hermans and G. W. Huber, Olefin conversion on nitrogen-doped carbon-supported cobalt catalyst: Effect of feedstock, *J. Catal*, 2017, **354**, 213-222.
29. D. Zhao, Z. Xu, J. P. Chada, C. A. Carrero, D. C. Rosenfeld, J. L. Rogers, I. Hermans, and G. W. Huber, Cobalt oxide on N-doped carbon for 1-butene oligomerization to produce linear octenes, *ACS Catal.*, 2017**, 7**, 7479-7489.
30. J. P. Chada, Z. Xu, D. Zhao, R. B. Watson, M. Brammer, M. Bigi, D. C. Rosenfeld, I. Hermans and G. W. Huber, Oligomerization of 1-butene over carbon-supported CoOx and subsequent isomerization/hydroformylation to n-nonanal, *Catal. Commun.,* 2018, **114**, 93-97.
31. Z. Xu, J. P. Chada, L. Xu, D. Zhao, D. C. Rosenfeld, J. L. Rogers, I. Hermans, M. Mavrikakis and G. W. Huber, Ethylene dimerization and oligomerization to 1-butene and higher olefins with chromium-promoted cobalt on carbon catalyst, *ACS Catal.*, 2018, **8**, 2488-2497.
32. D. Kiani and J. Baltrusaitis, Immobilization and activation of cobalt-amine catalyst on NH4OH-treated activated carbon for ethylene dimerization, *Catal. Today*, 2020, **365**, 24-34.
33. K. O'Connell and J. R. Regalbuto, High sensitivity silicon slit detectors for 1 nm powder XRD size detection limit, *Catal. Lett.,* 2015, **145**, 777-783.
34. D. Gu, C. -J. Jia, C. Weidenthaler, H. -J. Bongard, B. Spliethoff, W. Schmidt and F. Schüth, Highly ordered mesoporous cobalt-containing oxides: structure, catalytic properties, and active sites in oxidation of carbon monoxide, *J. Am. Chem. Soc.*, 2015, **137**, 11407-11418.

35. A. G. Shard, Detection limits in XPS for more than 6000 binary systems using Al and Mg Kα X-rays, *Surf. Interface Anal.*, 2014, **46**, 175-185.
36. P. E. Fanning and M. A. Vannice, A DRIFTS study of the formation of surface groups on carbon by oxidation, *Carbon*, 1993, **31**, 721-730.
37. P. Beltrame, L. Forni, A. Talamini, and G. Zuretti, Dimerization of 1-butene over nickel zeolitic catalysts: A search for linear dimers, *Appl. Catal. A,* 1994**, 110**, 39-48.
38. E. Iglesia, Design, synthesis, and use of cobalt-based Fischer-Tropsch synthesis catalysts, *Appl. Catal. A*, 1997, **161**, 59-78.
39. E. Iglesia, S. C. Reyes, R. J. Madon and S. L. Soled, Selectivity control and catalyst design in the Fischer-Tropsch synthesis: sites, pellets, and reactors, *Adv. Catal.*, 1993, **39**, 221-302.
40. R. A. Dictor and A. T. Bell, Fischer-Tropsch synthesis over reduced and unreduced iron oxide catalysts, *J. Catal.*, 1986, **97**, 121-136.
41. D. Zhao, X. Wang, J. B. Miller and G. W. Huber, The chemistry and kinetics of polyethylene pyrolysis: a process to produce fuels and chemicals, *ChemSusChem*, 2020, **13**, 1764-1774.

2.6 Supplementary Information

Supplementary Method: Calculating calibration constants for C_2 up to C_{10} olefins in GC-FID

A calibration constant (k_i) with i carbon atoms is defined as the ratio of the olefin concentration (mol%) with i carbon atoms and the corresponding GC area (a.u.). A linear correlation of $1/k_i$ as a function of i was observed for C_2 up to C_6 olefins from the Scotty gas standard (a mixture of 0.1 mol% of each C_2-C_6 LAO and 99.5 mol% of He). From the linear extrapolation of $1/k_i$ as a function of i, the calibration constants for C_8 and C_{10} olefins were calculated.

Supplementary Discussion: Obtaining the α parameter of a Schulz-Flory distribution

The equation defining the Schulz-Flory distribution is given as follows:

$$\frac{W_n}{n} = \alpha^{n-1}(1-\alpha)^2 \tag{S2.1}$$

where W_n is the product weight fraction (which in this case is the same as the carbon selectivity), n is the number of repeat units, and α is the chain growth probability. From rearrangement of the equation and taking the $\log_{10}$, the equation becomes:

$$\log_{10}\left(\frac{W_n}{n}\right) = (n-1)\log_{10}(\alpha) + 2\log_{10}(1-\alpha) \tag{S2.2}$$

$$\log_{10}\left(\frac{W_n}{n}\right) = n\log_{10}(\alpha) + [2\log_{10}(1-\alpha) - \log_{10}(\alpha)] \tag{S2.3}$$

By making a plot of $\log_{10}\left(\frac{W_n}{n}\right)$ as a function of n, the chain growth probability (α) could be calculated from 10^{slope}.

First order deactivation rate constant

The equation for first order deactivation is defined as:

$$\frac{da}{dt} = -k_{\mathrm{d}} a \tag{S2.4}$$

$$a = \frac{\text{rate}\,(t)}{\text{rate}\,(t_0)} \tag{S2.5}$$

Here k_{d} is the first order deactivation rate constant and a is the relative ethylene consumption rate at time t with respect to the initial ethylene consumption rate at t_0. From rearrangement of the equation and integration from $t = t_0$ to $t = t$, the following equation is obtained:

$$\ln\big(\text{rate}(t)\big) = -k_{\mathrm{d}}\, t + \ln\big(\text{rate}(t_0)\big) \tag{S2.6}$$

A plot of $\ln\big(\text{rate}(t)\big)$ versus t (which in this case is time on stream) therefore has a slope equal to $-k_{\mathrm{d}}$.

Table S2.1 BET surface areas of fresh and spent catalysts.

Sample	BET surface area ($m^2\ g^{-1}$)
Fresh[a]	418
Spent 80 °C[b]	70
Spent 200 °C[b]	105

[a]Fresh catalyst after pretreatment at 230 °C in argon. [b]Spent catalysts after 24 h reactions and Soxhlet extractions.

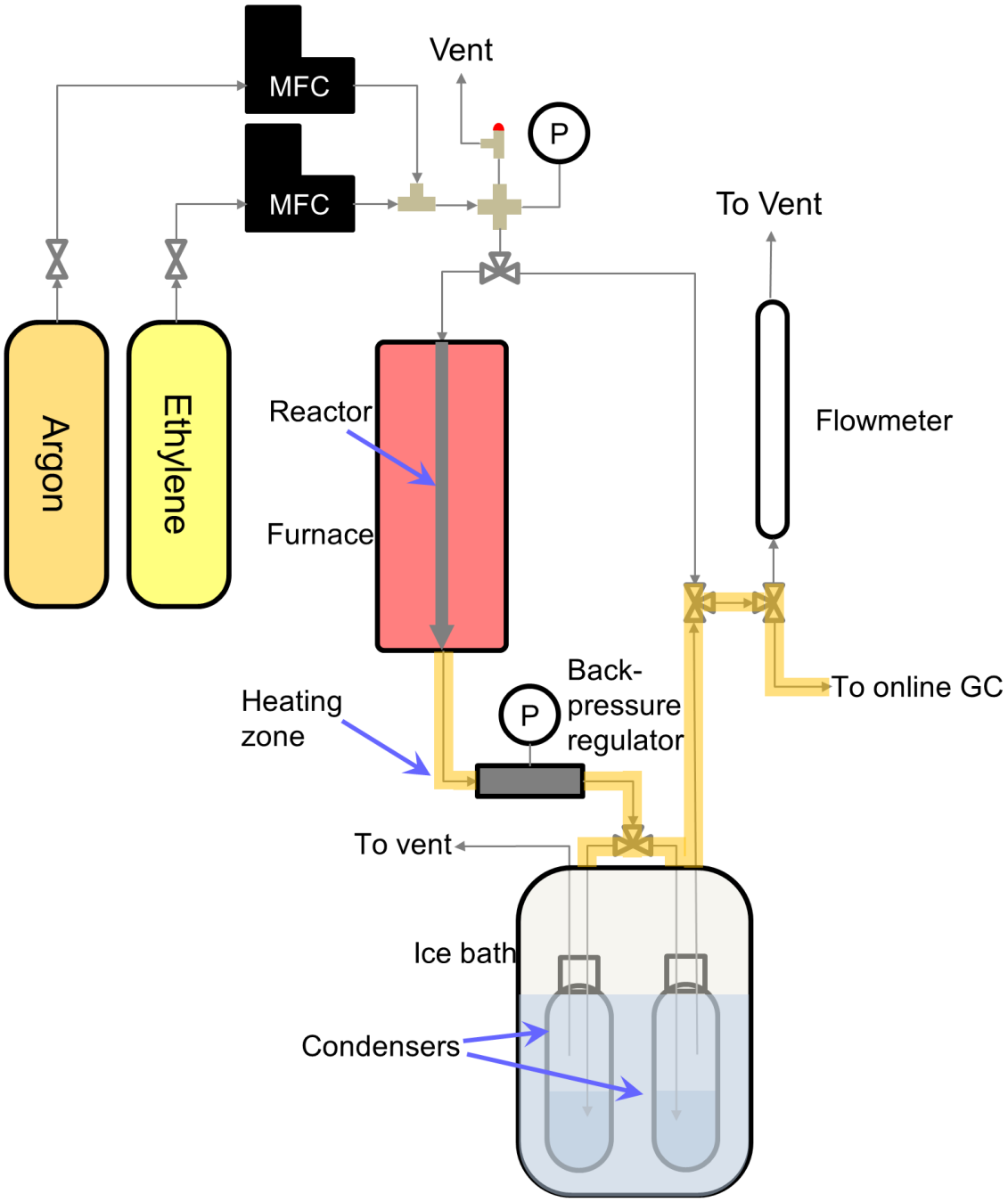

Figure S2.1 Process flow diagram of ethylene oligomerization reaction.

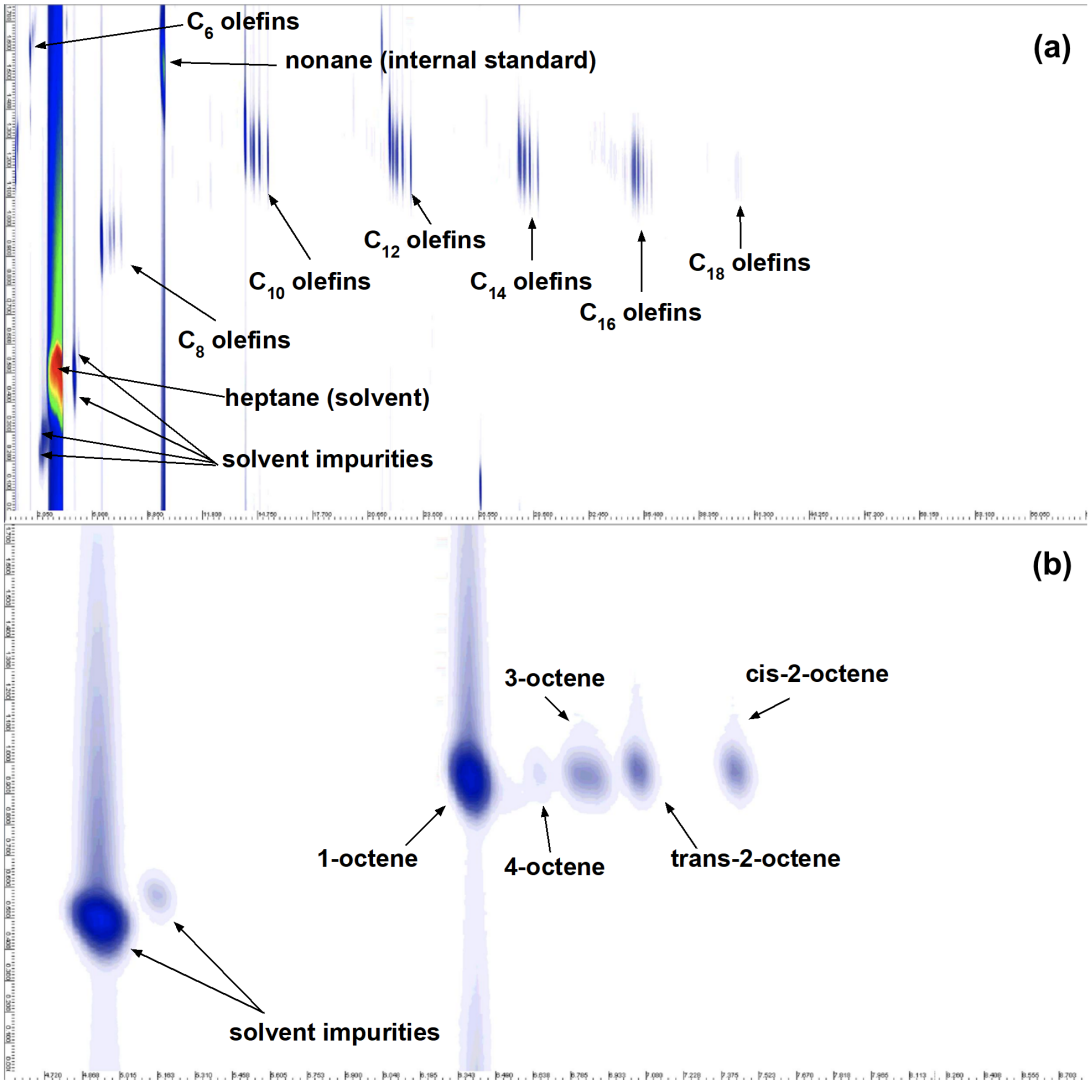

Figure S2.2 Representative 2D-GC-FID chromatograms from an ethylene oligomerization reaction at 200 °C, 16 bar ethylene, 16 bar argon, 12 wt% CoO_x/HTTC, and 0.72 h contact time. (a) Overall products. (b) C_8 olefin products.

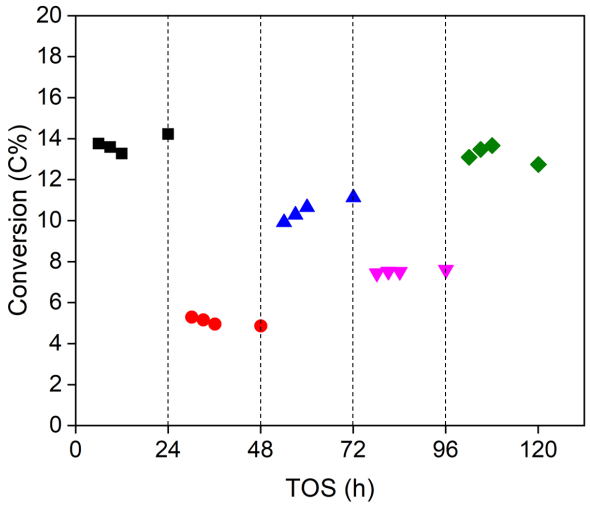

Figure S2.3 Ethylene conversion as a function of time on stream (TOS) at first 200 °C (black square), 140 °C (red circle), 180 °C (blue triangle), 160 °C (magenta upside-down triangle), and last 200 °C (green diamond). Reaction conditions: 16 bar ethylene, 16 bar argon, 12 wt% CoO_x/HTTC, and 1.45 h contact time.

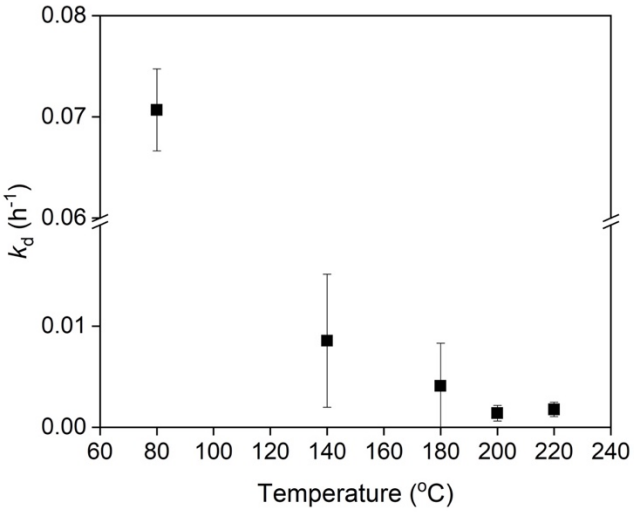

Figure S2.4 First order deactivation rate constant at different reaction temperatures during 24 h reactions. Reaction conditions: 16 bar ethylene, 16 bar argon, 12 wt% CoO_x/HTTC, and 0.18-1.45 h contact time. Bounds represent standard errors from the slopes of ln(Rate) versus time on stream (TOS) from the LINEST function in Excel. All conversions were below 20%.

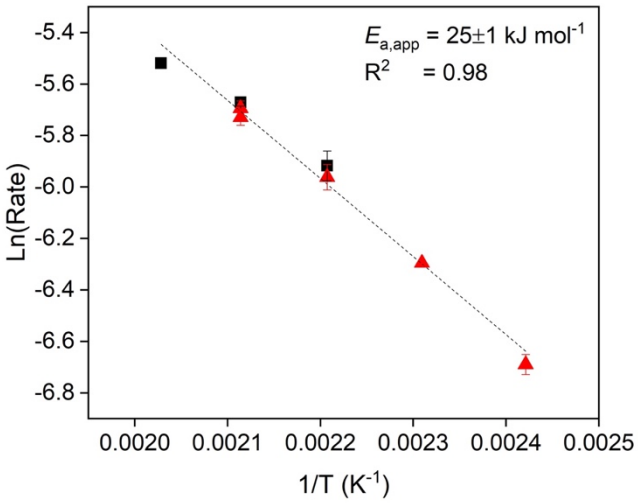

Figure S2.5 Ln(Rate) versus 1/T. Reactions with fresh catalysts at 180, 200, and 220 °C (black square) and sequential reactions at 200-140-180-160-200 °C (red triangle) with 24 h for each reaction temperature. Reaction conditions: 16 bar ethylene, 16 bar argon, 12 wt% CoO_x/HTTC, and 1.45 h contact time. Bounds represent standard deviations.

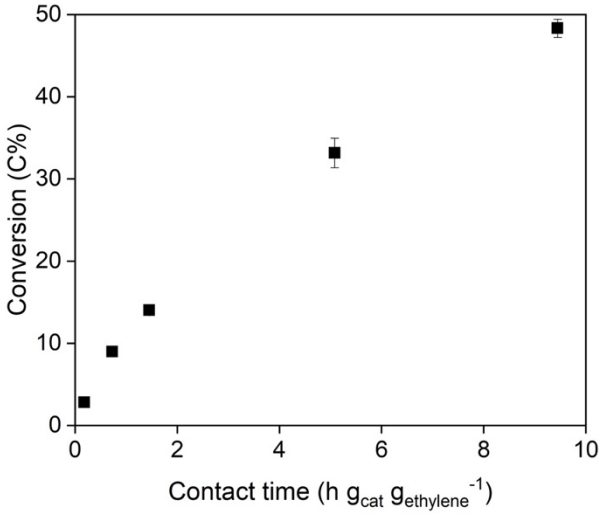

Figure S2.6 Conversion versus contact time. Reaction conditions: 200 °C, 16 bar ethylene, 16 bar argon, 12 wt% CoO_x/HTTC. Bounds represent standard deviations.

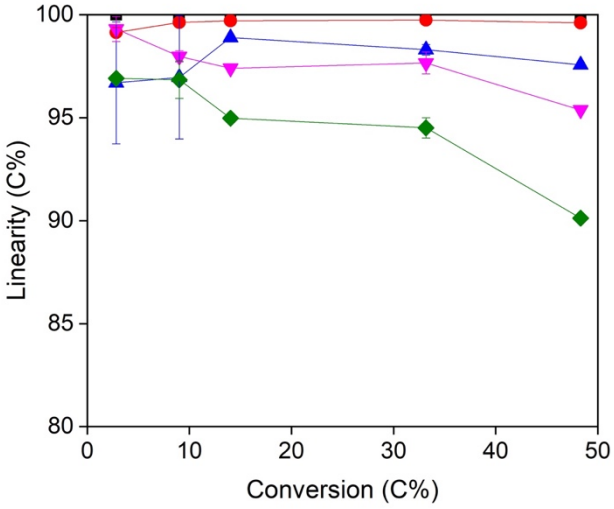

Figure S2.7 Product linearities versus conversion of C_4 (black square), C_6 (red circle), C_8 (blue triangle), C_{10} (magenta upside-down triangle), and C_{12} (green diamond) olefins. Reaction conditions: 200 °C, 16 bar ethylene, 16 bar argon, 12 wt% CoO_x/HTTC, and 0.18-9.45 h contact time. Bounds represent standard deviations.

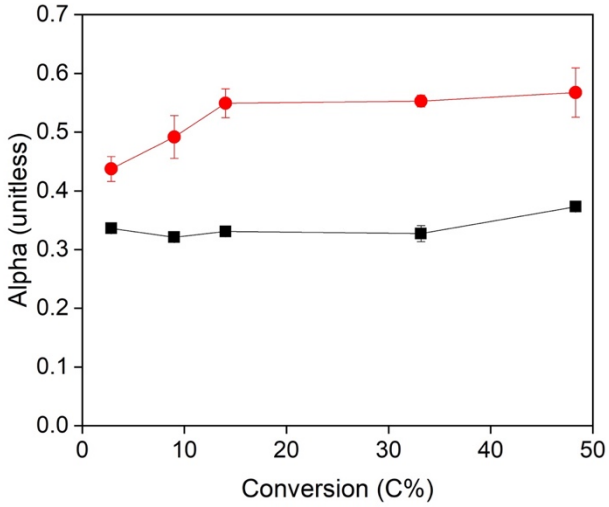

Figure S2.8 Chain growth probabilities from C_4 – C_{10} olefins (black square) and C_{10+} olefins (red circle) versus conversion. Reaction conditions: 200 °C, 16 bar ethylene, 16 bar argon, 12 wt% CoO_x/HTTC, and 0.18-9.45 h contact time. Bounds represent standard errors from the slopes of ln(Carbon selectivity / n) versus n from the LINEST function in Excel.

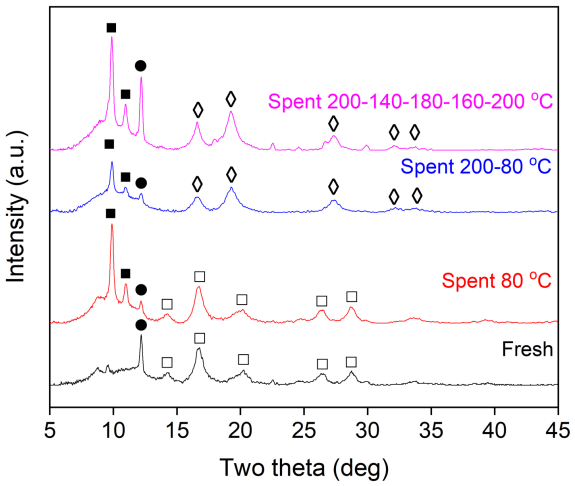

Figure S2.9 Mo-XRD patterns of fresh and spent catalysts with exposure to air. Characteristic peaks are carbon (graphite) - filled circle, polyethylene - filled square, Co_3O_4 - unfilled square, and CoO - unfilled diamond.

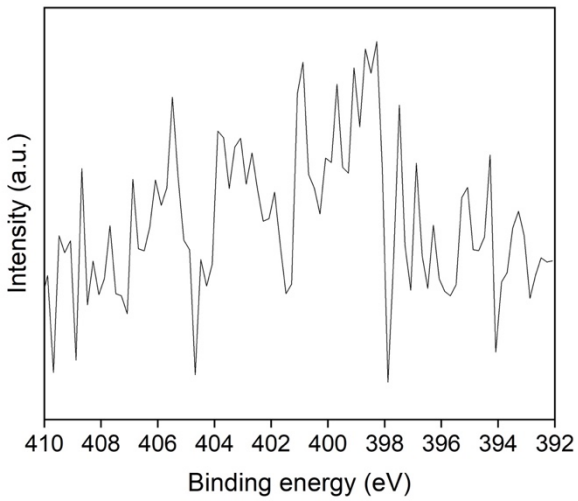

Figure S2.10 N 1s XPS region of fresh catalyst after pretreatment in argon at 230 °C.

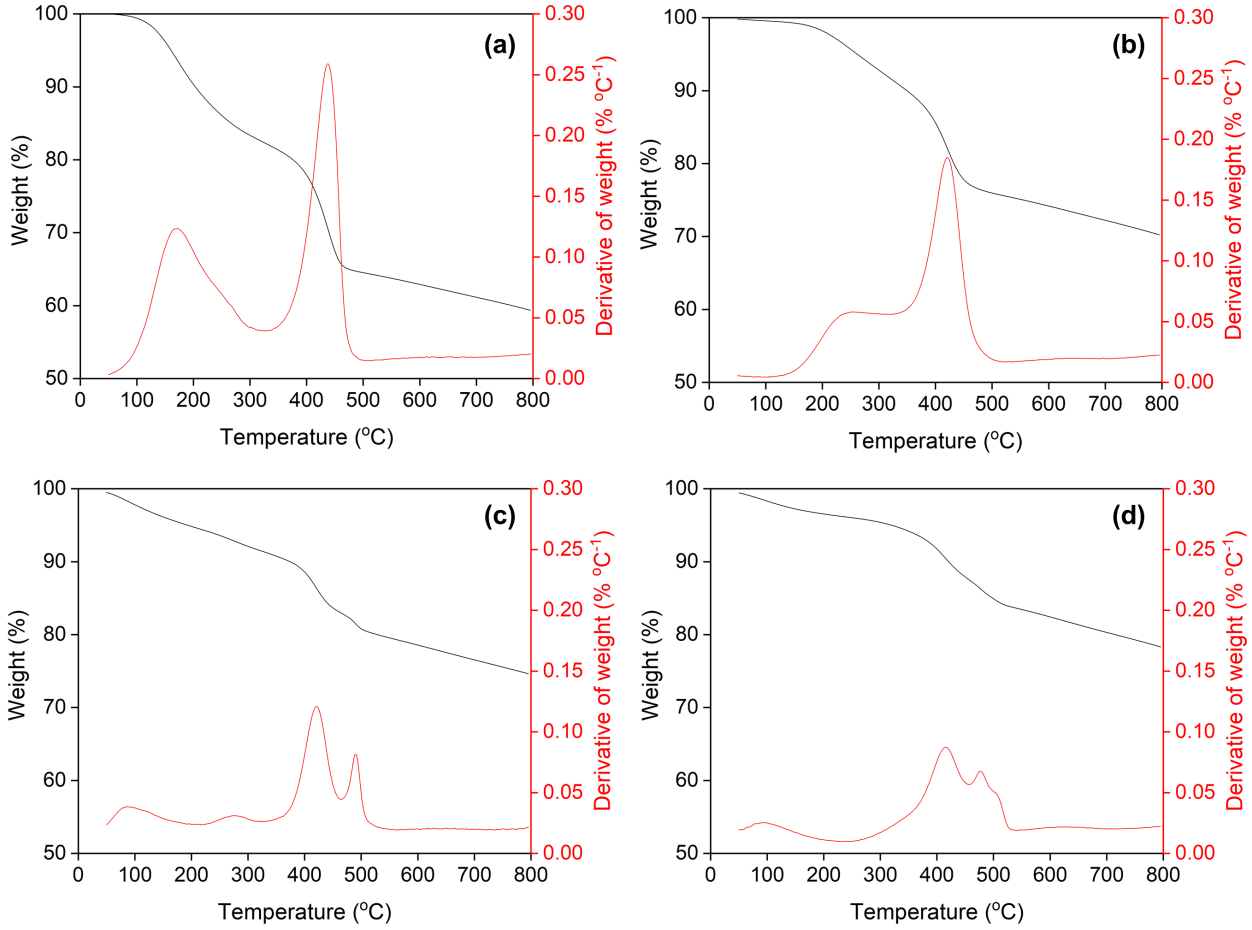

Figure S2.11 TGA curves of spent catalysts in N_2 before and after Soxhlet extractions. (a) Spent catalyst after a 24 h reaction at 80 °C before the Soxhlet extraction. (b) Spent catalyst after a 24 h reaction at 200 °C before the Soxhlet extraction. (c) Spent catalyst after a 24 h reaction at 80 °C after the Soxhlet extraction. (d) Spent catalyst after a 24 h reaction at 200 °C after the Soxhlet extraction. TGA conditions: 50 cm^3 (STP) min^{-1} of N_2, 10 °C min^{-1} ramp rate, and ~10 mg sample.

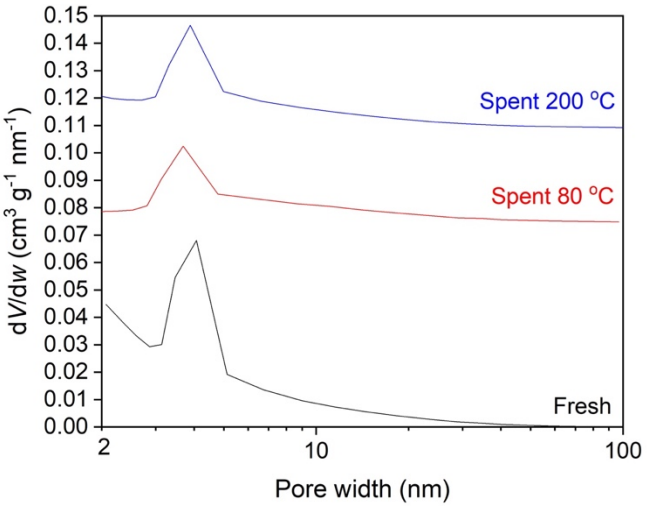

Figure S2.12 BJH pore size distributions of fresh catalyst after pretreatment in argon at 230 °C and spent catalysts after Soxhlet extractions.

Chapter 3. Reaction Kinetics Study of Ethylene Oligomerization into Linear Olefins over Carbon-Supported Cobalt Catalysts[2]

3.1 Introduction

The production of natural gas in the United States has been increasing since 2006 due to advancements in hydraulic fracturing technologies.[1,2] Steam cracking of the C_{2+} fraction of natural gas produces light C_2-C_4 olefins, which can be oligomerized for precursors of fuels (e.g., gasoline), into polymers, or into linear alpha olefins (LAOs).[3-7] Oligomerization of light olefins (e.g., propylene and butylenes) for gasoline applications was introduced in the 1930s using acid catalysts, following carbenium chemistry leading to highly branched hydrocarbons.[4,5] However, acid-catalyzed ethylene oligomerization does not typically occur until high temperature (>300 °C) with cracking also occurring at this temperature.[7,8] Ethylene, one of the most manufactured commodity chemicals, can be oligomerized at lower temperature (<200 °C) using transition metal catalysts to synthesize LAOs.[3,8] However, this process often involves homogeneous catalysts, activators, and solvents which typically requires further purification steps. Several heterogeneous transition metal catalysts, including nickel and cobalt catalysts, have been investigated as alternatives for olefin oligomerization into higher linear olefins in the absence of activators and/or solvents.[9-21] The highest product linearity of C_8 olefins reported for nickel catalysts is less than 60%.[15] However, this linearity was achieved at 5% 1-butene conversion, and increasing the conversion reduced the product linearity. Maintaining product linearity during the oligomerization process using heterogeneous catalysts without activators and/or solvents therefore remains a challenge. It is even more challenging to obtain linear alpha olefins (LAOs) which possess a higher

[2] This chapter is adapted from A. Jonathan, E. G. Tomashek, M. P. Lanci, J. A. Dumesic and G. W. Huber, Reaction kinetics study of ethylene oligomerization into linear olefins over carbon-supported cobalt catalysts, *J. Catal.*, 2021, DOI: https://doi.org/10.1016/j.jcat.2021.05.035.

value for use in polyethylene comonomers (C_4 - C_8), plasticizers (C_6 - C_{10}), lubricants (C_{10} - C_{12}), and detergents (C_{10} - C_{16}).[6,22]

Schultz et al. reported that olefin oligomerization reactions over ammoniated carbon-supported cobalt oxide catalysts (CoO_x/N-C) at 25 and 85 °C in batch reactors were highly selective to linear olefins.[16,18] Xu et al. further demonstrated that olefin oligomerization reactions over CoO_x/N-C were also highly selective to linear olefins at 80 °C in continuous flow reactors.[19,20,23] At 20% ethylene conversion and at the reaction temperature of 80 °C, the linearity of C_8 olefins was 77.6%, but only 5.2% was 1-octene.[20] Xu et al. suggested that both the catalyst activity for 1-butene oligomerization and the reducibility of the cobalt decreased with increasing pretreatment temperature (from 230 to 550 °C) in an inert atmosphere.[19] Xu et al. further claimed that the addition of Cr to the CoO_x/N-C (Cr-CoO_x/N-C) improved the catalyst activity and stability for ethylene oligomerization at the reaction temperature of 80 °C.[23] However, these data were collected in a regime where rapid catalyst deactivation occurred (at the reaction temperature of 80 °C) which disguised the activity and the stability of the catalysts. In addition, we have recently shown that a heterogeneous carbon-supported cobalt oxide catalyst without the addition of Cr and the ammonia treatment had a similar catalyst activity and deactivation rate to Cr-CoO_x/N-C for ethylene oligomerization.[21,23] This result suggests that the addition of Cr and ammonia to the cobalt oxide catalyst minimally impacted the activity and the stability for ethylene oligomerization.

We have recently demonstrated how to stabilize ethylene oligomerization over a carbon-supported cobalt oxide catalyst by performing the reaction at higher reaction temperature.[21] This catalyst is highly selective to linear olefins, including linear alpha olefins at the reaction temperature of 200 °C. The product linearities up to C_{12} olefins were above 90%, even at 48.3% ethylene conversion. The catalyst was also selective to linear alpha olefins (>60%) up to C_8 olefins

at low conversion (<20%). Based on these results, we have proposed a possible reaction scheme, shown in Figure 3.1, describing how linear alpha and linear internal olefins are produced. This reaction first involves an adsorption of ethylene. Another gaseous ethylene can react with the adsorbed ethylene or another growing oligomer by a chain growth step. The resulting oligomer can either desorb as a linear alpha olefin (LAO) or isomerize. Polyethylene formed in the catalyst pores may be one deactivation pathway. Catalyst characterizations without exposure to air showed that CoO is the cobalt phase when the catalyst is stable during oligomerization.

The key objective of this paper is to study the reaction kinetics of ethylene oligomerization over cobalt metal and cobalt oxide catalysts supported on carbon at 200 °C where deactivation is slower in the absence of Cr and the ammonia treatment. We will also show that cobalt metal supported on carbon is more active than cobalt oxide supported on carbon for ethylene oligomerization.

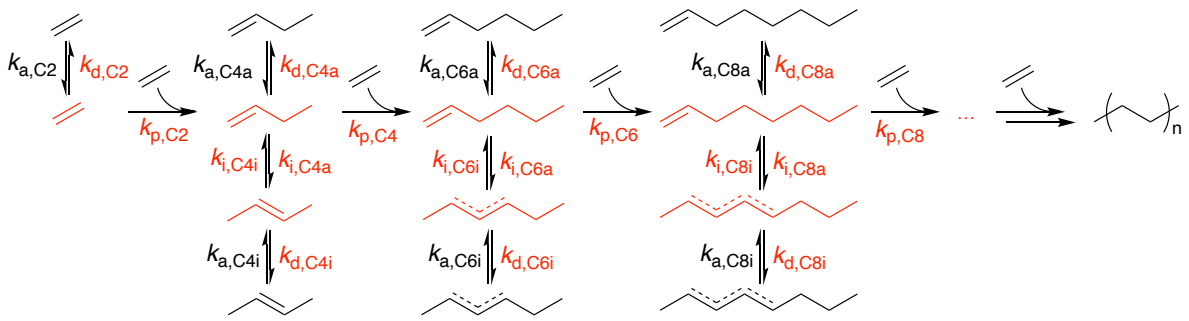

Figure 3.1 Reaction scheme for ethylene oligomerization over heterogeneous cobalt supported on carbon catalysts. The subscripts 'a', 'd', 'i', and 'p' in the rate constants, *k*, represent the adsorption, desorption, isomerization, and propagation rate constants, respectively. The letters 'a' and 'i' after the carbon number represent the double bond locations in the alpha and internal positions, respectively. Higher olefins may also react with C_{4+} alkyl chains forming internal olefins (not depicted). Species and reactions on the catalyst surface are labelled with red color. Figure is adapted from literature.[21]

3.2 Experimental Methods

3.2.1 Catalyst synthesis

The catalyst preparation method in this study was previously described in the literature.[21] Sieved activated carbon (Norit Darco MRX m-2278, 250-600 μm particle size, 600-800 m^2 g^{-1} BET surface area) was initially pretreated at 900 °C for 2 h under 100 cm^3 (STP) min^{-1} of helium at 10 °C min^{-1} ramp rate to make high-temperature-treated carbon (HTTC). After being cooled to room temperature, a solution composed of 1.89 g of $Co(NO_3)_2.6H_2O$ (Sigma Aldrich) and 1.22 g of deionized (DI) water was added to 2.0 g of the HTTC while being exposed to air to make an approximately 12 wt% cobalt nitrate on carbon catalyst. Finally, the catalyst was dried at 120 °C overnight.

3.2.2 Catalyst characterizations

Temperature-programmed desorption (TPD) experiments were performed using an AutoChem 2920 connected to a mass spectrometer (MS). Approximately 0.1 g of cobalt nitrate supported on carbon catalyst was used. The measurement was performed by heating the catalyst to 900 °C under 50 cm^3 (STP) min^{-1} of argon at 10 °C min^{-1} ramp rate, with the outlet stream being analyzed by the MS. The CO and CO_2 signals from the MS were converted to the corresponding molar concentrations using both CO and CO_2 calibration curves assuming an ideal gas law. The CO signal which originated from the CO_2 fragment (10% of CO_2 signal intensity) was subtracted from the total CO intensity.

Powder X-ray diffraction (XRD) experiments were performed using a Rigaku Rapid II diffractometer in the 2θ range of 2 to 45° with a Mo K_α source at 50 kV and 50 mA. The exposure time was set to 30 min. Prior to the XRD experiment, the catalyst was pretreated at 230 °C, 400

°C, or 560 °C for 2 h in argon at 1 °C min^{-1} ramp rate inside a reactor tube. After the pretreatment, both ends of the reactor tube were sealed with valves and the tube was transferred to a nitrogen-filled glove box. Inside the glove box, the catalyst was crushed into a powder and packed inside a glass capillary with one end sealed with glass and the other end with a vacuum grease (Apiezon H vacuum grease). The same procedure to prepare fresh samples for XRD without exposure to air was used to study spent catalysts after reactions at 200 °C with the catalysts pretreated at 230 °C, 400 °C, or 560 °C. The XRD patterns of standards were obtained from JADE 9 software. The XRD detection limit of supported nanoparticles is typically 2-2.5 nm.[24]

TGA experiments were carried out using a Thermal Analysis (TA) Instruments with Q500 system. For each experiment, approximately 10 mg of catalyst was heated to 800 °C at 10 °C min^{-1} ramp rate under 50 cm^3 (STP) min^{-1} of N_2.

3.2.3 Continuous flow reactions

Ethylene oligomerization reactions were performed in 30 cm (1 ft) downflow fixed bed reactors with an outer diameter of 0.64 cm (¼ in). The process flow diagram of these reactors is shown in the literature.[21] The ethylene and argon inlet flow rates in this study were varied from 20 to 160 cm^3 (STP) min^{-1} while maintaining the inlet concentration to be 50:50 by volume, except during the pressure effect study. The amount of catalyst was varied from 0.5 to 2.0 g. The contact time for each reaction is defined as the ratio of the mass of catalyst to the inlet mass flow rate of ethylene (h g_{cat} $g_{ethylene}^{-1}$). Prior to reaction studies, the catalyst was pretreated inside the reactor at 230 °C, 400 °C, or 560 °C in 100 cm^3 (STP) min^{-1} of argon for 2 h at 1 °C min^{-1} ramp rate. The catalyst was cooled to room temperature, pressurized to the desired reaction pressure using a back-pressure regulator (Equilibar), and reheated to the desired reaction temperature at 5 °C min^{-1} ramp

rate under argon, followed by a switch in feed. After the reactor and the back-pressure regulator, the stream was directed to a 120 mL condenser chilled in an ice bath to separate the relatively volatile species from the heavier species. These relatively volatile species were analyzed by an online gas chromatography with a flame ionization detector (online GC-FID, Shimadzu) approximately every 45 min. The condensed product was washed with approximately 10 g of heptane to ensure full collection and analyzed by a two-dimensional gas chromatography with a flame ionization detector (2D-GC-FID, Agilent) every 3 h.

The details of the product quantification method of each experiment were described in the literature.[21] In short, the online GC was able to detect C_2-C_{10} olefins while the 2D-GC was able to detect C_2-C_{24} olefins. The isomer distribution of C_4 olefins was quantified using the online GC, while the isomer distributions of C_{6+} olefins were quantified using the 2D-GC. Linear alpha olefin standards up to C_{24} were used to determine the retention times. GC peaks with longer retention times than the corresponding linear alpha olefin were assumed to be linear internal olefins. GC peaks with shorter retention times than the corresponding linear alpha olefin were assumed to be branched olefins. These assumptions were made based on the trend observed from C_4 to C_8 olefins. The isomer distributions of C_{14+} olefins were not quantified due to overlapping GC peaks. The average carbon balance for each experiment was above 95%, unless otherwise noted.

Equations 3.1 through 3.6 show how parameters in the manuscript are defined:

$$\text{Ethylene conversion: Conversion (C\%)} = \frac{\sum_{i=4}^{n}(i \times F_{\mathrm{C}_{i,\mathrm{out}}})}{2 \times F_{\mathrm{C}_{2,\mathrm{in}}}} \times 100 \tag{3.1}$$

$$\text{LAO isomer distribution: LAO of } \mathrm{C}_i \text{ (C\%)} = \frac{F_{\mathrm{C}_{i,\text{linear alpha,out}}}}{F_{\mathrm{C}_{i,\mathrm{out}}}} \times 100 \tag{3.2}$$

$$\text{Product linearity: Linearity of } \mathrm{C}_i \text{ (C\%)} = \frac{F_{\mathrm{C}_{i,\text{linear alpha,out}}} + F_{\mathrm{C}_{i,\text{linear internal,out}}}}{F_{\mathrm{C}_{i,\mathrm{out}}}} \times 100 \tag{3.3}$$

Product selectivity: Selectivity to C_i (C%) $= \frac{i \times F_{C_{i,\text{out}}}}{\sum_{i=4}^{n} i \times F_{C_{i,\text{out}}}} \times 100$ (3.4)

Ethylene consumption rate: Rate ($\text{mol}_{\text{ethylene}}\ g_{\text{cat}}^{-1}\ h^{-1}$) $= \frac{F_{C_{2,\text{in}}} \times \text{conversion}}{\text{mass of catalyst}}$ (3.5)

Carbon balance: Carbon balance (C%) $= \frac{\sum_{i=2}^{n}(i \times F_{C_{i,\text{out}}})}{2 \times F_{C_{2,\text{in}}}} \times 100$ (3.6)

where F is the molar flow rate in mol h^{-1} and C_i represents all olefins of a specific structure (linear, linear alpha, or total) containing i carbon atoms.

3.2.4 Transport limitation analysis

The Weisz-Prater criterion, shown in Equation 3.7, was used to test whether the ethylene oligomerization is kinetically limited, where Rate is the ethylene consumption rate per unit volume of catalyst, C_s is the ethylene surface concentration, R_p is the particle radius, D_{eff} is the ethylene effective diffusivity, and X is 0.6 for a 1st order reaction and 0.3 for a 2nd order reaction.[25] The calculation of each parameter along with the approximation are shown in the Supplementary Information. The calculated Rate, C_s, R_p, and D_{eff} are 2.96 x 10^{-5} mol cm^{-3} s^{-1}, 4.07 x 10^{-4} mol cm^{-3}, 3 x 10^{-2} cm, and 7.97 x 10^{-3} cm^2 s^{-1}, respectively, giving the result of the criterion to be 0.0082. This value is less than 0.6 (we will show that ethylene oligomerization over a cobalt supported on carbon catalyst has a first order dependence with ethylene partial pressure), thus the rate of ethylene oligomerization measured in this paper is in a kinetically-limited regime. The Weisz-Prater criterion in this study is valid at the beginning of the reaction when less polyethylene and other higher olefins were present on the catalyst. As time on stream (TOS) increases, the rate decreases due to deactivation and the diffusivity also decreases due to the presence of higher olefins and polyethylene, which makes it difficult to assess whether the condition is still satisfied.

$$\frac{\text{Rate}\times {R_\text{p}}^2}{C_\text{s}\times D_\text{eff}} \leq X \quad (3.7)$$

3.3 Results and Discussion

3.3.1 Effect of pretreatment temperature and contact time

Figure 3.2 shows the desorptions of CO and CO_2 from the temperature-programmed desorption (TPD) experiment of the cobalt nitrate supported on carbon catalyst under argon. Two CO_2 peaks were observed, one at 225 °C and the other one at 563 °C. A CO peak at 579 °C was also observed. Xu et al. have previously used X-ray diffraction (XRD), X-ray absorption spectroscopy (XAS), and Raman spectroscopy to show that the reduction of Co_3O_4 to CoO and the removal of the nitrate occur at around the temperature evidenced for the first CO_2 peak, and Co metal is formed as a major phase around the temperature evidenced for the second CO_2 peak.[19] The total amount of CO_2 that was desorbed is similar in value (2.4 mmol g_{cat}^{-1}) to the total amount of cobalt (2.0 mmol g_{cat}^{-1}) that was present on the catalyst, shown in Table S3.1, further demonstrating that the majority of the CoO was reduced to Co metal. The exact quantification may be complicated because oxygen might also come from the carbon support, the nitrate precursor, and water. The carbon forming CO_2 and CO likely comes from the catalyst support.

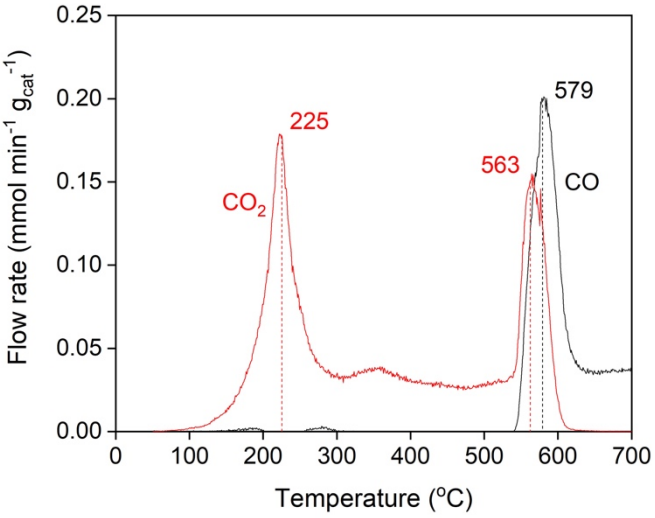

Figure 3.2 Temperature-programmed desorption (TPD) of 0.1 g of 12 wt% cobalt nitrate supported on high temperature treated carbon catalyst in 50 cm^3 (STP) min^{-1} of argon at 10 °C min^{-1} ramp rate. CO and CO_2 are shown in black and red colors, respectively.

We measured the activity of the catalysts for ethylene oligomerization at 200 °C after pretreatment in argon at 230 °C (PT230C), 400 °C (PT400C) and 560 °C (PT560C), as shown in Figure 3.3. Data points before 6 h time on stream (TOS) were excluded due to system transients. Figure 3.3 shows that the PT230C catalyst was stable during a 24 h reaction with an average conversion of 13.7%. The PT560C catalyst, on the other hand, had an initial conversion of 68.6%, but the catalyst deactivated to 32.3% conversion at 24 h TOS and to 23.1% conversion at 36 h TOS. The total pressure for the PT560C catalyst increased from 32 to 40 bar from 36 to 48 h TOS due to clogging from polyethylene. The PT400C catalyst had an initial conversion of 71.1%, but the catalyst deactivated to 47.2% conversion at 24 h TOS. This catalyst had the characteristics of both PT230C and PT560C catalysts because it was more active than the PT230C catalyst and more stable than the PT560C catalyst. The average carbon balances from the PT230C, PT400C, and PT560C catalysts were 99.2%, 96.4%, and 89.6%, respectively, suggesting the PT560C catalyst

produced the most polyethylene. These results also suggest that the conversion from the PT560C catalyst should have been higher due to the missing carbon balance.

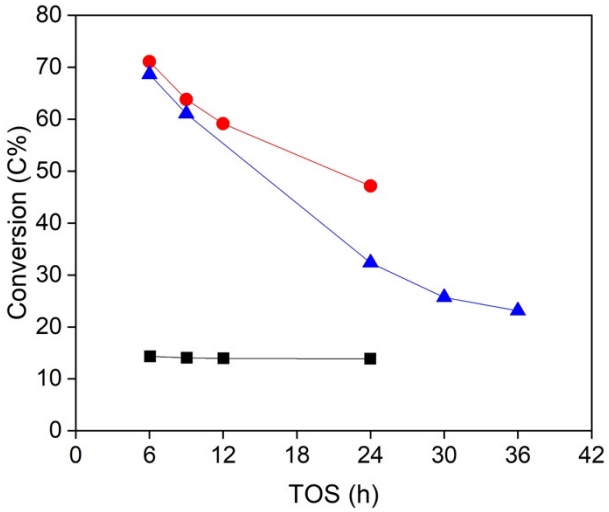

Figure 3.3 Ethylene conversions as a function of time on stream (TOS) with the catalysts pretreated at 230 °C (PT230C – black square), 400 °C (PT400C – red circle), and 560 °C (PT560C – blue triangle) in argon. Reaction conditions: 200 °C, 16 bar ethylene, 16 bar argon, 12 wt% cobalt supported on high temperature treated carbon catalysts, and 1.45 h contact time. Data points from the PT230C catalyst are from literature.[21]

The fresh and the spent catalysts were analyzed by X-ray diffraction (XRD) without exposure to air, as shown in Figure 3.4. The fresh PT230C catalyst was comprised mainly of Co_3O_4 whereas the spent PT230C catalyst showed CoO, suggesting that Co_3O_4 had been reduced to a more stable CoO cobalt phase during oligomerization. This result is consistent with XPS results without exposure to air.[21] The reduction of Co_3O_4 to CoO during the reaction also suggests that there is a time evolution of the cobalt species. On the other hand, the fresh and the spent PT560C catalysts showed the reflection characteristic of cobalt metal, demonstrating that cobalt metal is

even more active than CoO with an initial conversion higher by a factor of five. Both fresh and spent PT400C catalysts, however, only showed the reflection characteristic of CoO although the PT400C catalyst was more active than the PT230C catalyst and more stable than the PT560C catalyst. These catalysts likely contained small (<2.5 nm) Co metal nanoparticles which were below the detection limit of the XRD instrument. All spent PT230C, PT400C, and PT560C catalysts showed the reflection characteristic of polyethylene, suggesting polyethylene was present with relatively high crystallinity. The quantification of each cobalt phase from different pretreatment temperatures will be beneficial, especially for the catalysts pretreated at 230 and 400 °C. It is difficult to quantify each cobalt phase using XPS due to similar Co XPS peaks from different cobalt phases.[23,26,27] For example, Wang et al. assigned a peak at 781.5 eV to Co^{2+}, however, both Co_3O_4 (Co^{3+} and Co^{2+}) and CoO (Co^{2+}) have almost identical peaks around this value.[27] In addition, Wang et al. also assigned a peak near 795 eV to Co^0, however, Gu et al. showed that CoO has a major peak near 795 eV, which makes it difficult to quantify different cobalt phases.[26,27] A possible way to quantify these cobalt phases is through a linear combination fitting from *in-situ* XAS experiments.

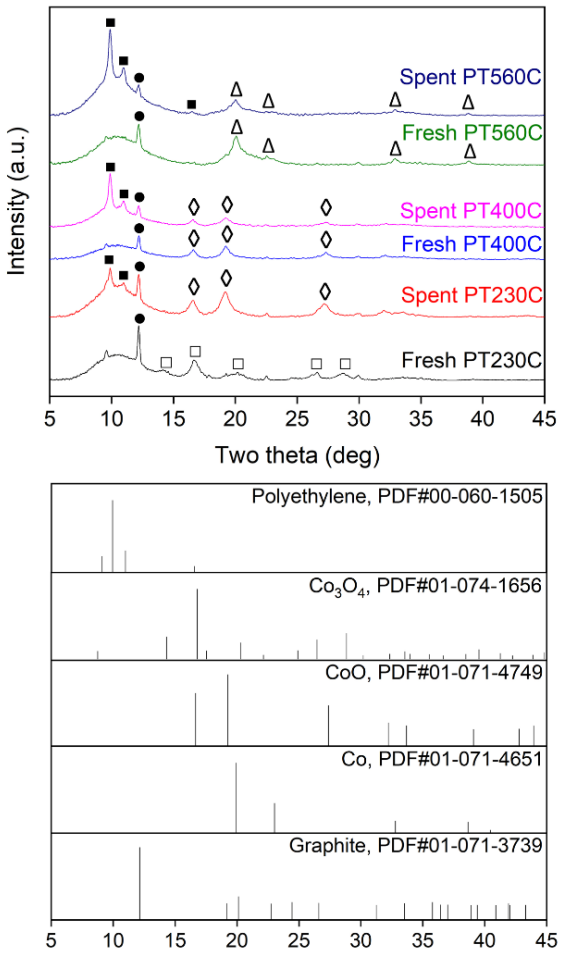

Figure 3.4 Mo X-ray diffraction (XRD) patterns of fresh catalysts after pretreatment in argon at 230 °C (Fresh PT230C), 400 °C (Fresh PT400C), and 560 °C (Fresh PT560C), and spent catalysts after reactions at 200 °C with pretreatment temperatures at 230 °C (Spent PT230C), 400 °C (Spent PT400C), and 560 °C (Spent PT560C) in argon. Characteristic peaks are carbon (graphite) - filled circle, polyethylene - filled square, Co_3O_4 - unfilled square, CoO - unfilled diamond, and Co metal - unfilled triangle. Data from Fresh PT230C and Spent PT230C catalysts along with the standard patterns are from literature.[21]

We performed thermogravimetric analysis (TGA) under N_2 of the spent PT230C, spent 400C, and spent PT560C catalysts after reactions at 200 °C and 24 h TOS, shown in Figure 3.5. Zhao et al. reported that decomposition of polyethylene showed a characteristic peak near 450 °C

with the same heating rate and system used here.[28] Assuming that polyethylene is the weight loss from 400 to 500 °C, Figure 3.5 shows approximately 10 wt% of the spent PT230C catalyst, 40 wt% of the spent PT400C catalyst, and 50 wt% of the spent PT560C catalyst were polyethylene. This result is consistent with the fact that more polyethylene is formed with the more active catalyst and the formation of polyethylene likely causes the catalyst to deactivate. The TGA curves of other spent catalysts in this study (Figure S3.1) show some variations in the amount of polyethylene, suggesting non-uniform polyethylene formation throughout the catalyst bed.

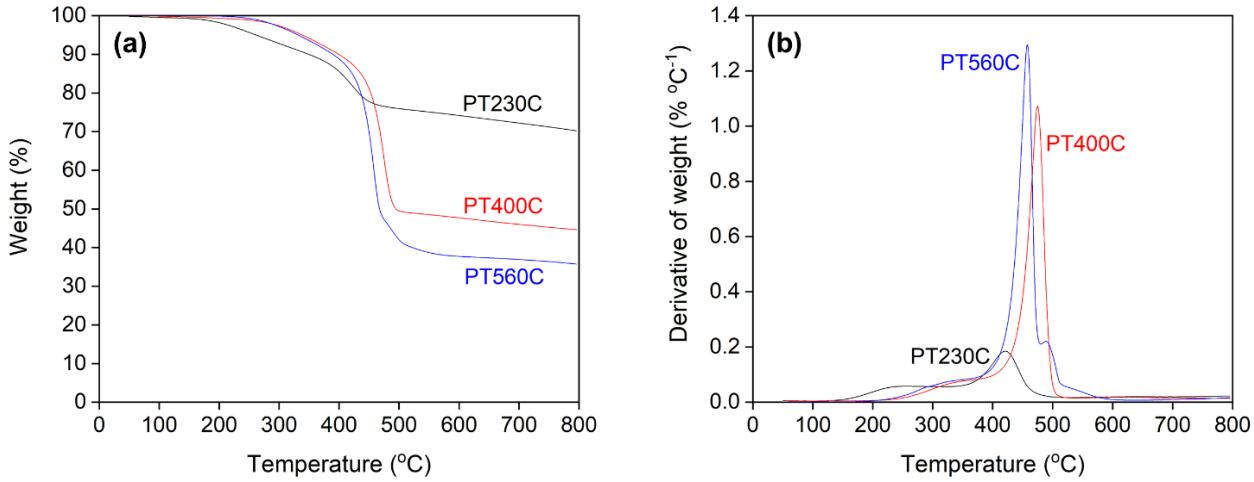

Figure 3.5 Thermogravimetric analysis (TGA) under N_2 of the spent 12 wt% PT230C catalyst after a 24 h reaction at 200 °C, 16 bar ethylene, 16 bar argon, and 1.45 h contact time, the spent 12 wt% PT400C catalyst after a 24 h reaction at 200 °C, 16 bar ethylene, 16 bar argon, and 1.45 h contact time, and the spent 12 wt% PT560C catalyst after a 24 h reaction at 200 °C, 16 bar ethylene, 16 bar argon, and 0.36 h contact time. (a) Weight percent versus temperature. (b) Derivative of weight percent versus temperature. TGA conditions: 50 cm^3 (STP) min^{-1} of N_2, 10 °C min^{-1} ramp rate, and ~10 mg sample. Data from the PT230C catalyst are from literature.[21]

Reactions with the PT560C catalyst (cobalt metal supported on carbon catalyst) were performed at different contact times, as shown in Figure 3.6. Figure 3.6 shows that the PT560C

catalyst deactivated at all of the contact times. A plot of ln(Rate) versus time on stream (TOS) was used to calculate the deactivation rate constant (k_d) (Figure S3.2) where the slope is the negative of the first order deactivation rate constant. The plot of k_d versus contact time (Figure 3.7) shows that there is no trend of k_d at different contact times.

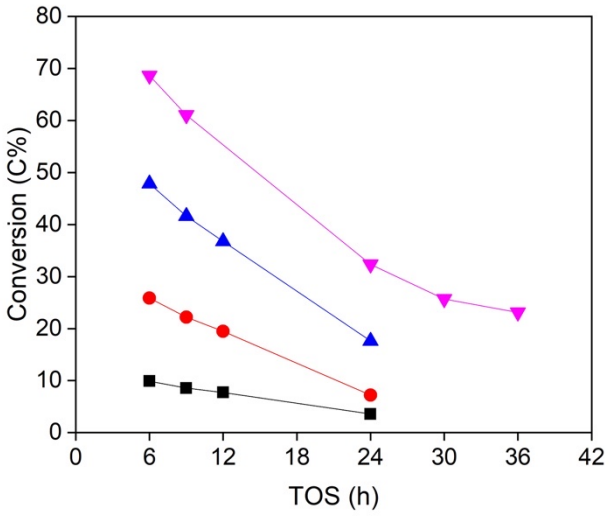

Figure 3.6 Ethylene conversions as a function of time on stream (TOS) at 0.18 h (black square), 0.36 h (red circle), 0.72 h (blue triangle), and 1.45 h (magenta upside-down triangle) contact times. Reaction conditions: 200 °C, 16 bar ethylene, 16 bar argon, and 12 wt% PT560C catalysts.

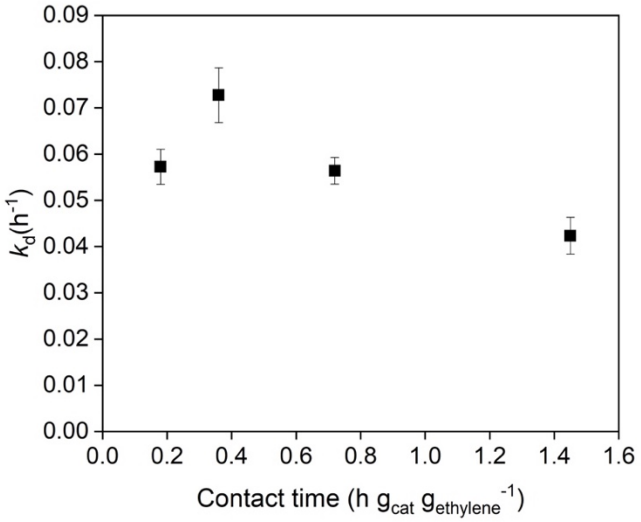

Figure 3.7 First order deactivation rate constant (k_d) versus contact time. Reaction conditions: 200 °C, 16 bar ethylene, 16 bar argon, and 12 wt% PT560C catalysts. Bounds represent standard errors from the slopes of ln(Rate) versus time on stream (TOS) from the LINEST function in Excel.

Figure 3.8 shows the LAO isomer distributions up to C_{12} olefins from the PT560C catalyst at two different times on stream (6 h and 24 h in Figures 3.8a and b, respectively). Isomer distributions of C_{14+} olefins were not quantified because of the overlapping GC peaks. Figure 3.8a shows that the LAO distribution decreases with increasing conversion and increased carbon number. This trend is not as prevalent on the data from the 24 h point (Figure 3.8b) likely due to catalyst deactivation. At higher conversion, which is analogous to higher contact time, the LAO products can be re-adsorbed on the catalyst and isomerize to produce linear internal olefins. Further propagations of linear internal olefins will make branched olefins. As the catalyst deactivates, there are fewer active sites resulting in the decrease in conversion. However, there is also more polyethylene which may decrease the rate of product diffusion thereby increasing the probability of the alpha olefins to isomerize to internal olefins.

The PT560C catalyst is less selective to LAOs than the PT230C catalyst. For example, the LAO isomer distributions up to C_8 olefins for the PT560C catalyst were above 30% at <10% ethylene conversion, whereas they were above 60% at <20% ethylene conversion for the PT230C catalyst.[21] This behavior is likely due to more polyethylene being present in the PT560C catalyst which slowed the diffusion of olefin products out of the catalyst pores and led to further isomerization. The LAO isomer distributions of the PT560C catalyst and PT400C catalyst (Figure S3.3) were similar. For example, at 68-72% conversions and 6 h TOS, the LAO isomer distributions of C_8 olefins from the PT560C and PT400C catalysts were 5.1% and 4.4%, respectively.

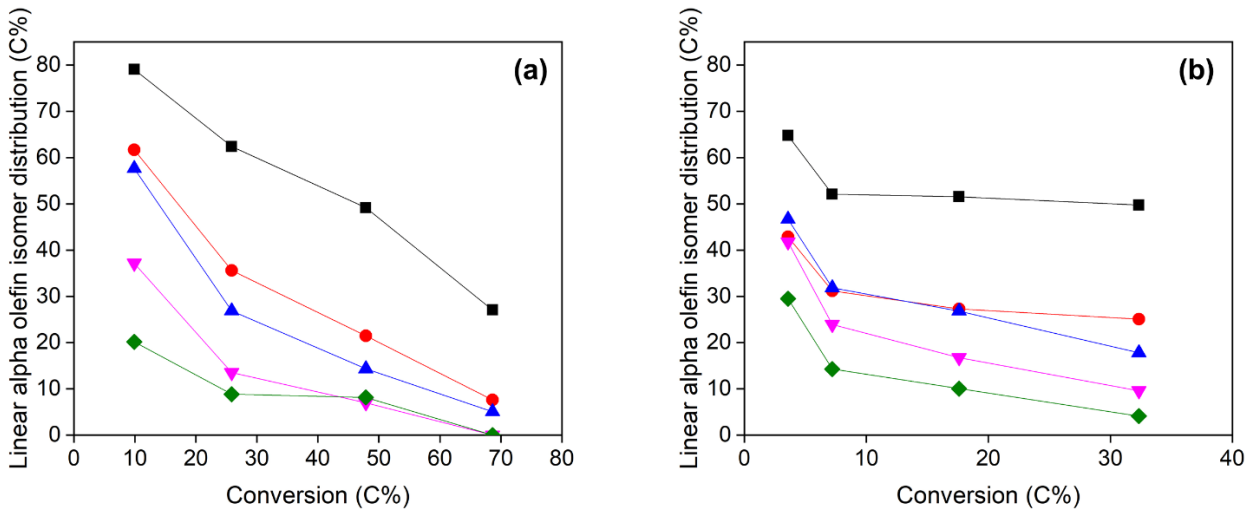

Figure 3.8 Linear alpha olefin (LAO) isomer distributions among C_4 (black square), C_6 (red circle), C_8 (blue triangle), C_{10} (magenta upside-down triangle), and C_{12} (green diamond) olefins versus ethylene conversion at (a) 6 h TOS and (b) 24 h TOS. Reaction conditions: 200 °C, 16 bar ethylene, 16 bar argon, 12 wt% PT560C catalysts, and 0.18-1.45 h contact time. Data points from different conversions are from different contact times.

Figures 3.9a and b show the product linearities from the PT560C catalyst up to C_{12} olefins at 6 h and 24 h TOS, respectively. The PT560C catalyst is selective to linear olefins since the product linearities up to C_{12} olefins were above 60%, even at 68.6% conversion. However, the PT560C catalyst has a lower selectivity to linear olefins than the PT230C catalyst. For example, at similar conversions (~ 48%), the C_4-C_{12} product linearities were above 80% and 90% for the PT560C and PT230C catalysts, respectively.[21] The product linearity decreased with increasing conversion and olefin molecular weight. However, the product linearities from 6 h and 24 h TOS were similar at similar conversions, further demonstrating that the polyethylene formation promotes a change in the diffusion resonance time, thus indirectly changes contact time for the products, leading to a higher apparent k_{ads} for an equivalent k_{des} for any individual species. The product linearities of the PT560C catalyst and PT400C catalyst (Figure S3.4) were similar. For instance, at similar 68-72% conversions and 6 h TOS, the product linearities of C_8 olefins from the PT560C and PT400C catalysts were 90.1% and 88.8%, respectively.

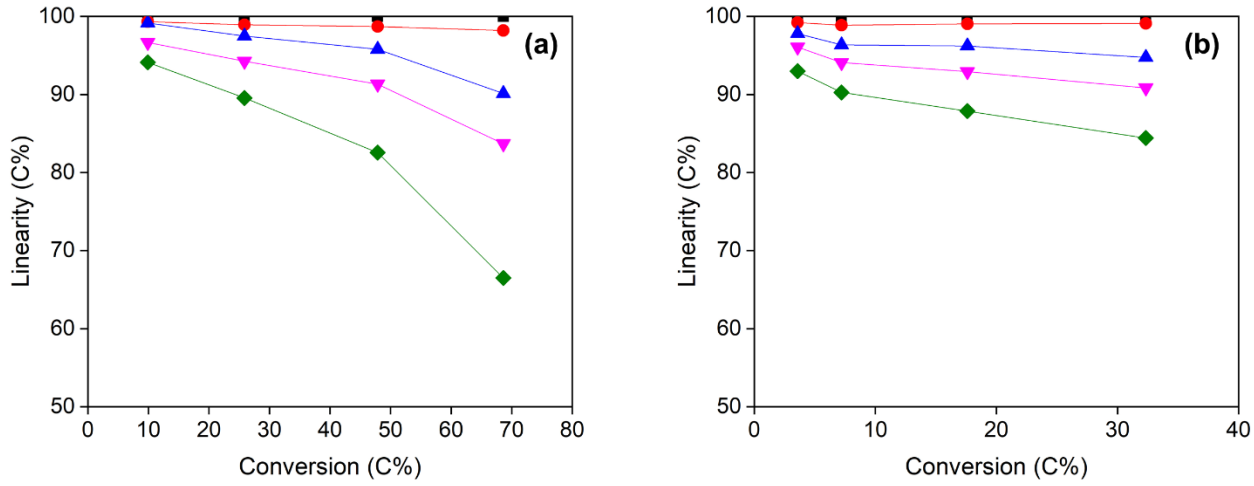

Figure 3.9 Product linearities of C_4 (black square), C_6 (red circle), C_8 (blue triangle), C_{10} (magenta upside-down triangle), and C_{12} (green diamond) olefins versus ethylene conversion at (a) 6 h TOS and (b) 24 h TOS. Reaction conditions: 200 °C, 16 bar ethylene, 16 bar argon, 12 wt% PT560C catalysts, and 0.18-1.45 h contact time. Data points from different conversions are from different contact times.

The product selectivities to different chain length olefins at 6 h and 24 h TOS from the PT560C catalyst are plotted versus ethylene conversion in Figures 3.10a and b, respectively. At 6 h TOS (Figure 3.10a), the selectivities to C_4, C_6, C_8, C_{10}, and C_{12+} olefins were relatively constant around 64%, 20%, 9%, 5%, and 4%, respectively, from 9.9% to 68.6% conversions. These selectivities were similar to the selectivities with the PT400C catalyst at 71.1% conversion (Figure S3.5). The selectivities to C_4, C_6, C_8, C_{10}, and C_{12+} olefins at 24 h TOS (Figure 3.10b) with the PT560C catalyst were also relatively constant around 51%, 21%, 11%, 9%, and 8%, respectively, from 3.6% to 32.3% conversions. We have previously observed the trend of approximately constant selectivities to C_4, C_6, C_8, C_{10}, and C_{12+} olefins around 55%, 22%, 10%, 5%, and 8%, respectively from 2.8% to 48.3% conversions and 0.18 to 9.45 h contact times with the cobalt oxide supported on carbon catalyst (PT230C catalyst).[21] This comparison indicates, at the reaction

conditions of this paper, the rate of propagation is relatively the same as the rate of termination (see Figure 3.1). The selectivity to higher olefins increased with increasing time on stream because the higher olefins took longer to diffuse out of the catalyst pores and the higher amount of polyethylene at longer time on stream further caused a bigger discrepancy between the diffusion rate of lighter and heavier olefins.

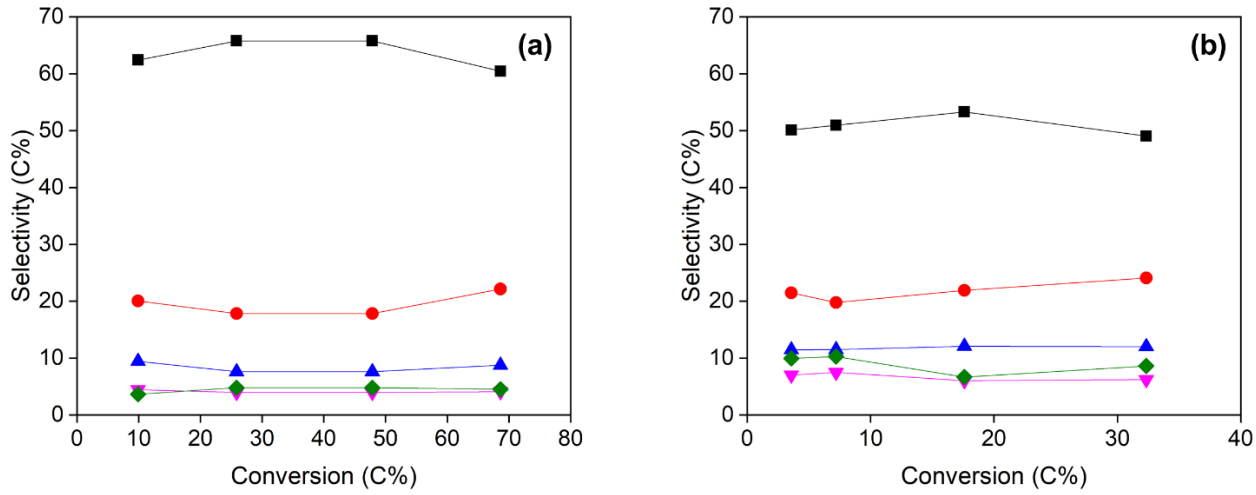

Figure 3.10 Product selectivities to C_4 (black square), C_6 (red circle), C_8 (blue triangle), C_{10} (magenta upside-down triangle), and C_{12+} (green diamond) olefins versus ethylene conversion at (a) 6 h TOS and (b) 24 h TOS. Reaction conditions: 200 °C, 16 bar ethylene, 16 bar argon, 12 wt% PT560C catalysts, and 0.18-1.45 h contact time. Data points from different conversions are from different contact times.

We have previously shown that ethylene oligomerization over a cobalt oxide supported on carbon catalyst followed a Schulz-Flory distribution with two different slopes (from C_4 to C_{10} olefins and C_{10+} olefins), where the change of the slope always occurred at C_{10} olefins (or $n = 5$ where n is the repeat unit).[21] Iglesia, Bell, and co-workers also observed two different slopes in the Schulz-Flory product distributions for CO hydrogenation with Fischer Tropsch synthesis

catalysts.[29-31] Iglesia and co-workers proposed that the intrapellet diffusion limitation of higher olefins caused the slope to change.[30] As shown in Figure 3.11, the products from ethylene oligomerization over a cobalt metal supported on carbon catalyst also follow a Schulz-Flory distribution with the change of the slope occurring at C_{10} olefins (or n = 5). The R^2 values with two different slopes were 0.997 and 0.999 whereas the R^2 value with a single slope was only 0.987, suggesting the two different slopes better fit the data. In addition, the values of two different slopes were -0.43 ± 0.02 and -0.28 ± 0.01 whereas the value of a single slope was -0.35 ± 0.02, which is out of the bound from the two slopes. Here, the bounds are defined as the standard errors. These results indicate that C_{10} and C_{12+} olefins are more influenced by the transport restrictions.

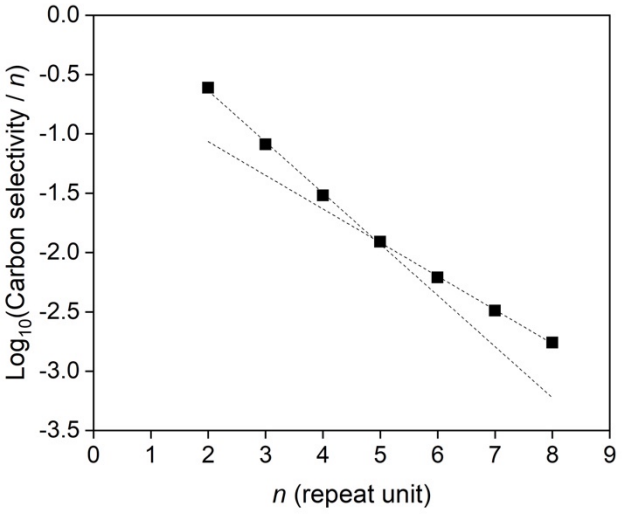

Figure 3.11 A typical product distribution for ethylene oligomerization over a PT560C catalyst as a function of repeat unit (n). Reaction conditions: 200 °C, 16 bar ethylene, 16 bar argon, 12 wt% PT560C catalyst, 1.45 h contact time, 24 h TOS, and 32.3% conversion.

The slope in the Schulz-Flory distribution is $\log_{10}(\alpha)$ where α is the chain growth probability. Because two different slopes were observed, one for C_4-C_{10} olefins and the other one for C_{10+} olefins, two different α values were calculated for each contact time and plotted versus conversion at 6 h (Figure 12a) and 24 h TOS (Figure 12b). Similar to the selectivity plots, the α values were relatively constant at different conversions. Comparing the α values at 6 and 24 h TOS, the average α value from C_4 to C_{10} olefins increased from 0.29 to 0.37 whereas the average α value from C_{10+} olefins increased from 0.44 to 0.51. For the ethylene oligomerization over cobalt oxide supported on carbon, the α value from C_4 to C_{10} olefins was relatively constant at 0.33 whereas the α value from C_{10+} olefins increased from 0.44 to 0.57 from 2.8% to 48.3% conversions.[21]

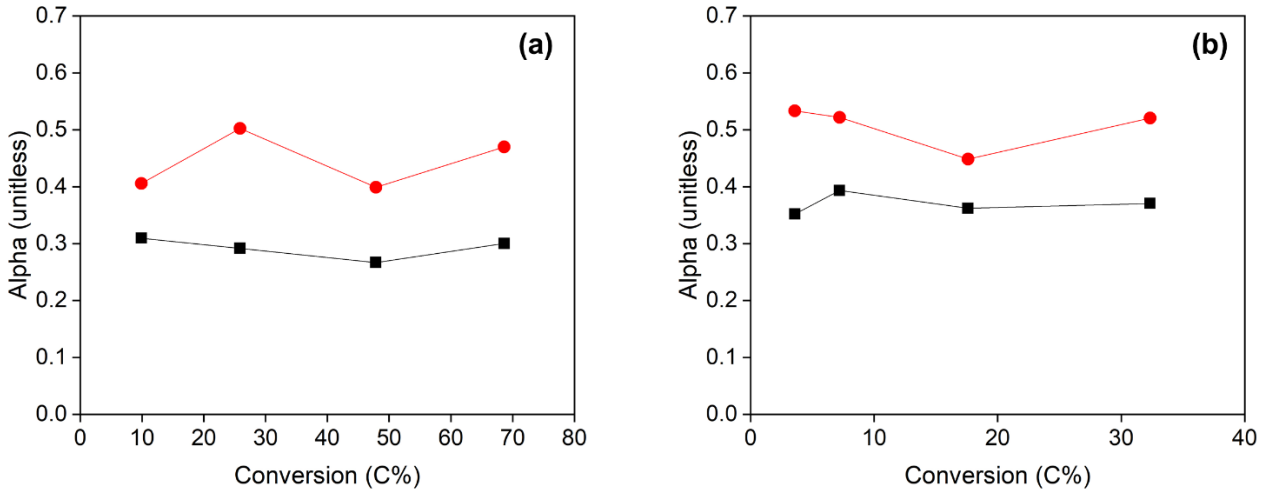

Figure 3.12 Chain growth probabilities of C_4-C_{10} olefins (black square) and C_{10+} olefins (red circle) versus ethylene conversion at (a) 6 h TOS and (b) 24 h TOS. Reaction conditions: 200 °C, 16 bar ethylene, 16 bar argon, 12 wt% PT560C catalysts, and 0.18-1.45 h contact time. Data points from different conversions are from different contact times.

3.3.2 Effect of reaction pressure

We investigated the effect of reaction pressure towards the catalyst stability, the product selectivity, and the product linearity of the cobalt oxide supported on carbon catalyst (PT230C catalyst) because the catalyst was more stable than the cobalt metal supported on carbon catalyst (PT560C catalyst). We performed sequential reactions at 200 °C at different total pressures at 32-11-25-18-32 bar with 24 h time on stream (TOS) at each pressure while maintaining the flow rates of ethylene and argon the same at 50:50 by volume. The plot of ethylene consumption rate as a function of TOS of these reactions is shown in Figure 3.13. Figure 3.13 shows that the catalyst was stable for 102 h since the average conversion from the first reaction at 32 bar was 8.3% while the conversion at 102 h (first data point from the last reaction at 32 bar) was 7.6% conversion. However, the catalyst deactivated after this last point was collected, likely due to pore blocking from polyethylene.

The average rates at different total pressures up to 96 h TOS were used to calculate the reaction order with respect to ethylene, as shown in Figure 3.14. The slope of this plot is the reaction order with respect to ethylene partial pressure, with a value of 1.1. In addition to these sequential reactions at different total pressures with the same catalyst bed, a reaction at 18 bar total pressure with a fresh catalyst bed was also performed for comparison. Figure 3.14 shows that the reaction with the fresh catalyst bed at 18 bar total pressure is similar to the reaction at 18 bar total pressure after the catalyst had been used at 32, 11, and 25 bar total pressures. The slight difference in activity from these catalysts was likely due to catalyst deactivation after the catalyst had been used at 32, 11, and 25 bar total pressures. We also performed ethylene oligomerization reactions with the fresh PT230C catalysts at the same 32 bar total pressure, but at different ethylene partial pressures for comparison, shown in Figure S3.6. The plot of ln(Rate) versus ln($P_{ethylene}$) from these

reactions, shown in Figure 3.15 has a slope of 0.95. The approximate first order dependence with respect to the reactant partial pressure and the Schulz-Flory distribution are consistent with the characteristic of the Cossee-Arlman mechanism, which is suggested to be the underlying mechanism for olefin oligomerization with this catalyst.[32,33]

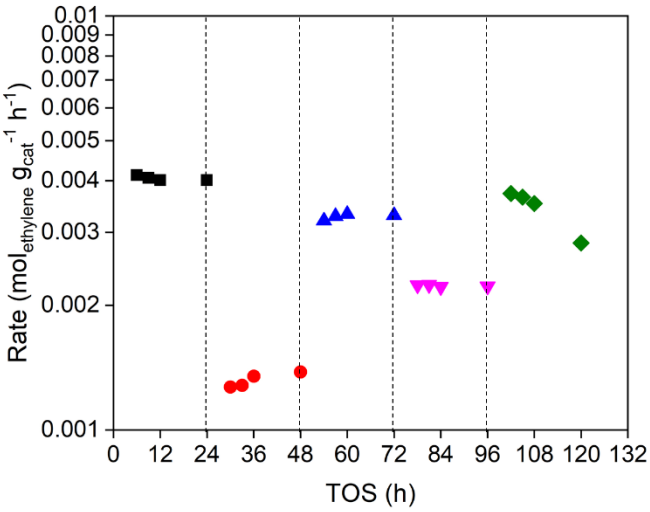

Figure 3.13 Ethylene consumption rate as a function of time on stream (TOS) at first 32 bar (black square), 11 bar (red circle), 25 bar (blue triangle), 18 bar (magenta upside-down triangle), and last 32 bar (green diamond) total pressures. Reaction conditions: 200 °C, 50:50 ethylene:argon (by volume), 12 wt% PT230C catalyst and 0.72 h contact time. All conversions were below 20%.

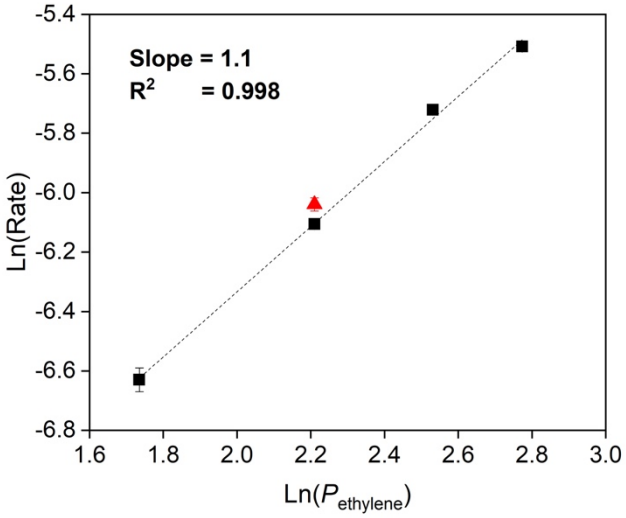

Figure 3.14 Ln(Rate) versus ln($P_{ethylene}$) from the 96 h sequential reactions at 32-11-25-18 bar total pressures (black square) and the reaction at 18 bar total pressure with a fresh catalyst bed (red triangle) at 200 °C, 50:50 ethylene:argon (by volume), 12 wt% PT230C catalyst, and 0.72 h contact time. Rate is defined as $mol_{ethylene}\ g_{cat}^{-1}\ h^{-1}$. Ethylene partial pressure ($P_{ethylene}$) is in bar. Bounds represent standard deviations. The slope and the R^2 value were calculated from the 96 h sequential reactions.

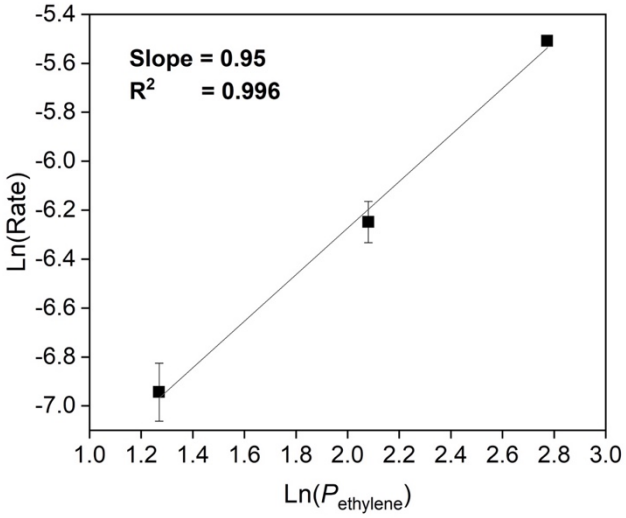

Figure 3.15 Ln(Rate) versus ln($P_{ethylene}$) from reactions with fresh 12 wt% PT230C catalysts at different ethylene partial pressures. Reaction conditions: 200 °C, 32 bar total pressure, 2 g of catalyst, 20-40 cm^3 (STP) min^{-1} of ethylene, and 40-160 cm^3 (STP) min^{-1} of argon. Rate is defined as $mol_{ethylene}$ g_{cat}^{-1} h^{-1}. Ethylene partial pressure ($P_{ethylene}$) is in bar. Bounds represent standard deviations.

We also investigated the effect of reaction pressure of the cobalt oxide supported on carbon catalyst (PT230C catalyst) towards the LAO isomer distribution, the product linearity, and the selectivity to each olefin chain. At the same 2.8% conversion, the LAO isomer distributions (Figure 3.16), the product linearities (Figure S3.7), and the product selectivities (Figure S3.8) at 11 bar and 32 bar total pressures with 50:50 ethylene and argon by volume are similar, suggesting that the total and the ethylene partial pressures have a negligible effect towards the LAO isomer distribution, the product linearity, and the product selectivity at similar conversion.

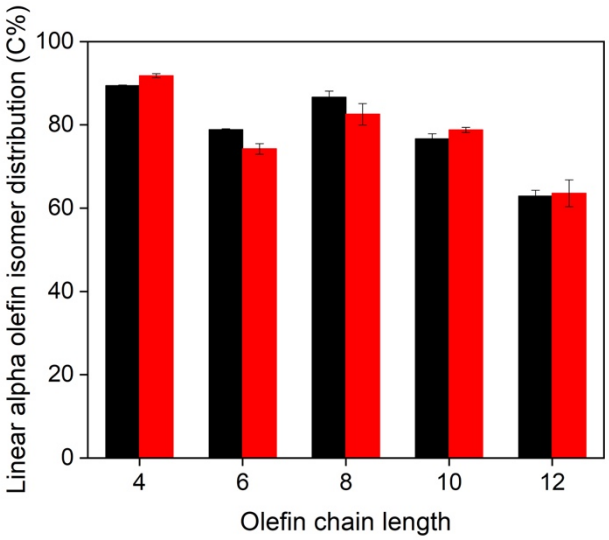

Figure 3.16 Linear alpha olefin (LAO) isomer distributions among C_4 to C_{12} olefins at 11 bar total pressure (black), 0.72 h contact time, and 2.8% ethylene conversion and 32 bar total pressure (red), 0.18 h contact time, and 2.8% ethylene conversion. Reaction conditions: 200 °C, 50:50 ethylene:argon (by volume), and 12 wt% PT230C catalysts. Bounds represent standard deviations. Data from the reaction with 32 bar total pressure are from literature.[21]

A possible rate expression for the ethylene oligomerization can be derived based on the observed reaction order with respect to ethylene partial pressure. Here, the reaction order from the cobalt oxide supported on carbon catalyst (PT230C catalyst) was used because the catalyst was more stable than the cobalt metal supported on carbon catalyst (PT560C catalyst). To derive the rate expression, the propagation of adsorbed olefins with gaseous ethylene was assumed to be the rate limiting step. This assumption has also been used for olefin oligomerization over supported nickel catalysts.[13,34] Under this assumption, the rate expression for ethylene consumption can be written as the Equation 3.8. The subscript 'p' in the rate constant (k) represents the propagation rate constant and the species inside the square brackets represents the surface coverage fraction of the corresponding species occupying a vacant site (*). Equation 3.8 can be simplified into the Equation 3.9 by assuming that the propagation rate constant is independent of the chain length. In

the case of the surface being highly covered by olefins (i.e., [*] ≅ 0), the site balance equation (Equation 3.10) can be simplified into the Equation 3.11. By substituting the summation term in the Equation 3.9 with the Equation 3.11, the rate expression can be simplified into Equation 3.12. Equation 3.12 shows a 1st order dependence of the rate with respect to ethylene partial pressure, which was observed in the experiments. Under these assumptions, the apparent activation energy ($E_{a,app}$) is also the same as the intrinsic activation energy in the k_p. We have previously obtained an $E_{a,app}$ of 25 kJ mol^{-1} by varying the reaction temperatures from 140 to 220 °C using the PT230C catalyst.[21] These results show that our reaction kinetics data are consistent with a mechanism that involves the rate determining step being the oligomerization of an adsorbed olefin with a gas phase olefin on a highly covered surface. These results can also be used as the basis of more rigorous future kinetic modelling to assess the validity of the propagation rate constant being independent of the olefin chain length as well as the case with the cobalt metal supported on carbon (PT560C) catalyst.

$$\text{Rate} = k_{p,C2}[C_2{}^*]P_{C2} + k_{p,C4}[C_4{}^*]P_{C2} + k_{p,C6}[C_6{}^*]P_{C2} + \ \ldots \ = P_{C2}\sum_{i=1}^{n} k_{p,C2i}[C_{2i}{}^*] \quad (3.8)$$

$$\text{Rate} = k_p P_{C2}\sum_{i=1}^{n}[C_{2i}{}^*] \quad (3.9)$$

$$1 = [\,^*] + [C_2{}^*] + [C_4{}^*] + [C_6{}^*] + \ \ldots \quad (3.10)$$

$$1 \approx [C_2{}^*] + [C_4{}^*] + [C_6{}^*] + \ \ldots \ = \sum_{i=1}^{n}[C_{2i}{}^*] \quad (3.11)$$

$$\text{Rate} = k_p P_{C2} \quad (3.12)$$

3.4 Conclusions

Ethylene oligomerization over carbon-supported cobalt catalysts is highly selective to linear olefins (>80% linearity up to C_{12} olefins at <48% conversion) and moderately selective up to C_8 linear alpha olefins (>30% LAO isomer distribution at <10% conversion) at the reaction temperature of 200 °C. Increasing the catalyst pretreatment temperature in argon from 230 to 560 °C reduces cobalt oxide to cobalt metal. Cobalt metal supported on carbon is more active than cobalt oxide supported on carbon, however, the catalyst deactivates likely due to higher rate of polyethylene formation on the cobalt metal catalyst. The 1st order deactivation rate constant is not a strong function of the contact time. Changing the total and ethylene partial pressures have a negligible impact towards the product selectivity, the product linearity, and the linear alpha olefin isomer distribution for the cobalt oxide supported on carbon catalyst. The rate of ethylene oligomerization is first order with respect to the ethylene partial pressure, which is consistent with a mechanism where the rate determining step is the reaction of ethylene with adsorbed olefins on a highly covered surface with olefins.

3.5 References

1. T. Ridha, Y. Li, E. Gençer, J. J. Siirola, J. T. Miller, F. H. Ribeiro and R. Agrawal, Valorization of shale gas condensate to liquid hydrocarbons through catalytic dehydrogenation and oligomerization, *Processes*, 2018, **6**, 139.
2. US Energy Information Administration, *Annual energy outlook 2019 with projections to 2050*, https://www.eia.gov/outlooks/aeo/pdf/aeo2019.pdf, (Accessed February 2021).
3. N. Rahimi and R. Karimzadeh, Catalytic cracking of hydrocarbons over modified ZSM-5 zeolites to produce light olefins: A review, *Appl. Catal. A*, 2011, **398**, 1-17.
4. V. N. Ipatieff, B. B. Corson and G. Egloff, Polymerization, a new source of gasoline, *Ind. Eng. Chem.*, 1935, **27**, 1077-1081.
5. V. N. Ipatieff and R. E. Schaad, Heptenes and heptanes from propylene and butylenes, *Ind. Eng. Chem.*, 1945, **37**, 362-364.
6. G. R. Lappin, L. H. Nemec, J. D. Sauer and J. D. Wagner, *Kirk-Othmer Encyclopedia of Chemical Technology*, John Wiley & Sons, Inc., 2000.
7. C. P. Nicholas, Applications of light olefin oligomerization to the production of fuels and chemicals, *Appl. Catal. A*, 2017, **543**, 82-97.

8. N. M. Eagan, M. D. Kumbhalkar, J. S. Buchanan, J. A. Dumesic and G. W. Huber, Chemistries and processes for the conversion of ethanol into middle-distillate fuels, *Nat. Rev. Chem.*, 2019, **3**, 223-249.
9. A. Finiels, F. Fajula and V. Hulea, Nickel-based solid catalysts for ethylene oligomerization - a review, *Catal. Sci. Technol.*, 2014, **4**, 2412-2426.
10. R. Y. Brogaard and U. Olsbye, Ethene oligomerization in Ni-containing zeolites: theoretical discrimination of reaction mechanisms, *ACS Catal.*, 2016, **6**, 1205-1214.
11. S. Moussa, P. Concepción, M. A. Arribas and A. Martínez, Nature of active sites and initiation mechanism for ethylene oligomerization on heterogeneous Ni-beta catalysts, *ACS Catal.*, 2018, **8**, 3903-3912.
12. A. N. Mlinar, G. B. Baur, G. G. Bong and A. T. Bell, Propene oligomerization over Ni-exchanged Na-X zeolites, *J. Catal.*, 2012, **296**, 156-164.
13. I. Agirrezabal-Telleria and E. Iglesia, Stabilization of active, selective, and regenerable Ni-based dimerization catalysts by condensation of ethene withinordered mesopores, *J. Catal.*, 2017, **352**, 505-514.
14. R. Joshi, G. Zhang, J. T. Miller and R. Gounder, Evidence for the coordination-insertion mechanism of ethene dimerization at nickel cations exchanged onto beta molecular sieves, *ACS Catal.*, 2018, **8**, 11407-11422.
15. A. Ehrmaier, Y. Liu, S. Peitz, A. Jentys, Y.-H. Chin, M. Sanchez-Sanchez, R. Bermejo-Deval and J. A. Lercher, Dimerization of Linear Butenes on Zeolite-Supported Ni^{2+}, *ACS Catal.*, 2019, **9**, 315-324.
16. R. G. Schultz, J. M. Schuck and B. S. Wildi, Olefin dimerization over cobalt-oxide-on-carbon catalysts: I. Propylene dimerization, *J. Catal.*, 1966, **6**, 385-396.
17. R. G. Schultz, R. M. Engelbrecht, R. N. Moore and L. T. Wolford, Olefin dimerization over cobalt-oxide-on-carbon catalysts: II. Butene and hexene dimerization, *J. Catal.*, 1966, **6**, 419-424.
18. R. G. Schultz, Olefin dimerization over cobalt-oxide-on-carbon catalysts: III. Oligomerization of ethylene, *J. Catal.*, 1967, **7**, 286-290.
19. Z. Xu, J. P. Chada, D. Zhao, C. A. Carrero, Y. T. Kim, D. C. Rosenfeld, J. L. Rogers, S. J. Rozeveld, I. Hermans and G. W. Huber, Production of linear octenes from oligomerization of 1-butene over carbon-supported cobalt catalysts, *ACS Catal.*, 2016, **6**, 3815–3825.
20. Z. Xu, D. Zhao, J. P. Chada, D. C. Rosenfeld, J. L. Rogers, I. Hermans and G. W. Huber, Olefin conversion on nitrogen-doped carbon-supported cobalt catalyst: Effect of feedstock, *J. Catal*, 2017, **354**, 213-222.
21. A. Jonathan, N. M. Eagan, D. L. Bruns, S. S. Stahl, M. P. Lanci, J. A. Dumesic and G. W. Huber, Ethylene oligomerization into linear olefins over cobalt oxide on carbon catalyst, *Catal. Sci. Technol.*, 2021, **11**, 3599-3608.
22. E. O. C. Greiner, M. Blagoev and Y. Yamaguchi, *Chemical Economics Handbook: Linear alpha-Olefins*, IHS Chemical, 2013.
23. Z. Xu, J. P. Chada, L. Xu, D. Zhao, D. C. Rosenfeld, J. L. Rogers, I. Hermans, M. Mavrikakis and G. W. Huber, Ethylene dimerization and oligomerization to 1-butene and higher olefins with chromium-promoted cobalt on carbon catalyst, *ACS Catal.*, 2018, **8**, 2488-2497.
24. K. O'Connell and J. R. Regalbuto, High sensitivity silicon slit detectors for 1 nm powder XRD size detection limit, *Catal. Lett.,* 2015, **145**, 777-783.
25. M. A. Vannice, *Kinetics of Catalytic Reactions*, Springer, 2005.

26. D. Gu, C. -J. Jia, C. Weidenthaler, H. -J. Bongard, B. Spliethoff, W. Schmidt and F. Schüth, Highly ordered mesoporous cobalt-containing oxides: structure, catalytic properties, and active sites in oxidation of carbon monoxide, *J. Am. Chem. Soc.*, 2015, **137**, 11407-11418.
27. L. Wang, E. Guan, Y. Wang, L. Wang, Z. Gong, Y. Cui, X. Meng, B. C. Gates and F. -S. Xiao, Silica accelerates the selective hydrogenation of CO_2 to methanol on cobalt catalysts, *Nat. Commun.*, 2020, **11**, 1033.
28. D. Zhao, X. Wang, J. B. Miller and G. W. Huber, The chemistry and kinetics of polyethylene pyrolysis: a process to produce fuels and chemicals, *ChemSusChem*, 2020, **13**, 1764-1774.
29. E. Iglesia, Design, synthesis, and use of cobalt-based Fischer-Tropsch synthesis catalysts, *Appl. Catal. A*, 1997, **161**, 59-78.
30. E. Iglesia, S. C. Reyes, R. J. Madon and S. L. Soled, Selectivity control and catalyst design in the Fischer-Tropsch synthesis: sites, pellets, and reactors, *Adv. Catal.*, 1993, **39**, 221-302.
31. R. A. Dictor and A. T. Bell, Fischer-Tropsch synthesis over reduced and unreduced iron oxide catalysts, *J. Catal.*, 1986, **97**, 121-136.
32. E. D. Metzger, R. J. Comito, Z. Wu, G. Zhang, R. C. Dubey, W. Xu, J. T. Miller and M. Dincă, Highly selective heterogeneous ethylene dimerization with a scalable and chemically robust MOF catalyst, *ACS Sustain. Chem. Eng.*, 2019, **7**, 6654-6661.
33. P. Cossee, Ziegler-Natta Catalysis I. Mechanism of Polymerization of α-Olefins with Ziegler-Natta Catalysts, *J. Catal.*, 1964, **3**, 80-88.
34. S. Pellizzeri, M. Barona, V. Bernales, P. Miró, P. Liao, L. Gagliardi, R.Q. Snurr and R.B. Getman, Catalytic descriptors and electronic properties of single-site catalysts for ethene dimerization to 1-butene, *Catal. Today*, 2018, **312**, 149-157.

3.6 Supplementary Information

Supplementary Experimental: Weisz-Prater criterion

The following discussion outlines how to determine whether an ethylene oligomerization reaction over a cobalt supported on carbon catalyst is kinetically limited using the Weisz-Prater criterion.[1] The reaction is kinetically limited if the following Equation S3.1:

$$\frac{\text{Rate} \times {R_\text{p}}^2}{C_\text{s} \times D_\text{eff}} \leq X \qquad \text{(S3.1)}$$

is satisfied where:

- Rate = ethylene consumption rate per unit volume [=] mol cm^{-3} s^{-1}
- R_p = catalyst particle radius [=] cm
- C_s = reactant surface concentration [=] mol cm^{-3}
- D_eff = effective diffusivity [=] cm^2 s^{-1}
- X = 0.6 for 1st order reaction and 0.3 for 2nd order reaction

Because ethylene oligomerization over a cobalt supported on carbon catalyst is 1st order with respect to ethylene partial pressure, X = 0.6.

For ethylene oligomerization over a cobalt metal supported on carbon catalyst, an initial rate approach (which is the y-intercept from the plot of ln(Rate) vs TOS) was used due to catalyst deactivation. Based on Figure S3.2, the y-intercept is approximately -1.5. Note that the rate itself is defined as $mol_{ethylene}$ g_{cat}^{-1} h^{-1}, thus:

$$\text{Rate} = 2.23 \times 10^{-2} \ \frac{\text{mol}_\text{ethylene}}{\text{g}_\text{cat}\ \text{h}}$$

To convert the rate per gram of catalyst into the rate per unit volume of catalyst, the cobalt precursor was assumed to only fill the catalyst pore. Given that the density of the carbon support (Cabot Corporation) is 0.42 g cm^{-3} and the cobalt weight loading of the catalyst is 12 wt%, the rate per volume was calculated as follow:

$$\text{Rate} = 0.42\ \frac{\text{g}_\text{C}}{\text{cm}^3} \times \frac{1\ \text{g}_\text{cat}}{0.88\ \text{g}_\text{C}} \times 2.23 \times 10^{-2}\ \frac{\text{mol}_\text{ethylene}}{\text{g}_\text{cat}\ \text{h}} \times \frac{1\ \text{h}}{3600\ \text{s}}$$

$$\boxed{\text{Rate} = 2.96\ \times 10^{-5}\ \frac{\text{mol}}{\text{cm}^3\ \text{s}}}$$

All ethylene oligomerization reactions in the current study were performed at 16 bar ethylene, 16 bar argon, and at 200 °C (473 K), except during the pressure effect study. Assuming that the surface concentration of ethylene is the same as the bulk concentration of ethylene and the behavior follows an ideal gas law, the surface concentration was calculated using the following Equation S3.2:

$$C_\text{s} = \frac{P_\text{ethylene}}{R \times T} \qquad \text{(S3.2)}$$

$$C_\text{s} = \frac{16\ \text{bar}}{8.314\ \frac{\text{J}}{\text{mol K}} \times 473\ \text{K}} \times \frac{10^5\ \text{Pa}}{1\ \text{bar}} \times \frac{1\ \text{m}^3}{10^6 \text{cm}^3}$$

$$\boxed{C_\text{s} = 4.07 \times 10^{-4}\ \frac{\text{mol}}{\text{cm}^3}}$$

The carbon support in this study was sieved to obtain a particle diameter of 250 to 600 μm. By using the worst case scenario (which is the biggest particle size), the particle radius is therefore:

$$\boxed{R_\text{p} = 0.03\ \text{cm}}$$

Based on the BJH pore size distribution from our previous study, a peak at ~4 nm was observed, giving a pore radius of 2 nm.[2] Because this is in between 1 nm to 100 nm pore radius, the effective diffusivity (D_{eff}) could be approximated to be the Knudsen diffusivity (D_{K}).[3] The formula of the Knudsen diffusivity is given by the following Equation S3.3:

$$D_{\text{K}} = (9.7 \times 10^3) \times R_{\text{pore}} \times \left(\frac{T}{MW}\right)^{0.5} [=] \frac{\text{cm}^2}{\text{s}} \qquad \text{(S3.3)}$$

where:

- R_{pore} = pore radius [=] cm
- T = temperature [=] K
- MW = molecular weight [=] g mol^{-1}

Therefore:

$$D_{\text{K}} = (9.7 \times 10^3) \times (2 \times 10^{-7}\ \text{cm}) \times \left(\frac{473\ \text{K}}{28\frac{\text{g}}{\text{mol}}}\right)^{0.5}$$

$$\boxed{D_{\text{K}} = 7.97 \times 10^{-3}\ \frac{\text{cm}^2}{\text{s}} \approx D_{\text{eff}}}$$

Going back to the Weisz-Prater Criterion:

$$\frac{\text{Rate} \times {R_{\text{p}}}^2}{C_{\text{s}} \times D_{\text{eff}}} \leq X$$

$$\frac{\left(2.96 \times 10^{-5}\ \frac{\text{mol}}{\text{cm}^3\ \text{s}}\right) \times (0.03\ \text{cm})^2}{\left(4.07 \times 10^{-4}\frac{\text{mol}}{\text{cm}^3}\right) \times \left(7.97 \times 10^{-3}\ \frac{\text{cm}^2}{\text{s}}\right)} \leq 0.6$$

$$\boxed{0.0082 \leq 0.6}$$

Because the criterion is satisfied, then the ethylene oligomerization reaction over cobalt metal supported on carbon catalyst is kinetically limited.

Table S3.1 Total mol of cobalt in the 12 wt% cobalt nitrate supported on high temperature treated carbon catalyst as well as both CO and CO_2 being produced during the temperature-programmed desorption (TPD) in 50 cm^3 (STP) min^{-1} of argon at 10 °C min^{-1} ramp rate. The amount of CO was calculated up to 650 °C, assuming a straight line baseline from 536 to 650 °C.

Species	Amount (mmol g_{cat}^{-1})
Cobalt	2.0
CO	0.8
CO_2	2.4

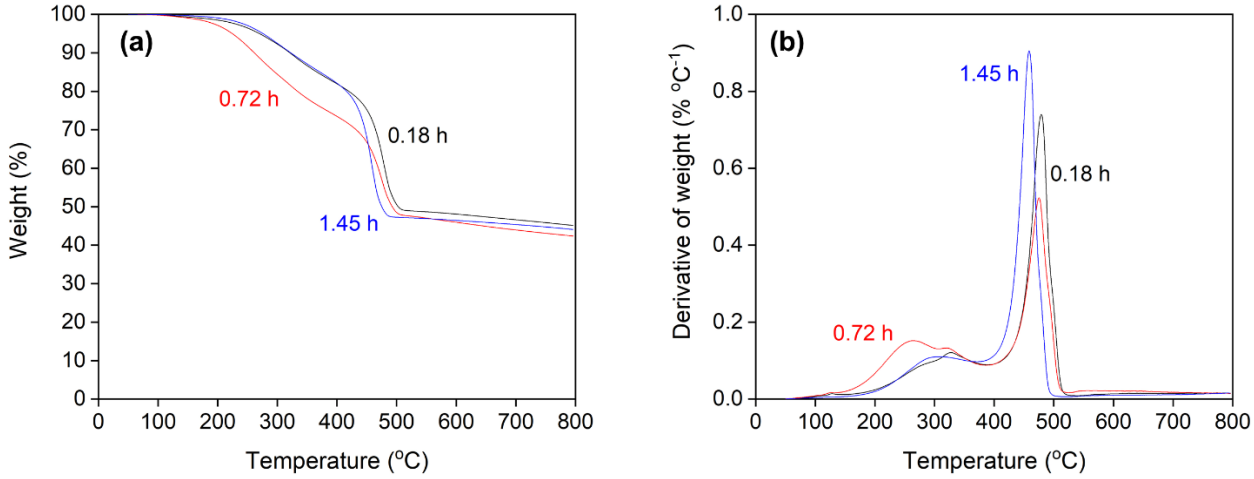

Figure S3.1 Thermogravimetric analysis (TGA) under N_2 of the spent 12 wt% PT560C catalysts after reactions at 200 °C, 16 bar ethylene, 16 bar argon, and 0.18 h, 0.72 h, and 1.45 h contact times. The reaction at 1.45 h contact time was performed for 36 h TOS whereas other reactions were performed for 24 h TOS. (a) Weight percent versus temperature. (b) Derivative of weight percent versus temperature. TGA conditions: 50 cm^3 (STP) min^{-1} of N_2, 10 °C min^{-1} ramp rate, and ~10 mg sample.

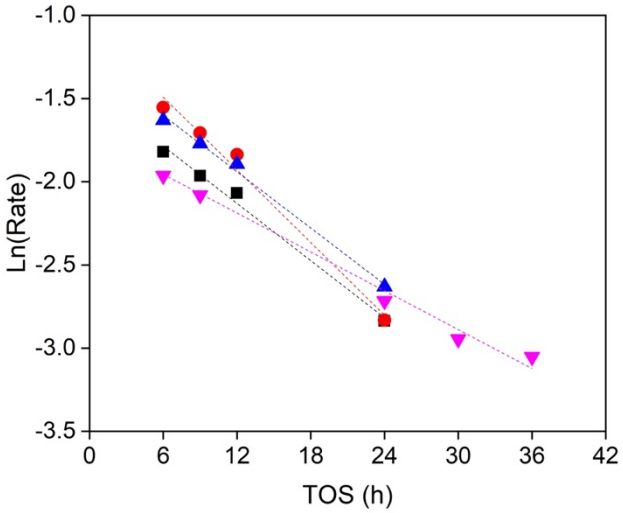

Figure S3.2 Ln(Rate) versus time on stream (TOS) at 0.18 h (black square), 0.36 h (red circle), 0.72 h (blue triangle), and 1.45 h (magenta upside-down triangle) contact times. Rate is defined as $mol_{ethylene}\ g_{cat}^{-1}\ h^{-1}$. Reaction conditions: 200 °C, 16 bar ethylene, 16 bar argon, and 12 wt% PT560C catalysts.

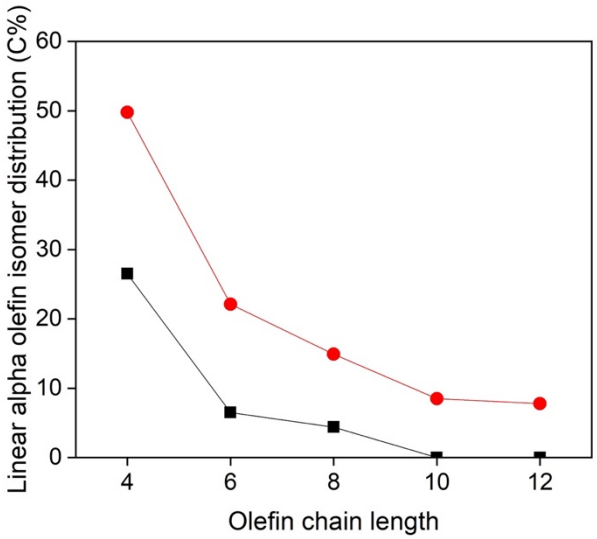

Figure S3.3 Linear alpha olefin (LAO) isomer distributions among C_4, C_6, C_8, C_{10}, and C_{12} olefins at 6 h TOS and 71.1% conversion (black square) and 24 h TOS and 47.2% conversion (red circle). Reaction conditions: 200 °C, 16 bar ethylene, 16 bar argon, 12 wt% PT400C catalysts, and 1.45 h contact time. Conversion is lower at higher TOS due to catalyst deactivation.

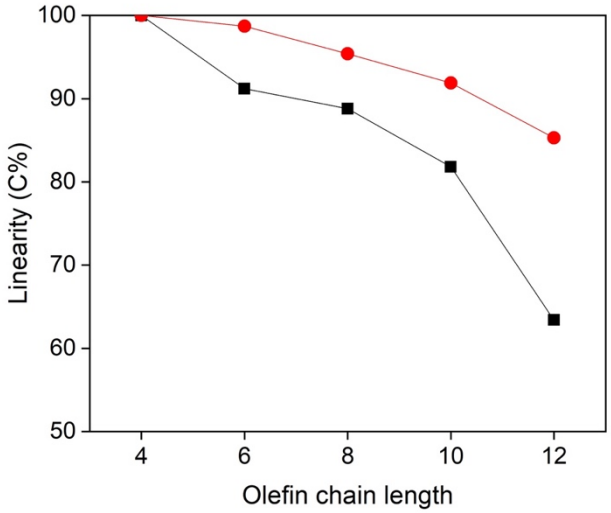

Figure S3.4 Product linearities of C_4, C_6, C_8, C_{10}, and C_{12} olefins at 6 h TOS and 71.1% conversion (black square) and 24 h TOS and 47.2% conversion (red circle). Reaction conditions: 200 °C, 16 bar ethylene, 16 bar argon, 12 wt% PT400C catalysts, and 1.45 h contact time. Conversion is lower at higher TOS due to catalyst deactivation.

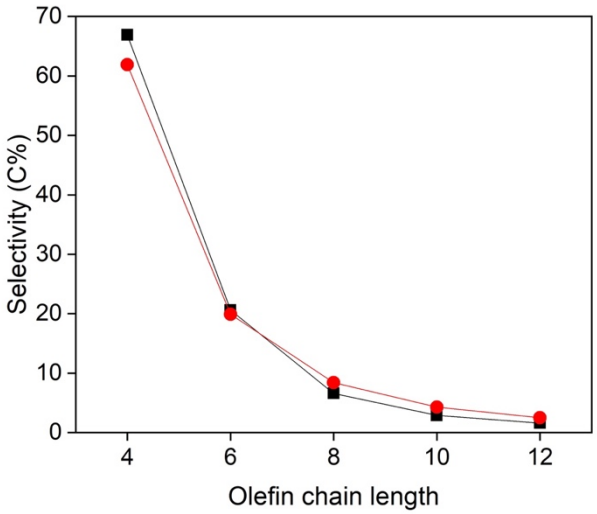

Figure S3.5 Product selectivities to C_4, C_6, C_8, C_{10}, and C_{12} olefins at 6 h TOS and 71.1% conversion (black square) and 24 h TOS and 47.2% conversion (red circle). Reaction conditions: 200 °C, 16 bar ethylene, 16 bar argon, 12 wt% PT400C catalysts, and 1.45 h contact time. Conversion is lower at higher TOS due to catalyst deactivation.

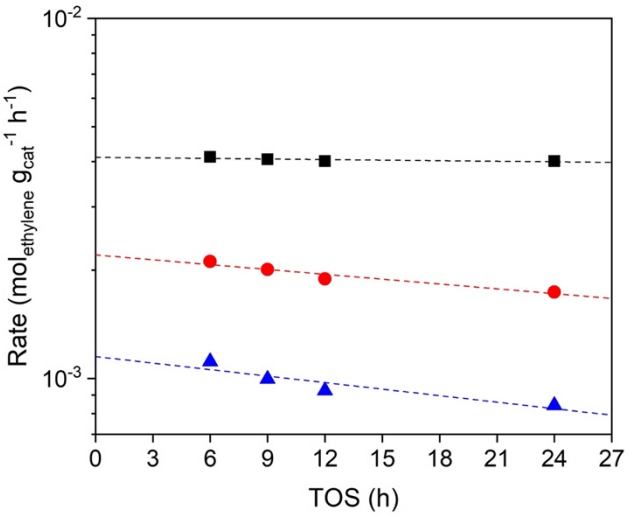

Figure S3.6 Ethylene consumption rates as a function of time on stream (TOS) with ethylene and argon concentrations (by volume) of 50:50 (black square), 25:75 (red circle), and 11:89 (blue triangle). Reaction conditions: 200 °C, 32 bar total pressure, 2 g of catalyst, 20-40 cm^3 (STP) min^{-1} of ethylene, and 40-160 cm^3 (STP) min^{-1} of argon. All conversions were below 20%. Dashed lines are added to guide the eye.

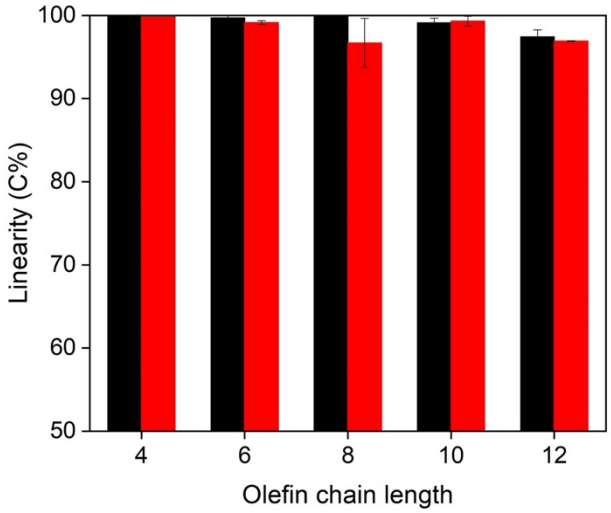

Figure S3.7 Product linearities of C_4 to C_{12} olefins at 11 bar total pressure (black), 0.72 h contact time, and 2.8% ethylene conversion and 32 bar total pressure (red), 0.18 h contact time, and 2.8% ethylene conversion. Reaction conditions: 200 °C, 50:50 ethylene:argon (by volume), and 12 wt% PT230C catalysts. Bounds represent standard deviations. Data from the reaction with 32 bar total pressure are from literature.[2]

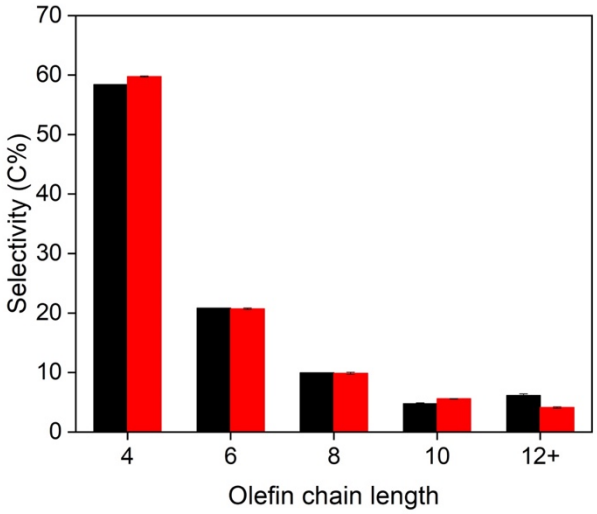

Figure S3.8 Product selectivities to C_4 to C_{12+} olefins at 11 bar total pressure (black), 0.72 h contact time, and 2.8% ethylene conversion and 32 bar total pressure (red), 0.18 h contact time, and 2.8% ethylene conversion. Reaction conditions: 200 °C, 50:50 ethylene:argon (by volume), and 12 wt% PT230C catalysts. Bounds represent standard deviations. Data from the reaction with 32 bar total pressure are from literature.[2]

Supplementary References

1. M. A. Vannice, *Kinetics of Catalytic Reactions*, Springer, 2005.
2. A. Jonathan, N. M. Eagan, D. L. Bruns, S. S. Stahl, M. P. Lanci, J. A. Dumesic and G. W. Huber, Ethylene oligomerization into linear olefins over cobalt oxide on carbon catalyst, *Catal. Sci. Technol.*, 2021, **11**, 3599-3608.
3. M. E. Davis and R. J. Davis, *Fundamentals of Chemical Reaction Engineering*, McGraw-Hill, 2003.

Chapter 4. Effect of Catalyst Support on Cobalt Catalysts for Ethylene Oligomerization into Linear Olefins[3]

4.1 Introduction

Light (C_2 - C_4) olefin oligomerization is an attractive process to synthesize higher (C_6 - C_{16}) linear alpha olefins (LAOs) for use in various applications, including polyethylene comonomers, plasticizers, lubricants, and detergents.[1,2] The abundant source of ethylene from the advent of hydraulic fracturing technologies and dehydration of ethanol, the largest biofuel in the world make ethylene a promising feedstock for this reaction.[3-6] Light olefin oligomerization into linear alpha olefins is commercially done with homogeneous transition metal catalysts in processes like Gulfene, SHOP, and Ethyl.[7] However, the implementation of these catalysts typically requires extra purification steps, activators, and/or solvents. Therefore, the use of heterogeneous transition metal catalysts as alternatives for this reaction is desirable. Various attempts have been made to synthesize selective heterogeneous transition metal catalysts to linear olefins, most commonly with solid acid supported Ni catalysts.[8-17] To improve the selectivity to linear olefins, these experiments were typically performed at low conversion (<20%). For example, Gounder and co-workers reported that ethylene dimerization over Ni-Li-Zn[Beta] at <2% ethylene conversion resulted in <30% of all butenes being 1-butene.[15] Lercher and co-workers also reported that 1-butene oligomerization over Ni-Ca-LTA at 5% conversion resulted in 53% selectivity to linear octenes, the highest selectivity to linear octenes reported to date with heterogeneous nickel catalysts in the absence of activators and solvents.[16]

[3] This chapter is adapted from A. Jonathan, R. G. Dastidar, C. Wang, J. A. Dumesic and G. W. Huber, Effect of catalyst support on cobalt catalysts for ethylene oligomerization into linear olefins, under review.

Olefin oligomerization reactions over heterogeneous carbon-supported cobalt catalysts have been reported to have high selectivities to linear olefins.[18-23] Schultz et al. reported that dimerization reactions of propylene, 1-butene, and 1-hexene with ammoniated cobalt oxide supported on carbon catalysts (CoO_x/N-C) in batch reactors yielded 52%, 65%, and 83% selectivities to linear dimers, respectively.[18,19] These catalysts were prepared by impregnating the carbon support with an ammonium hydroxide solution before and after the impregnation with cobalt. Recently, Xu et al. reported that CoO_x/N-C selectively dimerized 1-butene to linear octenes in continuous flow reactors at the reaction temperature of 80 °C.[21] At 29% 1-butene conversion, the linearity of C_8 olefins was above 78%. Xu et al. also reported that ethylene oligomerization over CoO_x/N-C at 80 °C and 20% ethylene conversion yielded octenes with 78% linearity.[22] However, the amount of 1-octene was only 5% at this conversion. In addition, the catalysts also suffered from deactivation at the reaction temperature of 80 °C.

Recently, we have shown that a heterogeneous carbon-supported cobalt oxide on carbon catalyst is stable and highly selective to linear and alpha olefins when performing the reaction at 200 °C.[24] At 14% ethylene conversion, the linear alpha olefin (LAO) isomer distributions of C_4, C_6, and C_8 olefins were 90.2%, 77.6%, and 69.1%, respectively. The product linearities up to C_{12} olefins were all above 90%, even at 48% ethylene conversion. We have shown that both the bulk and the surface cobalt phases were CoO, suggesting that this is the stable cobalt phase during oligomerization. We have also shown that increasing the catalyst pretreatment temperature in argon from 230 °C to 560 °C reduces CoO_x to Co metal, which improves the catalytic activity.[25] However, Co metal supported on carbon catalyst deactivated due to polyethylene formation on the catalyst (approximately 50% of the spent catalyst was polyethylene after a 24 h reaction).

Although heterogeneous cobalt supported on carbon catalysts are highly selective to linear and alpha olefins with Co metal being the more active cobalt phase, the effect of the catalyst support on cobalt catalysts for olefin oligomerization has not been thoroughly investigated. In addition, the differences in the carbon morphology and the surface functional groups on the catalyst supports could potentially influence the activity and the selectivity of these catalysts. Other carbon-supported transition metal catalysts, including Pt, Pd, and bimetallic RhRe have been reported to have their activities influenced by the morphology and the functional groups of the carbon support for dehydrogenation, hydrogenation, and hydrogenolysis reactions.[26-29] In this study, we compare two different carbon supports, high-temperature-treated carbon (HTTC) and acid-washed carbon (AWC) as the catalyst supports for cobalt with the purpose of understanding the effect of surface functional groups for ethylene oligomerization. In addition, we also investigate the effect of increasing the catalyst support particle size to impose more transport restrictions to the products from ethylene oligomerization over heterogeneous cobalt supported on carbon catalysts. Finally, we compare two different activated carbon supports for cobalt catalysts for olefin oligomerization.

4.2 Experimental Methods

4.2.1 Catalyst synthesis

High-temperature-treated carbon (HTTC) was synthesized by heating activated carbon (Norit Darco MRX m-2278 or Darco BG1) at 900 °C for 2 h in 100 cm^3 (STP) min^{-1} of helium at 10 °C min^{-1} ramp rate. The HTTC was cooled to room temperature under helium and exposed to air thereafter. For the synthesis of acid-washed carbon (AWC), 10 g of activated carbon was submerged in 100 mL of HNO_3 (70%, ACS grade) and heated at 90 °C for 1 h in a reboiler. The

AWC was subsequently washed with DI water to remove the leftover acid and dried in an oven at 110 °C overnight. All carbon supports in this study were initially sieved to obtain a particle size in the range of 250 – 600 μm (average of 425 μm), except for the catalyst support particle size study where 600 – 850 μm (average of 725 μm) and 850 – 1000 μm (average of 925 μm) particle sizes were used. To synthesize a 12 wt% carbon-supported cobalt catalyst, 2.0 g of carbon support was impregnated with a solution composed of 1.89 g of $Co(NO_3)_2 \cdot 6H_2O$ (Sigma Aldrich) and 1.22 g of deionized (DI) water. The catalyst was dried on a hotplate at 120 °C overnight.

4.2.2 Continuous flow reactions

Ethylene oligomerization reactions were performed in 30 cm downflow fixed bed reactors with 0.64 cm (¼ in) OD tubing. The diagram of this system is shown in literature.[24] Both ethylene and argon flow rates in this study were set to 20 cm^3 (STP) min^{-1} while the amount of catalyst was varied from 0.5 to 2 g. The contact time (h g_{cat} $g_{ethylene}^{-1}$) in this study is defined as the ratio of the mass of catalyst and the inlet mass flow rate of ethylene. Prior to the reaction, the carbon-supported cobalt catalyst was initially pretreated at 230 °C for 2 h in 100 cm^3 (STP) min^{-1} of argon at 1 °C min^{-1} ramp rate. The catalyst was then cooled to room temperature in argon, pressurized to 32 bar (450 psig) using a back-pressure regulator (Equilibar), and heated to 200 °C at 5 °C min^{-1} ramp rate in argon, followed by a switch in feed. The outlet stream of the reactor was directed to a 120 mL condenser chilled in an ice bath to separate the relatively volatile species. These species were directed to an online GC-FID (Shimadzu, 2014) and analyzed approximately every 45 min. The condensed product was washed with approximately 10 g of heptane to ensure full collection and analyzed by a 2D-GC-FID (Agilent) approximately every 3 h. Data points before 6 h time on stream (TOS) were excluded due to system transients. For calculations of the linear alpha olefin

isomer distribution, the product linearity, and the product selectivity, average data points from 24 h to 30 h time on stream (TOS) were used due to noticeable transients in product selectivities before 24 h. The bounds from the average data points represent the standard deviations from these data points.

The product quantification of each method is described in detail elsewhere.[24] In short, the online GC-FID was able to detect C_2 up to C_{10} olefins whereas the 2D-GC-FID was able to detect C_2 up to C_{24} olefins. Linear alpha olefin (LAO) standards up to C_{24} olefins were used to determine retention times. GC peaks with earlier retention times than the corresponding LAO were assumed to be branched olefins whereas those with later retention times than the corresponding LAO were assumed to be linear internal olefins. These assumptions were made based on the trend observed in C_4 to C_8 olefins. The isomer distribution of C_4 olefins was determined using the online GC-FID whereas the isomer distributions of other olefins were determined using the 2D-GC-FID. Carbon balances in all reactions were above 95%.

The parameters in the manuscript are defined as follows:

$$\text{Ethylene conversion (C\%)} = \frac{\sum_{i=4}^{n} i \times F_{\mathrm{C}_{i,\mathrm{out}}}}{2 \times F_{\mathrm{C}_{2,\mathrm{in}}}} \times 100 \tag{4.1}$$

$$\text{Product selectivity to } \mathrm{C}_i \text{ (C\%)} = \frac{i \times F_{\mathrm{C}_{i,\mathrm{out}}}}{\sum_{i=4}^{n} i \times F_{\mathrm{C}_{i,\mathrm{out}}}} \times 100 \tag{4.2}$$

$$\text{LAO isomer distribution of } \mathrm{C}_i \text{ (C\%)} = \frac{F_{\mathrm{C}_{i,\text{linear alpha,out}}}}{F_{\mathrm{C}_{i,\mathrm{out}}}} \times 100 \tag{4.3}$$

$$\text{Product linearity of } \mathrm{C}_i \text{ (C\%)} = \frac{F_{\mathrm{C}_{i,\text{linear alpha,out}}} + F_{\mathrm{C}_{i,\text{linear internal,out}}}}{F_{\mathrm{C}_{i,\mathrm{out}}}} \times 100 \tag{4.4}$$

$$\text{Ethylene consumption rate } (\mathrm{mol}_{\text{ethylene}}\ \mathrm{g}_{\text{cat}}^{-1}\ \mathrm{h}^{-1}) = \frac{F_{\mathrm{C}_{2,\mathrm{in}}} \times \text{conversion}}{\text{mass of catalyst}} \tag{4.5}$$

$$\text{Carbon balance (C\%)} = \frac{\sum_{i=2}^{n} i \times F_{\mathrm{C}_{i,\mathrm{out}}}}{2 \times F_{\mathrm{C}_{2,\mathrm{in}}}} \times 100 \tag{4.6}$$

Here, F is the molar flow rate in mol h^{-1} and C_i is the olefin chain with i carbon atoms.

4.2.3 X-ray photoelectron spectroscopy (XPS) procedure

XPS experiments were carried out in a K-alpha spectrometer (Thermo Scientific) with an Al K_α X-ray source. All samples were analyzed with the flood gun on and without exposure to air. In a typical experiment, the catalyst was initially pretreated at 230 °C in argon for 2 h and transferred to a glovebox without exposure to air. The pretreated catalyst was packed into a vessel (Transfer Vessel K-Alpha), sealed under vacuum inside the glovebox, and transferred to the XPS instrument. The Co 2p spectra were taken over 50 scans with 0.1 eV step size, 50 ms dwell time, and 50 kV pass energy. All other spectra were taken over 20 scans with 0.2 eV step size, 50 ms dwell time, and 50 kV pass energy. All binding energy (BE) values were calibrated to the binding energy of C 1s peak for graphite at 284.5 eV. The baseline of each spectrum was corrected using a straight line. All Co 2p spectra were normalized to have comparable intensities in all samples.

4.2.4 X-ray diffraction (XRD) procedure

Powder XRD experiments were carried out in a Rigaku Rapid II diffractometer with a Mo K_α X-ray source at 50 mA and 50 kV in the 2θ range of 2 to 45°. In a typical experiment, the catalyst was initially ground to make a powder and packed inside a polyimide tube (American Durafilm) with both ends sealed with a clay. The catalyst was analyzed with 30 min exposure time. The baseline of the XRD pattern was corrected using JADE 9 software. All XRD patterns were normalized to have comparable intensities in all samples.

4.2.5 Thermogravimetric analysis (TGA) procedure

TGA experiments were carried out using a Thermal Analysis (TA) Instruments Q500 system. In a typical experiment, 10 mg of sample was heated to 800 °C in 50 cm^3 (STP) min^{-1} of N_2 at 10 °C min^{-1} ramp rate.

4.2.6 N_2 Physisorption procedure

N_2 physisorption experiments were carried out in an ASAP 2020 (Micrometrics) instrument at -196 °C. In a typical experiment, 200 mg of sample was initially degassed at 120 °C for 6 h prior to the N_2 physisorption analysis. The BET surface area of the sample was obtained from the N_2 physisorption data in the relative pressure (P/P_0) range of 0.06 to 0.24. The BJH pore size distribution (dV/dw where V is the pore volume and w is the pore width) of the sample was obtained from the N_2 desorption isotherm.

4.2.7 Temperature-programmed desorption (TPD) procedure

TPD experiments were carried out using an AutoChem 2920 (Micrometrics) connected to a mass spectrometer (MS). In a typical experiment, 100 mg of sample was heated to 900 °C in 50 cm^3 (STP) min^{-1} of He at 10 °C min^{-1} ramp rate with the outlet stream being analyzed by the MS. The signals from m/z = 28 and m/z = 44 were converted to the molar concentrations of CO and CO_2, respectively with CO and CO_2 calibrations assuming an ideal gas law. The total CO signal (m/z = 28) was subtracted by 10% of the total CO_2 signal (m/z = 44) to correct the CO fragment which originated from CO_2.

4.2.8 Inductive coupled plasma-atomic emission spectroscopy (ICP-AES) procedure

Bulk elemental compositions of the MRX and BG1 carbon supports were analyzed using the Thermo iCAP 7000 series ICP-EOS. In a typical experiment, 2 mL of concentrated H_2SO_4, 5 mL of concentrated HNO_3, and 1 to 5 mL of concentrated HF were added to 0.15 to 0.50 g of sample in a Teflon beaker. The beaker was put on a hotplate at a temperature below the softening point of Teflon (i.e., <300 °C). 10 mL of concentrated HCl and 30 mL of water were subsequently added to the beaker to ensure the digested material was dissolved into the solution. The solution was cooled to room temperature and transferred to a 100 mL volumetric flask. The sample was analyzed directly or through suitable dilution into the ICP instrument.

4.3 Results and Discussion

4.3.1 Effect of surface functional groups

Norit Darco MRX m-2278 was treated with both a high temperature treatment (HTTC) and an acid wash (AWC) after which the cobalt was added by impregnating the carbon support with a solution of cobalt nitrate. The high temperature treatment of carbon has been shown in literature to reduce oxygen surface functional groups and sulfur impurities whereas the acid wash treatment of carbon has been shown in literature to increase the oxygen content of carbon and oxidize the surface functional groups.[30-33] Prior to a reaction, the cobalt nitrate catalyst was pretreated at 230 °C in argon to make a carbon-supported cobalt oxide catalyst. The detailed synthesis procedures are discussed in detail in the experimental section. Ethylene oligomerization reactions were performed with these two cobalt oxide catalysts (CoO_x/HTTC and CoO_x/AWC) at 1.45 h contact time to compare their activities. Figure 4.1 shows that CoO_x/HTTC was stable for over 30 h TOS

with an average conversion of 15.0%. CoO_x/AWC was also stable for over 30 h TOS, however with an average conversion of only 8.2%.

We further performed ethylene oligomerization reaction over CoO_x/HTTC at 0.36 h contact time to compare the selectivities of these two catalysts at similar (5.0 – 8.2%) conversions. Figure 4.2a shows that the linear alpha olefin (LAO) isomer distributions up to C_{12} olefins from the CoO_x/HTTC were above 56.3% whereas they were only above 26.0% with the CoO_x/AWC. These results show that the oxidized surface functional groups, such as carboxylic acids, catalyze the isomerization of linear alpha olefins into linear internal olefins. The product linearities (Figure S4.1) from CoO_x/HTTC and CoO_x/AWC were above 96.9% and 96.0%, respectively. The slight difference in the product linearity was likely due to the conversion of linear internal olefins into branched olefins. The olefin chain length selectivities for these two catalysts are shown in Figure 4.2b. Both CoO_x/HTTC and CoO_x/AWC primarily produced C_4 olefins with 58.5% and 69.3% selectivities, respectively. CoO_x/AWC was more selective to shorter olefins (e.g., C_4 olefins) because it produced more linear internal olefins, which have low rates for oligomerization into larger linear alpha olefins. Xu et al. have studied co-feed experiments of 1-hexene and internal hexenes oligomerization over ammoniated cobalt oxide on carbon catalysts (CoO_x/N-C) demonstrating that internal olefins have lower activities than alpha olefins.[22] A mixture of 99% 1-hexene and 1% internal hexenes yielded 8.9% C_{12} olefins whereas a mixture of 12% 1-hexene and 88% internal hexenes yielded 2.9% C_{12} olefins at the same reaction conditions. These results are consistent with our result that CoO_x/AWC was less active than CoO_x/HTTC because it produced more linear internal olefins, which had lower oligomerization activity.

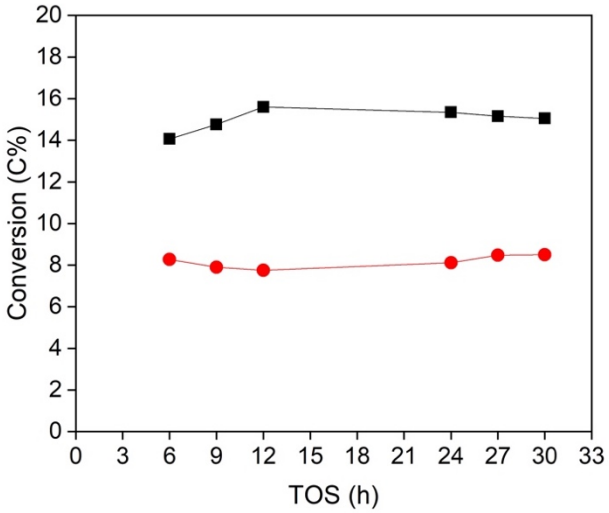

Figure 4.1 Ethylene conversions as a function of time on stream (TOS) of 12 wt% CoO_x/HTTC (black square) and 12 wt% CoO_x/AWC (red circle). Reaction conditions: 200 °C, 16 bar ethylene, 16 bar argon, and 1.45 h contact time.

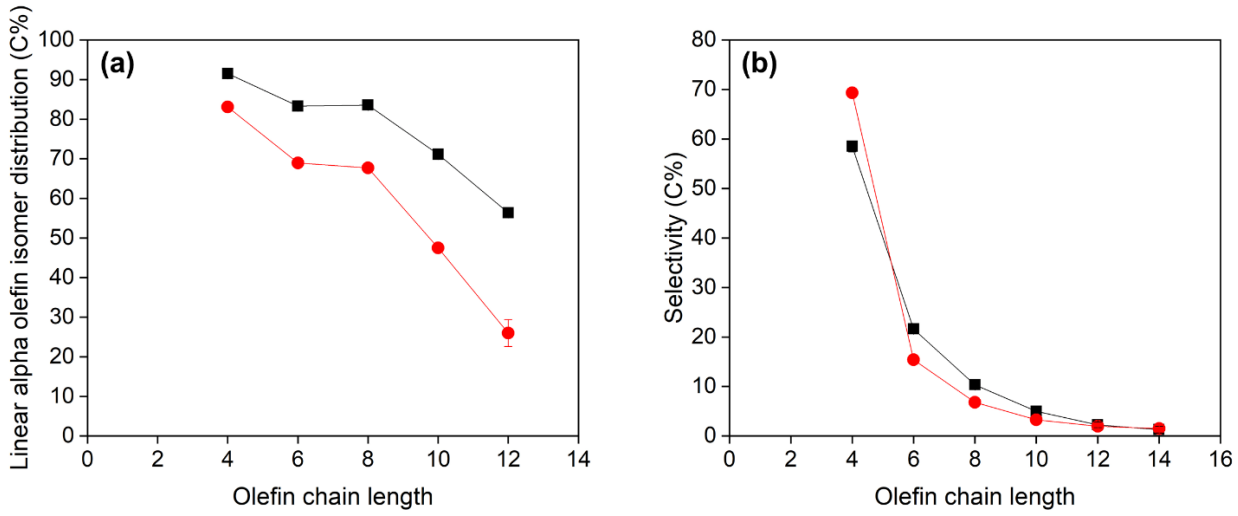

Figure 4.2 (a) Linear alpha olefin (LAO) isomer distributions and (b) selectivities to each olefin chain length from ethylene oligomerization over 12 wt% CoO_x/HTTC (black square) and 12 wt% CoO_x/AWC (red circle) at similar (5.0-8.2%) conversions. Reaction conditions for 12 wt% CoO_x/HTTC: 200 °C, 16 bar ethylene, 16 bar argon, 0.36 h contact time, and 5.0% average conversion. Reaction conditions for 12 wt% CoO_x/AWC: 200 °C, 16 bar ethylene, 16 bar argon, 1.45 h contact time, and 8.2% average conversion.

X-ray photoelectron spectroscopy (XPS) experiments were performed on both fresh CoO_x/HTTC and CoO_x/AWC without exposure to air to determine the surface cobalt phase of each catalyst prior to ethylene oligomerization. The XPS spectra of these fresh catalysts along with the spectra of Co_3O_4 and CoO are shown in Figure 4.3. Co_3O_4 and CoO can be distinguished by comparing the satellite peaks in the Co 2p region.[34] Co_3O_4 has one satellite peak at 790 eV whereas CoO has two satellite peaks at 786 and 802 eV. Both fresh CoO_x/HTTC and CoO_x/AWC predominantly show the characteristic of CoO with the CoO_x/AWC showing more prominent 786 and 802 eV satellite peaks. We have previously performed XPS without exposure to air of the spent CoO_x/HTTC after a 24 h reaction and showed that these 786 and 802 eV satellite peaks became more prominent after the oligomerization reaction, suggesting a higher fraction of CoO in the catalyst after the reaction.[24]

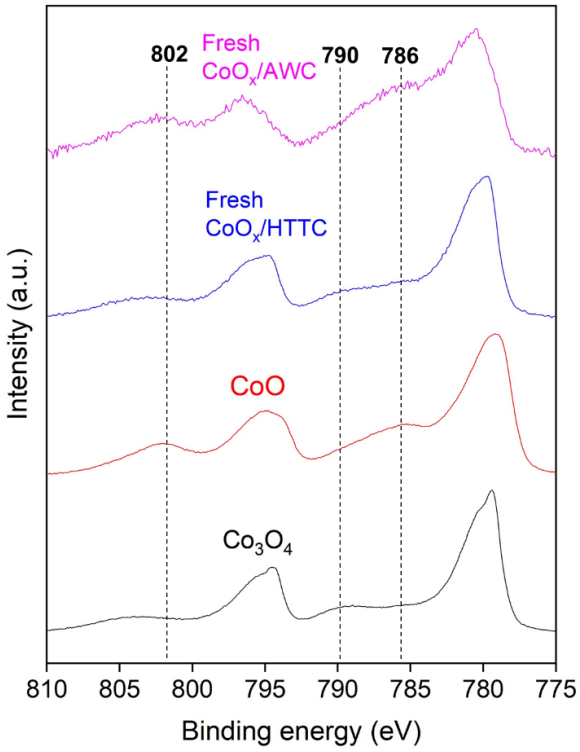

Figure 4.3 XPS spectra of fresh 12 wt% CoO_x/HTTC and fresh 12 wt% CoO_x/AWC along with Co_3O_4 and CoO standards. The XPS spectra of Co_3O_4 and CoO standards are adapted from literature.[24]

X-ray diffraction (XRD) experiments were performed on both fresh and spent catalysts after 30 h ethylene oligomerization. The XRD patterns of these catalysts and some standards (e.g., Co_3O_4, CoO, Co, polyethylene, and graphite) are shown in Figure 4.4. Both fresh CoO_x/HTTC and CoO_x/AWC show the reflections of Co_3O_4, suggesting the bulk cobalt phase was Co_3O_4 on both catalysts. However, both spent catalysts show reflections of CoO, suggesting the Co_3O_4 had been reduced to CoO during the oligomerization reactions. Therefore, the activity difference from CoO_x/HTTC and CoO_x/AWC is not due to the difference in the cobalt phase because both catalysts had the characteristics of CoO after reactions. The reflection characteristic of polyethylene was also observed on both spent catalysts, suggesting polyethylene was formed with relatively high

crystallinity. The presence of polyethylene was further confirmed by TGA of both spent catalysts under N_2, shown in Figure S4.2. The two spent catalysts have TGA peaks around 450 °C, consistent with the TGA peak of polyethylene.[35]

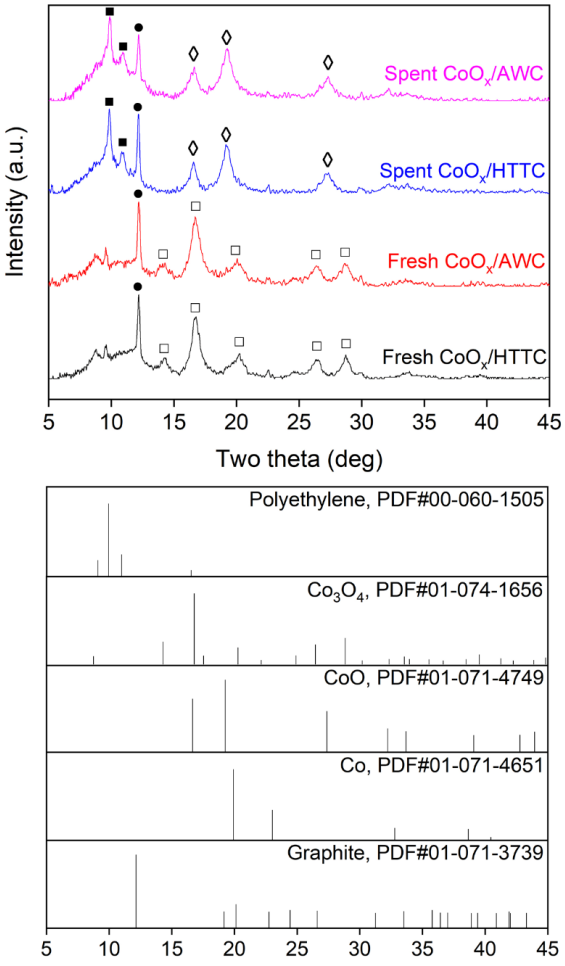

Figure 4.4 Mo-XRD patterns of fresh and spent 12 wt% CoO_x/HTTC and 12 wt% CoO_x/AWC. Characteristic peaks are carbon (graphite) – filled square, polyethylene – filled square, Co_3O_4 – unfilled square, CoO – unfilled diamond. The Mo-XRD patterns of the standards are adapted from literature.[25]

The crystallite sizes of Co_3O_4 and CoO from the fresh and spent catalysts were calculated using the Scherrer's equation at two theta angles of 16.7° and 19.2°, respectively. Table 4.1 shows that the Co_3O_4 crystallite sizes of the fresh CoO_x/HTTC and CoO_x/AWC were 5.1 nm and 4.4 nm, respectively. After the reactions where Co_3O_4 had been reduced to CoO, the CoO crystallite sizes of the spent CoO_x/HTTC and CoO_x/AWC were 4.6 nm and 4.0 nm, respectively. These results show that CoO_x/HTTC was more active than CoO_x/AWC even with larger CoO_x crystallite sizes. The smaller CoO_x crystallite sizes from the CoO_x/AWC can be explained by higher adsorption of Co^{2+} ion during the impregnation of the carbon support because of the electronegativity of the oxygen surface functional groups. As a result, the metal dispersion increased whereas the crystallite size decreased. This phenomenon has been reported previously in the literature for synthesis of carbon-supported transition metal catalysts.[29,33,36]

N_2 physisorption experiments were performed on both HTTC and AWC in the absence of cobalt to measure the BET surface area and the pore size distribution of the catalyst supports. Table 4.1 shows that the BET surface areas of both HTTC and AWC were similar at 564 and 547 $m^2 g^{-1}$, respectively. The BJH pore size distributions of these two carbon supports, shown in Figure S4.3 were also similar with a peak at 4 nm. Therefore, the BET surface areas and the BJH pore size distributions of these carbon supports did not influence the activity difference of the catalysts. We also performed XPS on both HTTC and AWC to compare the support elemental compositions, shown in Table 4.1. The carbon, oxygen, and nitrogen contents of HTTC were 96.1%, 3.0%, and 0.9%, respectively whereas they were 81.8%, 16.8%, and 1.4%, respectively in AWC. The higher oxygen content in the AWC was expected because the carbon support was oxidized in nitric acid. In addition, the nitrogen content in the AWC was slightly higher after the acid wash treatment with nitric acid.

Table 4.1 High-temperature-treated carbon (HTTC) and acid-washed carbon (AWC) BET surface areas by N_2 physisorption, Co_3O_4 crystallite sizes on fresh 12 wt% Co_3O_4/C, CoO crystallite sizes on spent 12 wt% CoO/C, and surface elemental analyses by XPS.

Catalyst support	**Co_3O_4 crystallite size on fresh 12 wt% CoO_x/C (nm)**	**CoO crystallite size on spent 12 wt% CoO_x/C (nm)**	**BET surface area (m^2 g^{-1})**	**Surface elemental analysis (mol%)**		
				C	O	N
HTTC	5.1	4.6	564	96.1	3.0	0.9
AWC	4.4	4.0	547	81.8	16.8	1.4

Temperature-programmed desorption (TPD) experiments under argon were performed on both HTTC and AWC to probe the oxygen functional groups on both carbon supports. Additionally, a TPD experiment was also performed on the regular carbon support (C) to determine whether the high temperature treatment of carbon reduced the oxygen functional groups of the carbon support. The evolutions of both CO and CO_2 could determine specific oxygen functional groups on the carbon support. It has been reported that the peak assignment of either CO and CO_2 to a specific oxygen functional group depends on the gas flow rate, the temperature ramp, and the structure of the material.[37,38] Therefore, a certain range of temperature was used to assign a CO or CO_2 peak to a certain oxygen functional group. Figure 4.5a shows the desorption of CO_2 from regular carbon (C), high-temperature-treated carbon (HTTC), and acid-washed carbon (AWC). Both C and HTTC had broad CO_2 peaks from 50 to 900 °C with the maximum CO_2 flow rates of 0.002 and 0.0007 mmol min^{-1} g_{cat}^{-1}, respectively. In contrast, the AWC had two peaks around 350 °C and 650 °C with the CO_2 flow rates of 0.037 and 0.011 mmol min^{-1} g_{cat}^{-1}, respectively. The peaks around 350 and 650 °C are consistent with the characteristic peaks of carboxylic acids and lactones, respectively.[37-40] Figure 4.5b shows the desorption of CO from regular carbon (C), high-

temperature-treated carbon (HTTC), and acid-washed carbon (AWC). All carbon supports had increasing CO flow rates during the temperature ramp from 50 to 850 °C. The CO flow rates at 850 °C from C, HTTC, and AWC were 0.017, 0.003, and 0.061 mmol min^{-1} g_{cat}^{-1}, respectively. The peak assignment of CO above 600 °C is relatively difficult since it can be attributed to phenols, carbonyls, ethers, and quinones.[37-39] Both Figures 4.5a-b show that the acid wash treatment of carbon increased the oxygen content and oxidized the surface functional groups whereas the high temperature treatment of carbon reduced the oxygen content and the surface functional groups.

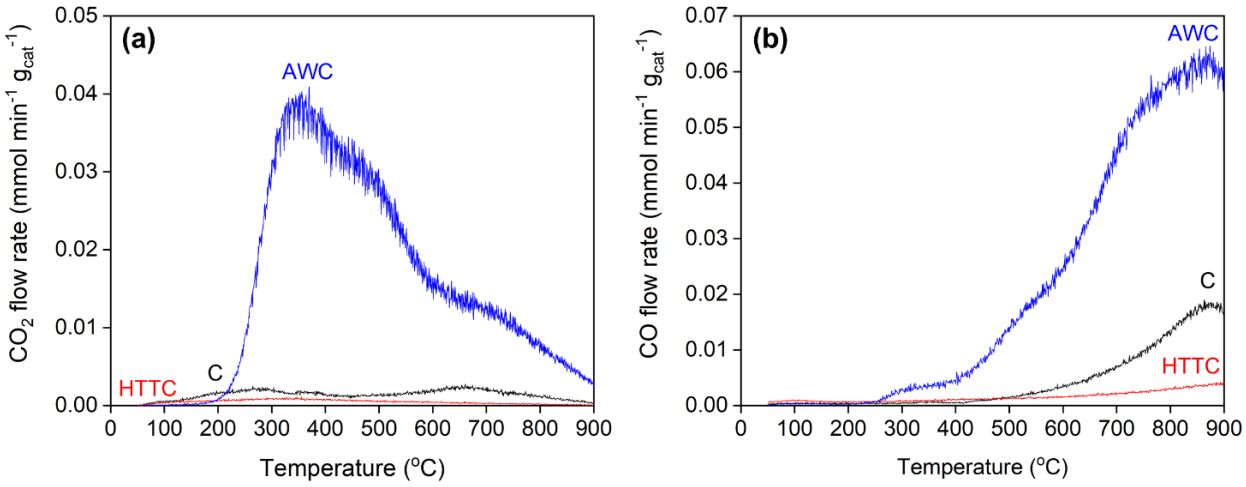

Figure 4.5 Temperature-programmed desorption (TPD) experiments of regular carbon support (C), high-temperature-treated carbon (HTTC), and acid-washed carbon (AWC). (a) CO_2 flow rate as a function of temperature. (b) CO flow rates as a function of temperature. Reaction conditions: 0.1 g of sample, 50 cm^3 (STP) min^{-1} of argon, and 10 °C min^{-1} ramp rate.

We also performed TPD experiments on cobalt nitrate on both HTTC and AWC supports ($Co(NO_3)_2$/HTTC and $Co(NO_3)_2$/AWC). Figures 4.6a-b show the evolution of CO_2 and CO as a function of temperature, respectively. Both $Co(NO_3)_2$/HTTC and $Co(NO_3)_2$/AWC had two CO_2 peaks around 220 and 560 °C. The CO_2 flow rates around 220 °C from $Co(NO_3)_2$/HTTC and

$Co(NO_3)_2$/AWC were 0.15 and 0.41 mmol min^{-1} g_{cat}^{-1}, respectively. The higher CO_2 flow rate from $Co(NO_3)_2$/AWC around 220 °C could be attributed to the reduction of Co_3O_4 to CoO as observed by XPS on the fresh catalysts after pretreatment in argon at 230 °C. We have recently shown that Co metal was formed as the major cobalt phase around the temperature of the second CO_2 peak.[25] Figure 4.6b shows that both catalysts still produced CO even at 900 °C.

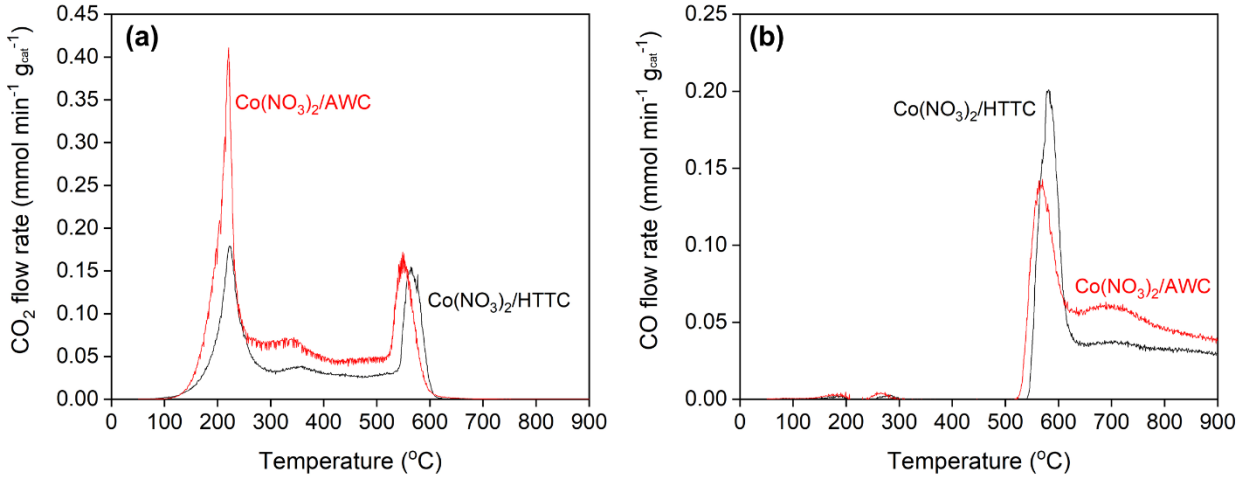

Figure 4.6 Temperature-programmed desorption (TPD) experiments of 12 wt% $Co(NO_3)_2$/HTTC and 12 wt% $Co(NO_3)_2$/AWC. (a) CO_2 flow rate as a function of temperature. (b) CO flow rates as a function of temperature. Reaction conditions: 0.1 g of sample, 50 cm^3 (STP) min^{-1} of argon, and 10 °C min^{-1} ramp rate.

4.3.2 Effect of catalyst support particle size

In addition to the surface functional groups, the effect of catalyst support particle size towards the product selectivity of the catalyst was also investigated with CoO_x/HTTC. Iglesia et al. reported that the product selectivity from Fischer Tropsch synthesis reactions can be tuned to larger hydrocarbons by imposing transport restrictions to the products while maintaining the reactant to be kinetically limited.[41,42] They proposed a transport parameter, χ which is proportional

to square of the catalyst support particle size, the void fraction, the Co site density per unit area, and inversely proportional to the average pore radius. In this study, we varied the catalyst support particle size from 425 to 925 μm because the change in the catalyst support particle size contributes the largest in the χ parameter. At the same 1.45 h contact time, the average ethylene conversions from these catalysts varied from 13.3 to 16.0% (Figure S4.4a). At these similar conversions, the product selectivities (Figure S4.4b), the LAO isomer distributions (Figure S4.4c), and the product linearities (Figure S4.4d) of each olefin chain length from these catalysts were similar, suggesting the product selectivity from olefin oligomerization with this catalyst cannot be tuned by varying the χ parameter. This is likely due to the presence of the polyethylene and other oligomers on the catalyst surface.

4.3.3 Effect of different carbon supports

Two different activated carbon supports, Norit Darco MRX (MRX) and Darco BG1 (BG1) were used to prepare cobalt supported on carbon catalysts. Both carbon supports were treated at 900 °C for 2 h in helium to reduce sulfur impurities and oxygen surface functional groups.[32] The high-temperature-treated carbon supports were subsequently impregnated with a solution of cobalt nitrate to obtain a 12 wt% Co loading while being exposed to air. Each catalyst was pretreated at 230 °C in argon prior to reaction to make either CoO_x/MRX being on the MRX support or CoO_x/BG1 being on the BG1 support. Ethylene oligomerization reactions were performed with these two catalysts at 200 °C, 32 bar, and 1.45 h contact time to compare their activities. Figure 4.7 shows both catalysts were stable for over 24 h time on stream (TOS). However, CoO_x/MRX had an average ethylene conversion of 15.0% whereas CoO_x/BG1 had an average conversion of only 2.6%. We further performed ethylene oligomerization with the CoO_x/MRX at 0.36 h contact

time to compare the selectivities of these two catalysts at similar (2.6-5.0%) conversions. At these similar conversions, the product selectivities (Figure 4.8), the linear alpha olefin (LAO) isomer distributions (Figure S4.5), and the product linearities (Figure S4.6) from these two catalysts were similar. We hypothesize that the difference in activity by a factor of six from these two catalysts at the same reaction conditions could be influenced by the cobalt oxidation state as well as the impurities from the carbon supports.

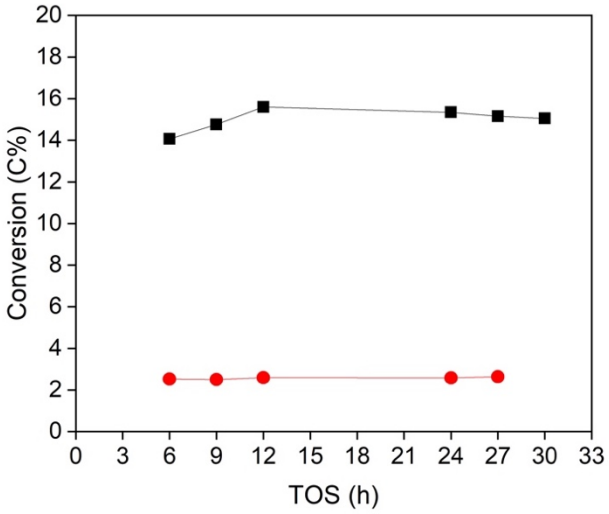

Figure 4.7 Ethylene conversions as a function of time on stream (TOS) of 12 wt% CoO_x/MRX (black square) and 12 wt% CoO_x/BG1 (red circle). Reaction conditions: 200 °C, 16 bar ethylene, 16 bar argon, and 1.45 h contact time.

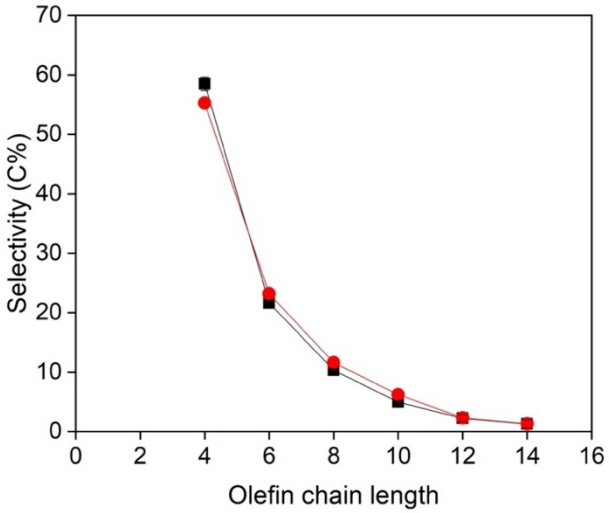

Figure 4.8 Selectivities to each olefin chain length from ethylene oligomerization over 12 wt% CoO_x/MRX (black square) and 12 wt% CoO_x/BG1 (red circle) at similar (2.6-5.0%) conversions. Reaction conditions for 12 wt% CoO_x/MRX: 200 °C, 16 bar ethylene, 16 bar argon, 0.36 h contact time, and 5.0% average conversion. Reaction conditions for 12 wt% CoO_x/BG1: 200 °C, 16 bar ethylene, 16 bar argon, 1.45 h contact time, and 2.6% average conversion.

X-ray photoelectron spectroscopy (XPS) experiments were performed on these two fresh catalysts without exposure to air to obtain the surface cobalt phase on both catalysts, shown in Figure 4.9. These two fresh catalysts have predominantly CoO phase, suggesting that the carbon supports from these two catalysts had a similar influence towards the surface cobalt phase. In addition to XPS, X-ray diffraction (XRD) experiments were also performed on the fresh and spent CoO_x/MRX and CoO_x/BG1 to obtain the bulk cobalt phase of each catalyst, shown in Figure 4.10. Both fresh catalysts show the characteristic reflection of Co_3O_4. After the reaction at 200 °C, the bulk cobalt phase on both catalysts became CoO, consistent with the CoO being the stable cobalt phase. Because CoO was the cobalt phase on both catalysts after the reaction at 200 °C, the activity difference between these two catalysts was likely not influenced by the cobalt phase. However,

Figure 4.10 shows that the spent CoO_x/MRX had the characteristic reflection of polyethylene whereas it was not observed on the spent CoO_x/BG1. The difference in the reflection of polyethylene could be explained by two reasons. First, CoO_x/MRX produced more polyethylene than CoO_x/BG1. Second, the polyethylene produced by the CoO_x/MRX had higher crystallinity than the polyethylene from the CoO_x/BG1. Both spent catalysts were analyzed by TGA (Figure S4.7) under N_2 to determine the amount of carbon deposition on the spent catalysts. The spent CoO_x/MRX lost 30% of its initial weight whereas the spent CoO_x/BG1 lost 21% of its initial weight during the temperature ramp to 700 °C, consistent with more carbon deposition with the more active catalyst. Both spent catalysts had TGA peaks around 450 °C, suggesting polyethylene was present on both spent catalysts.

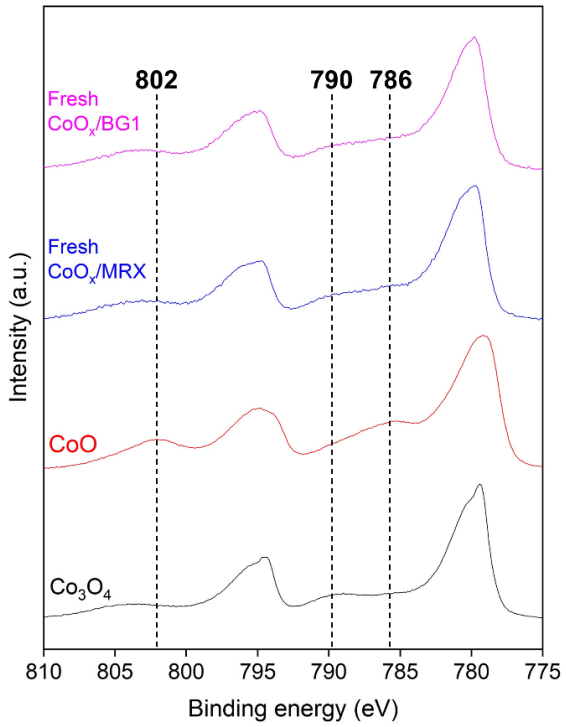

Figure 4.9 XPS spectra of fresh 12 wt% CoO_x/MRX and fresh 12 wt% CoO_x/BG1 along with Co_3O_4 and CoO standards. The XPS spectra of Co_3O_4 and CoO standards are adapted from literature.[24]

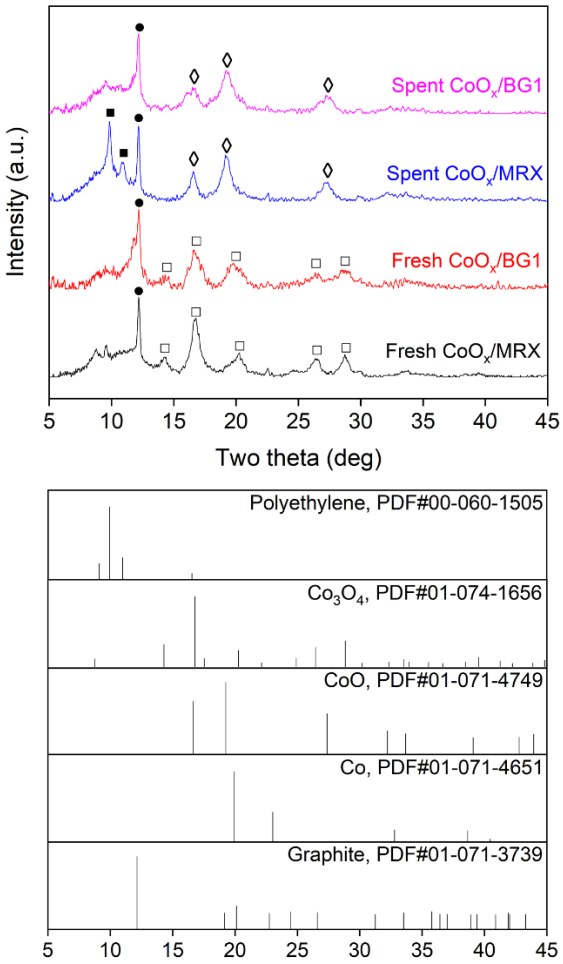

Figure 4.10 Mo-XRD patterns of fresh and spent 12 wt% CoO_x/MRX and 12 wt% CoO_x/BG1. Characteristic peaks are carbon (graphite) – filled square, polyethylene – filled square, Co_3O_4 – unfilled square, CoO – unfilled diamond. The Mo-XRD patterns of the standards are adapted from literature.[25]

The crystallite sizes of Co_3O_4 and CoO from the fresh and spent CoO_x/MRX and CoO_x/BG1 were compared using the Scherrer's equation at two theta angles of 16.7° and 19.2°, respectively. Prior to the reactions, the Co_3O_4 crystallite sizes of the CoO_x/MRX and the CoO_x/BG1 were 5.1 and 3.2 nm, respectively. After the reaction, the CoO crystallite sizes were 4.6 nm and 3.1 nm, respectively. These results show that although the CoO_x/MRX was more active

by a factor of six, the crystallite sizes were larger by ~50%. Therefore, the difference in the crystallite sizes of these two catalysts did not explain the activity difference between these two catalysts. N_2 physisorption experiments were performed on both MRX high-temperature-treated carbon (HTTC) and BG1 HTTC. The BJH pore size distributions of these two HTTC supports, shown in Figure S4.8 were similar with a peak at 4 nm, suggesting the activity difference was not influence by the pore structure. The BET surface areas of the MRX HTTC and the BG1 HTTC were 564 $m^2\ g^{-1}$ and 452 $m^2\ g^{-1}$, respectively which could partially explain why the CoO_x/MRX was more active than the CoO_x/BG1.

We analyzed the bulk elemental compositions of both MRX HTTC and BG1 HTTC to determine the levels of impurities that were present on both carbon supports. Table 4.2 shows that higher levels of impurities were present on the BG1 HTTC than on the MRX HTTC, especially Al, Ca, Fe, and Mg. The biggest difference in the impurity levels for these two carbon supports was in the amount of Ca. MRX HTTC only had 2,072 ppm of Ca whereas the BG1 HTTC had 33,615 ppm of Ca. We hypothesize that the higher amount of at least one of these impurities contributes to the activity difference between the two carbon-supported cobalt oxide catalysts.

Table 4.2 Bulk elemental compositions of MRX HTTC and BG1 HTTC by ICP-AES.

Element	Amount (ppm by weight)	
	MRX HTTC	BG1 HTTC
Al	5,092	12,685
Ca	2,072	33,615
Fe	2,518	16,530
K	497	885
Li	<49	<49
Mg	741	6,304
Mn	<49	203
Na	1,184	1,357

4.4 Conclusions

High-temperature-treated carbon-supported cobalt oxide catalyst (CoO_x/HTTC) is nearly twice as active as the acid-washed carbon-supported cobalt oxide catalyst (CoO_x/AWC) due to more linear alpha olefin formation which results in higher oligomerization activity. Both catalysts had CoO as the cobalt phase after reactions, suggesting the activity difference between these two catalysts was not related to the cobalt phase. The CoO_x crystallite sizes from CoO_x/AWC were smaller than the CoO_x crystallite sizes from CoO_x/HTTC even though the CoO_x/HTTC catalyst had a higher activity. TPD and XPS experiments showed that the high temperature treatment reduced the oxygen content of the carbon support whereas the acid wash treatment of carbon increased the oxygen content by oxidizing the surface functional groups. The catalyst support particle size of CoO_x/HTTC was varied from 425 to 925 μm to impose more transport restrictions to the products, however, the product selectivities remained similar. The oligomerization activity

is higher by a factor of six when the cobalt is supported on a carbon with lower Al, Ca, Fe, and Mg impurities, suggesting at least one of these impurities lowers the oligomerization activity.

4.5 References

1. E. O. C. Greiner, M. Blagoev and Y. Yamaguchi, *Chemical Economics Handbook: Linear alpha-Olefins*, IHS Chemical, 2013.
2. G. R. Lappin, L. H. Nemec, J. D. Sauer and J. D. Wagner, *Kirk-Othmer Encyclopedia of Chemical Technology*, John Wiley & Sons, Inc., 2000.
3. N. M. Eagan, M. D. Kumbhalkar, J. S. Buchanan, J. A. Dumesic and G. W. Huber, Chemistries and processes for the conversion of ethanol into middle-distillate fuels, *Nat. Rev. Chem.*, 2019, **3**, 223-249.
4. N. Rahimi and R. Karimzadeh, Catalytic cracking of hydrocarbons over modified ZSM-5 zeolites to produce light olefins: A review, *Appl. Catal. A*, 2011, **398**, 1-17.
5. M. Balat and H. Balat, Recent trends in global production and utilization of bio-ethanol fuel, *Appl. Energy*, 2009, **86**, 2273-2282.
6. K. Kohse-Höinghaus, P. Oßwald, T. A. Cool, T. Kasper, N. Hansen, F. Qi, C. K. Westbrook and P. R. Westmoreland, Biofuel combustion chemistry: from ethanol to biodiesel, *Angew. Chem. Int. Ed.*, 2010, **49**, 3572-3597.
7. A. Forestière, H. Olivier-Bourbigou and L. Saussine, Oligomerization of monoolefins by homogeneous catalysts, *Oil Gas Sci. Technol.,* 2009, **64**, 649-667.
8. R. Y. Brogaard and U. Olsbye, Ethene oligomerization in Ni-containing zeolites: theoretical discrimination of reaction mechanisms, *ACS Catal.*, 2016, **6**, 1205-1214.
9. S. Moussa, P. Concepción, M. A. Arribas and A. Martínez, Nature of active sites and initiation mechanism for ethylene oligomerization on heterogeneous Ni-beta catalysts, *ACS Catal.*, 2018, **8**, 3903-3912.
10. C. P. Nicholas, Applications of light olefin oligomerization to the production of fuels and chemicals, *Appl. Catal. A*, 2017, **543**, 82-97.
11. A. N. Mlinar, G. B. Baur, G. G. Bong and A. T. Bell, Propene oligomerization over Ni-exchanged Na-X zeolites, *J. Catal.*, 2012, **296**, 156-164.
12. I. Agirrezabal-Telleria and E. Iglesia, Stabilization of active, selective, and regenerable Ni-based dimerization catalysts by condensation of ethene withinordered mesopores, *J. Catal.*, 2017, **352**, 505-514.
13. E. D. Metzger, R. J. Comito, Z. Wu, G. Zhang, R. C. Dubey, W. Xu, J. T. Miller and M. Dincă, Highly selective heterogeneous ethylene dimerization with a scalable and chemically robust MOF catalyst, *ACS Sustain. Chem. Eng.*, 2019, **7**, 6654-6661.
14. A. Finiels, F. Fajula and V. Hulea, Nickel-based solid catalysts for ethylene oligomerization - a review, *Catal. Sci. Technol.*, 2014, **4**, 2412-2426.
15. R. Joshi, G. Zhang, J. T. Miller and R. Gounder, Evidence for the coordination-insertion mechanism of ethene dimerization at nickel cations exchanged onto beta molecular sieves, *ACS Catal.*, 2018, **8**, 11407-11422.
16. A. Ehrmaier, Y. Liu, S. Peitz, A. Jentys, Y.-H. Chin, M. Sanchez-Sanchez, R. Bermejo-Deval and J. A. Lercher, Dimerization of Linear Butenes on Zeolite-Supported Ni^{2+}, *ACS Catal.*, 2019, **9**, 315-324.

17. H. Olivier-Bourbigou, P. A. R. Breuil, L. Magna, T. Michel, M. F. Espada Pastor and D. Delcroix, Nickel Catalyzed Olefin Oligomerization and Dimerization, *Chem. Rev.*, 2020, **120**, 7919-7983.
18. R. G. Schultz, J. M. Schuck and B. S. Wildi, Olefin dimerization over cobalt-oxide-on-carbon catalysts: I. Propylene dimerization, *J. Catal.*, 1966, **6**, 385-396.
19. R. G. Schultz, R. M. Engelbrecht, R. N. Moore and L. T. Wolford, Olefin dimerization over cobalt-oxide-on-carbon catalysts: II. Butene and hexene dimerization, *J. Catal.*, 1966, **6**, 419-424.
20. R. G. Schultz, Olefin dimerization over cobalt-oxide-on-carbon catalysts: III. Oligomerization of ethylene, *J. Catal.*, 1967, **7**, 286-290.
21. Z. Xu, J. P. Chada, D. Zhao, C. A. Carrero, Y. T. Kim, D. C. Rosenfeld, J. L. Rogers, S. J. Rozeveld, I. Hermans and G. W. Huber, Production of linear octenes from oligomerization of 1-butene over carbon-supported cobalt catalysts, *ACS Catal.*, 2016, **6**, 3815–3825.
22. Z. Xu, D. Zhao, J. P. Chada, D. C. Rosenfeld, J. L. Rogers, I. Hermans and G. W. Huber, Olefin conversion on nitrogen-doped carbon-supported cobalt catalyst: Effect of feedstock, *J. Catal*, 2017, **354**, 213-222.
23. Z. Xu, J. P. Chada, L. Xu, D. Zhao, D. C. Rosenfeld, J. L. Rogers, I. Hermans, M. Mavrikakis and G. W. Huber, Ethylene dimerization and oligomerization to 1-butene and higher olefins with chromium-promoted cobalt on carbon catalyst, *ACS Catal.*, 2018, **8**, 2488-2497.
24. A. Jonathan, N. M. Eagan, D. L. Bruns, S. S. Stahl, M. P. Lanci, J. A. Dumesic and G. W. Huber, Ethylene oligomerization into linear olefins over cobalt oxide on carbon catalyst, *Catal. Sci. Technol.*, 2021, **11**, 3599-3608.
25. A. Jonathan, E. G. Tomashek, M. P. Lanci, J. A. Dumesic and G. W. Huber, Reaction kinetics study of ethylene oligomerization into linear olefins over carbon-supported cobalt catalysts, *J. Catal.*, 2021, DOI: https://doi.org/10.1016/j.jcat.2021.05.035.
26. I. C. Gerber and P. Serp, A theory/experience description of support effects in carbon-supported catalysts, *Chem. Rev.*, 2019, **120**, 1250-1349.
27. P. U. Karanjkar, S. P. Burt, X. Chen, K. J. Barnett, M. R. Ball, M. D. Kumbhalkar, X. Wang, J. B. Miller, I. Hermans, J. A. Dumesic and G. W. Huber, Effect of carbon supports on RhRe bifunctional catalysts for selective hydrogenolysis of tetrahydropyran-2-methanol, *Catal. Sci. Technol.*, 2016, **6**, 7841-7851.
28. E. Auer, A. Freund, J. Pietsch and T. Tacke, Carbons as supports for industrial precious metal catalysts, *Appl. Catal. A*, 1998, **173**, 259-271.
29. F. Coloma, A. Sepúlveda-Escribano, J. L. G. Fierro and F. Rodríguez-Reinoso, Gas phase hydrogenation of crotonaldehyde over Pt/activated carbon catalysts. Influence of the oxygen surface groups on the support, *Appl. Catal. A*, 1997, **150**, 165-183.
30. Y. Otake and R. G. Jenkins, Characterization of oxygen-containing surface complexes created on a microporous carbon by air and nitric acid treatment, *Carbon*, 1993, **31**, 109-121.
31. P. Vinke, M. van der Eijk, M. Verbree, A. F. Voskamp, and H. van Bekkum, Modification of the surfaces of a gasactivated carbon and a chemically activated carbon with nitric acid, hypochlorite, and ammonia, *Carbon*, 1994, **32**, 675-686.
32. P. E. Fanning and M. A. Vannice, A DRIFTS study of the formation of surface groups on carbon by oxidation, *Carbon*, 1993, **31**, 721-730.
33. I. Gerber, M. Oubenali, R. Bacsa, J. Durand, A. Gonçalves, M. F. R. Pereira, F. Jolibois, L. Perrin, R. Poteau and P. Serp, Theoretical and Experimental Studies on the Carbon-Nanotube

Surface Oxidation by Nitric Acid: Interplay between Functionalization and Vacancy Enlargement, *Chem. Eur. J.*, 2011, **17**, 11467-11477.
34. D. Gu, C. -J. Jia, C. Weidenthaler, H. -J. Bongard, B. Spliethoff, W. Schmidt and F. Schüth, Highly ordered mesoporous cobalt-containing oxides: structure, catalytic properties, and active sites in oxidation of carbon monoxide, *J. Am. Chem. Soc.*, 2015, **137**, 11407-11418.
35. D. Zhao, X. Wang, J. B. Miller and G. W. Huber, The chemistry and kinetics of polyethylene pyrolysis: a process to produce fuels and chemicals, *ChemSusChem*, 2020, **13**, 1764-1774.
36. F. Coloma, A. Sepulveda-Escribano, J. L. G. Fierro and F. Rodriguez-Reinoso, Preparation of platinum supported on pregraphitized carbon blacks, *Langmuir*, 1994, **10**, 750-755.
37. S. Kundu, Y. Wang, W. Xia and M. Muhler, Thermal stability and reducibility of oxygen-containing functional groups on multiwalled carbon nanotube surfaces: a quantitative high-resolution XPS and TPD/TPR study, *J. Phys. Chem. C*, 2008, **112**, 16869-16878.
38. J. L. Figueiredo, M. F. R. Pereira, M. M. A. Freitas and J. J. M Orfao, Modification of the surface chemistry of activated carbons, *Carbon*, 1999, **37**, 1379-1389.
39. M. L. Toebes, J. M. P. van Heeswijk, J. H. Bitter, A. J. van Dillen and K. P. de Jong, The influence of oxidation on the texture and the number of oxygen-containing surface groups of carbon nanofibers, *Carbon*, 2004, **42**, 307-315.
40. P. Brender, R. Gadiou, J.-C. Rietsch, P. Fioux, J. Dentzer, A. Ponche and C. Vix-Guterl, Characterization of carbon surface chemistry by combined temperature programmed desorption with in situ X-ray photoelectron spectrometry and temperature programmed desorption with mass spectrometry analysis, *Anal. Chem.*, 2012, **84**, 2147-2153.
41. E. Iglesia, S. C. Reyes, R. J. Madon and S. L. Soled, Selectivity control and catalyst design in the Fischer-Tropsch synthesis: sites, pellets, and reactors, *Adv. Catal.*, 1993, **39**, 221-302.
42. E. Iglesia, Design, synthesis, and use of cobalt-based Fischer-Tropsch synthesis catalysts, *Appl. Catal. A*, 1997, **161**, 59-78.

4.6 Supplementary Information

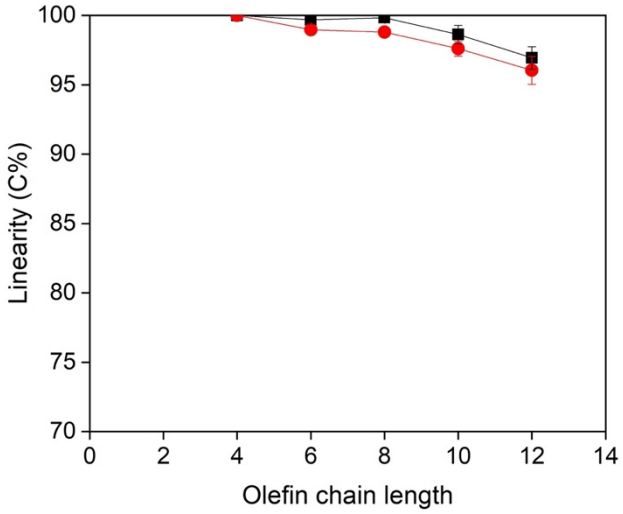

Figure S4.1 Product linearities of each olefin chain length from ethylene oligomerization over 12 wt% CoO_x/HTTC (black square) and 12 wt% CoO_x/AWC (red circle) at similar (5.0-8.2%) conversions. Reaction conditions for 12 wt% CoO_x/HTTC: 200 °C, 16 bar ethylene, 16 bar argon, 0.36 h contact time, and 5.0% average conversion. Reaction conditions for 12 wt% CoO_x/AWC: 200 °C, 16 bar ethylene, 16 bar argon, 1.45 h contact time, and 8.2% average conversion.

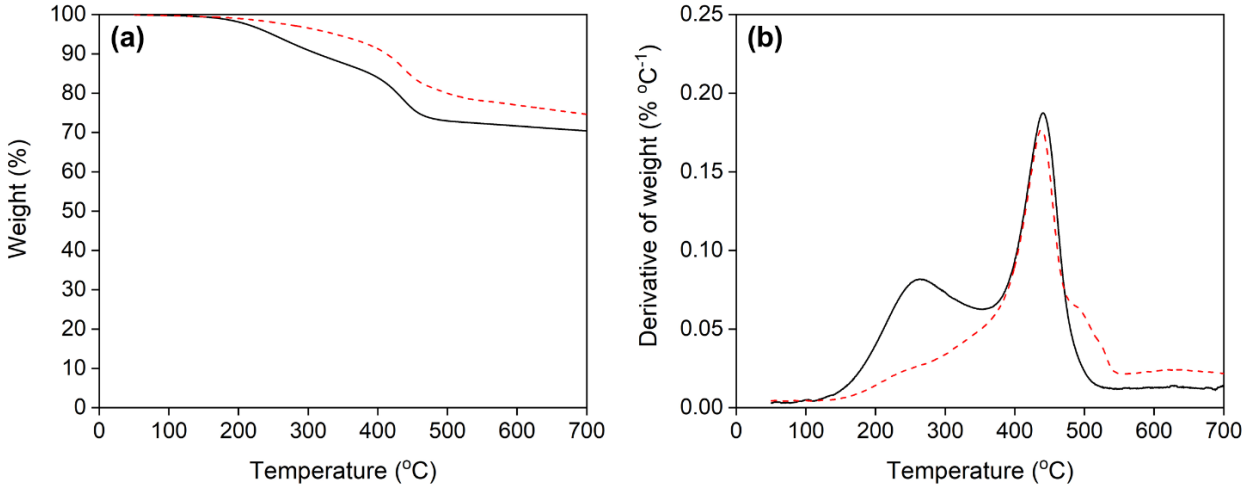

Figure S4.2 Thermogravimetric analysis (TGA) curves of the spent 12 wt% CoO_x/HTTC (black solid line) and the spent 12 wt% CoO_x/AWC (red dashed line) after reactions at 200 °C, 16 bar ethylene, 16 bar argon, and 1.45 h contact time. TGA conditions: 50 cm^3 (STP) min^{-1} of N_2, 10 °C min^{-1} ramp rate, and ~10 mg sample. (a) Weight percent versus temperature. (b) Derivative of weight percent versus temperature.

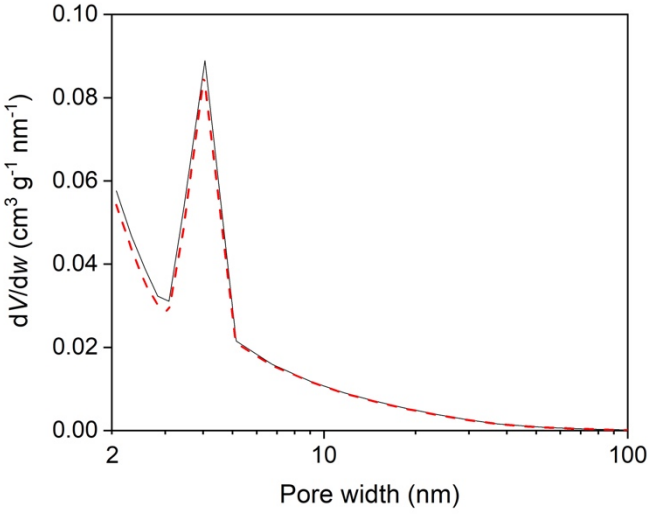

Figure S4.3 BJH pore size distributions of HTTC (black solid line) and AWC (red dashed line).

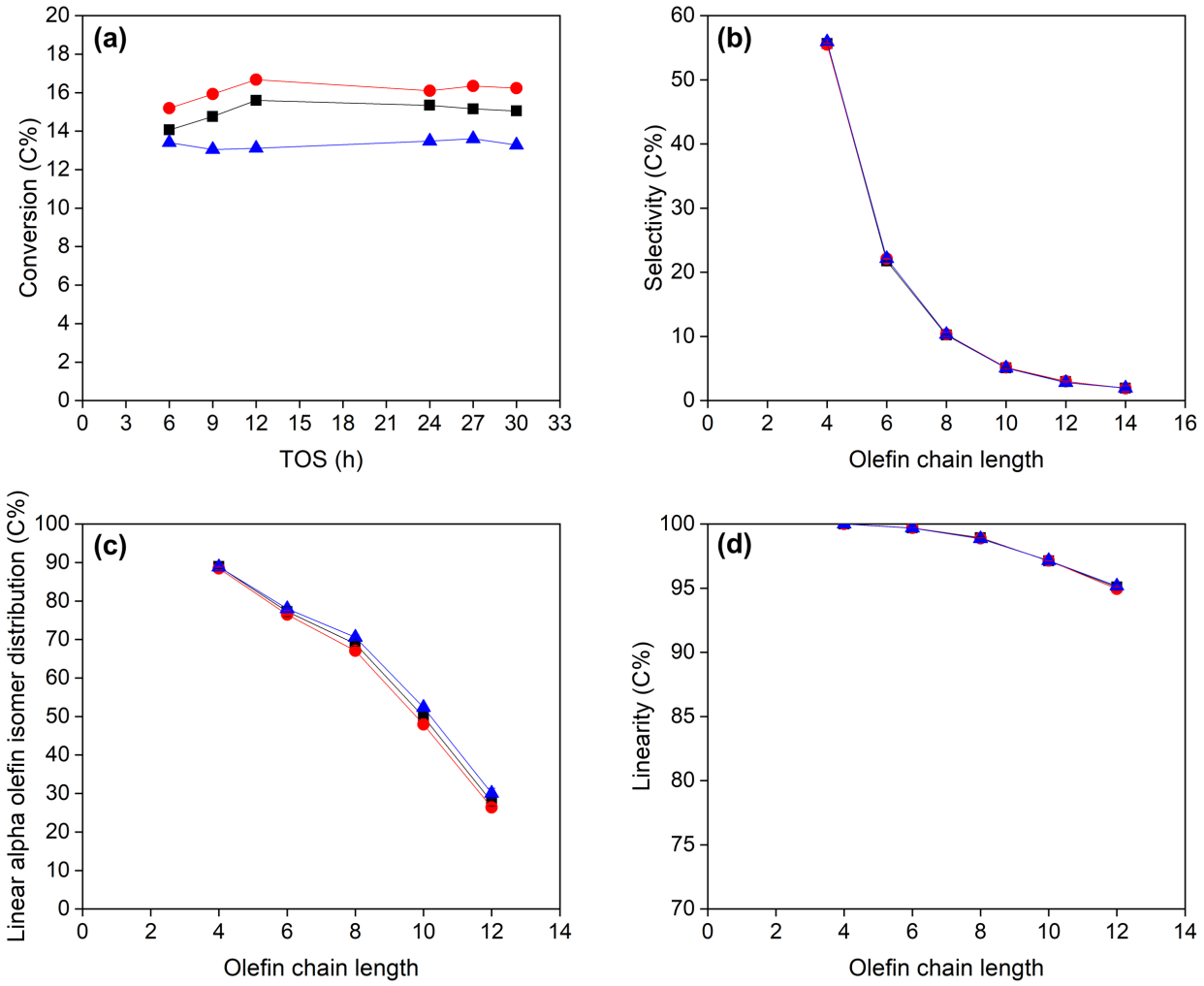

Figure S4.4 Ethylene conversions and product selectivities with 12 wt% CoO_x/HTTC and 425 µm (black square), 725 µm (red circle), and 925 µm (blue triangle) particle sizes. (a) Ethylene conversions as a function of time on stream (TOS). (b) Product selectivities to each olefin chain length. (c) Linear alpha olefin (LAO) isomer distributions of each olefin chain length. (d) Product linearities of each olefin chain length. Reaction conditions: 200 °C, 16 bar ethylene, 16 bar argon, and 1.45 h contact time.

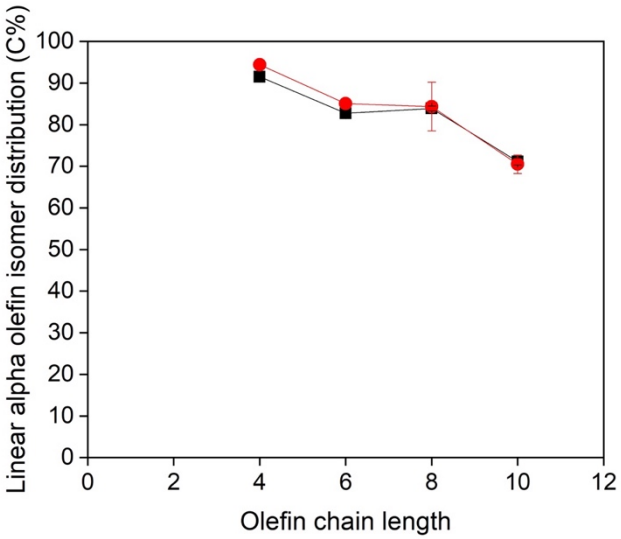

Figure S4.5 Linear alpha olefin (LAO) isomer distributions of each olefin chain length from ethylene oligomerization over 12 wt% CoO_x/MRX (black square) and 12 wt% CoO_x/BG1 (red circle) at similar (2.6-5.0%) conversions. Reaction conditions for 12 wt% CoO_x/MRX: 200 °C, 16 bar ethylene, 16 bar argon, 0.36 h contact time, and 5.0% average conversion. Reaction conditions for 12 wt% CoO_x/BG1 (red circle): 200 °C, 16 bar ethylene, 16 bar argon, 1.45 h contact time, and 2.6% average conversion.

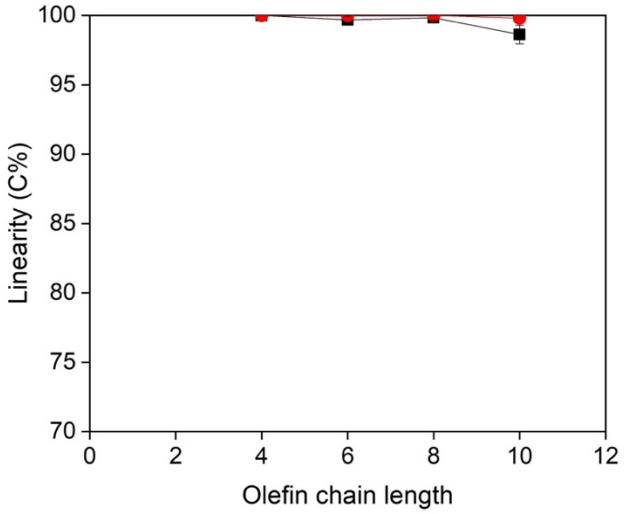

Figure S4.6 Product linearities of each olefin chain length from ethylene oligomerization over 12 wt% CoO_x/MRX (black square) and 12 wt% CoO_x/BG1 (red circle) at similar (2.6-5.0%) conversions. Reaction conditions for 12 wt% CoO_x/MRX: 200 °C, 16 bar ethylene, 16 bar argon, 0.36 h contact time, and 5.0% average conversion. Reaction conditions for 12 wt% CoO_x/BG1 (red circle): 200 °C, 16 bar ethylene, 16 bar argon, 1.45 h contact time, and 2.6% average conversion.

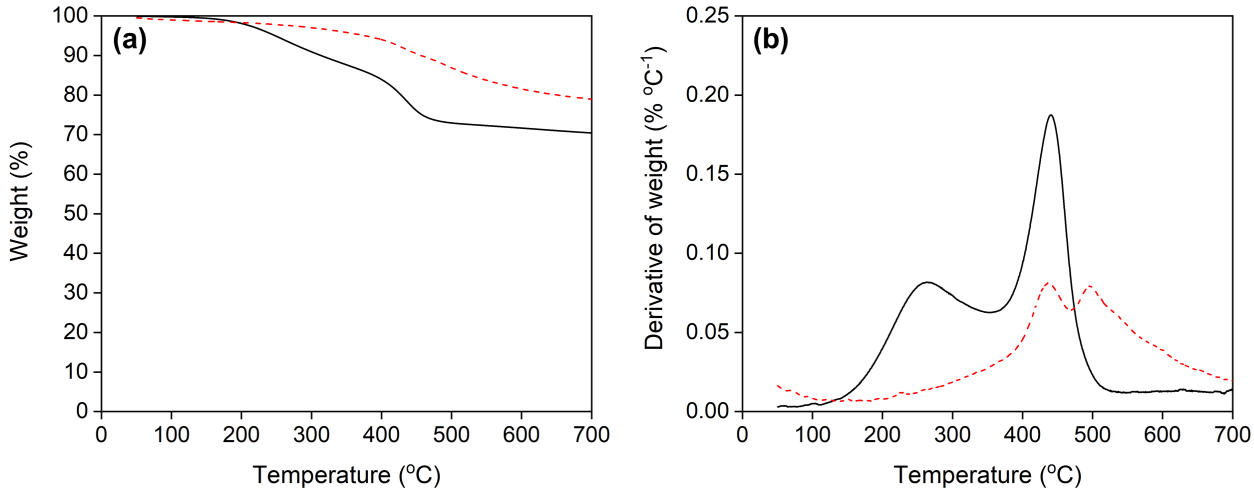

Figure S4.7 Thermogravimetric analysis (TGA) curves of the spent 12 wt% CoO_x/MRX (black solid line) and the spent 12 wt% CoO_x/BG1 (red dashed line) after reactions at 200 °C, 16 bar ethylene, 16 bar argon, and 1.45 h contact time. TGA conditions: 50 cm^3 (STP) min^{-1} of N_2, 10 °C min^{-1} ramp rate, and ~10 mg sample. (a) Weight percent versus temperature. (b) Derivative of weight percent versus temperature.

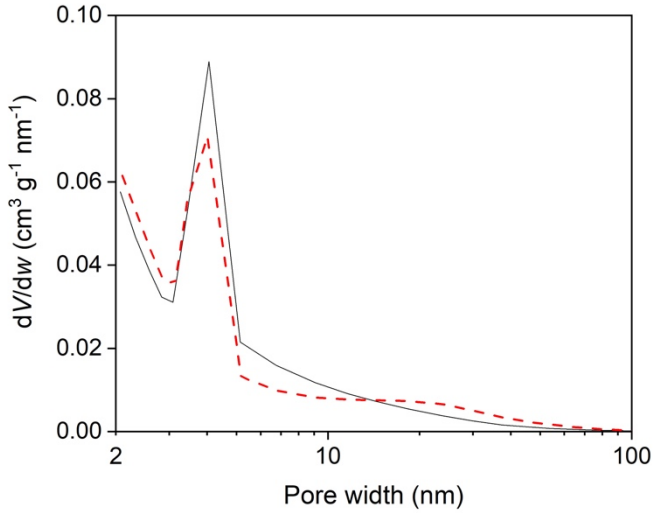

Figure S4.8 BJH pore size distributions of MRX HTTC (black solid line) and BG1 HTTC (red dashed line).

Chapter 5. Conclusions and Future Directions

5.1 Conclusions

In this dissertation, we investigated heterogeneous cobalt catalysts for ethylene oligomerization into higher linear and alpha olefins. We showed that a heterogeneous carbon-supported cobalt oxide catalyst can selectively oligomerize ethylene into higher linear and alpha olefins when performing the reaction at reaction temperatures near 200 °C. The linear alpha olefin (LAO) isomer distributions of C_4 to C_8 olefins were above 60% at <20% ethylene conversion. The product linearities up to C_{12} olefins were above 90%, even at 48% ethylene conversion. The catalyst was also stable for 120 h when performing sequential reactions with the same catalyst bed at the following reaction temperatures: 200-140-160-180-200 °C. To our knowledge, this is the most selective heterogeneous catalyst for synthesis of higher linear and alpha olefins in the absence of activators and solvents. The product distribution follows the Schulz-Flory distribution, suggesting the Cossee-Arlman mechanism as the underlying mechanism for olefin oligomerization over a heterogeneous carbon-supported cobalt catalyst. Catalyst characterizations without exposure to air of the spent catalyst after 24 h reaction at 200 °C showed CoO as the bulk and surface cobalt phases, suggesting that this is the stable cobalt phase during oligomerization. The ethylene oligomerization reaction also produced polyethylene which can lead to catalyst deactivation.

We showed that the cobalt phase from the heterogeneous carbon-supported cobalt catalyst is sensitive to the catalyst pretreatment temperature under inert atmosphere. Increasing the pretreatment temperature from 230 °C to 560 °C in argon reduces CoO_x to Co metal which also improves the oligomerization activity at the reaction temperature of 200 °C. However, cobalt metal supported on carbon deactivated during the oligomerization reaction due to polyethylene formation

(approximately 50% of the spent catalyst was polyethylene after a 24 h reaction). Cobalt metal supported on carbon is less selective to linear and alpha olefins than cobalt oxide supported on carbon. For example, the linear alpha olefin (LAO) isomer distributions of C_4 to C_8 olefins from the cobalt metal catalyst were more than 30% at <10% ethylene conversion, whereas they were above 60% at <20% ethylene conversion with the cobalt oxide catalyst. In addition, the product linearities up to C_{12} olefins were more than 80% at 48% ethylene conversion with the cobalt metal catalyst, whereas they were more than 90% at the same conversion with the cobalt oxide catalyst. The ethylene oligomerization reaction has a 1^{st} order dependence with respect to ethylene partial pressure, consistent with a mechanism where the rate determining step is the propagation of adsorbed olefins with gaseous ethylene on a highly covered surface with olefins.

The effect of the catalyst support on cobalt catalysts for ethylene oligomerization into linear and alpha olefins was also investigated. Two different carbon supports, high-temperature-treated carbon (HTTC) and acid-washed carbon (AWC), were used as the catalyst supports for cobalt oxide in this study with the purpose of understanding the effect of surface functional groups towards oligomerization. The high temperature treatment of carbon reduced the oxygen content and the oxygen surface functional groups, whereas the acid wash treatment of carbon in nitric acid increased the oxygen content and oxidized the surface functional groups. Carboxylic acids were present as the major surface functional groups on the acid-washed carbon as observed by temperature-programmed desorption (TPD) experiments. Both HTTC and AWC supported cobalt oxide catalysts were stable during ethylene oligomerization reactions for 30 h TOS. However, the HTTC supported cobalt oxide catalyst was nearly twice as active as the AWC supported cobalt oxide catalyst. At similar conversions, the HTTC supported cobalt oxide catalyst was more selective to linear alpha olefins (LAOs) and higher olefins than the AWC supported cobalt oxide

catalyst. The surface functional groups (e.g., carboxylic acids) from the AWC catalyzed the isomerization of linear alpha olefins into linear internal olefins which have lower rates for oligomerization into larger olefins. Despite lower activity, the CoO_x crystallite sizes from the AWC catalyst were smaller due to higher adsorption of Co^{2+} during the impregnation of the carbon support from the oxygen functional groups. After reactions at 200 °C, both catalysts had the characteristics of CoO, suggesting that the cobalt phase did not influence the activity difference between these two catalysts. We also reported that increasing the catalyst support particle size to impose more transport restrictions to the products had a minimal impact towards the product selectivities, linearities, and linear alpha olefin isomer distributions. Finally, the oligomerization activity of a heterogeneous cobalt oxide supported on carbon was higher by a factor of six when the cobalt was supported on a carbon which had less impurities (e.g., Al, Ca, Fe, and Mg), suggesting these impurities likely influenced the activity of the catalyst.

Overall, we have demonstrated that heterogeneous cobalt catalysts can selectively oligomerize ethylene into higher linear and alpha olefins in the absence of activators and solvents. Our findings show the potential of improving current existing technology to produce higher linear and alpha olefins as precursors of fuels and chemicals.

5.2 Future Directions

5.2.1 Catalyst characterizations with operando X-ray techniques

In this dissertation, X-ray diffraction (XRD) and X-ray photoelectron spectroscopy (XPS) experiments were performed on the carbon-supported cobalt catalysts to determine what cobalt phases were present before and after the ethylene oligomerization reactions. Reduction of Co_3O_4 to CoO was observed by XRD and XPS when the catalyst had been pretreated at 230 °C in argon

and was used for ethylene oligomerization for 24 h at the reaction temperature of 200 °C. However, this reduction was not observed by both XRD and XPS when the oligomerization was instead performed at 80 °C for 24 h. It is unclear whether reduction of Co_3O_4 did not occur at this reaction temperature or the reduction occurred slowly during the reaction at 80 °C. In addition, there might also be a time evolution of cobalt species forming Co metal after the reduction of Co_3O_4 to CoO during the reaction at 200 °C. As observed in the experiments, Co metal is more active than CoO, although the catalyst deactivated due to polyethylene formation. There might be competing reactions between the reduction of CoO to Co metal as well as catalyst deactivation of Co metal due to polyethylene formation which result in the pseudo stable catalyst during the reaction at 200 °C. To answer these questions, *operando* X-ray techniques, such as *operando* X-ray absorption spectroscopy (XAS), *operando* X-ray diffraction (XRD), and *operando* X-ray photoelectron spectroscopy (XPS) will be beneficial to elucidate what the cobalt phases are and how the cobalt phases evolve during the reaction.[1-3] Additionally, *operando* XAS can be used to determine the composition of each cobalt phase during the reaction. One challenge for performing *operando* X-ray experiments is setting up the apparatus for high pressure experiments (e.g., 32 bar), which are used in this study.

5.2.2 Kinetic modelling of ethylene oligomerization over heterogeneous cobalt catalysts

Reaction kinetics data including the apparent activation energy, the reaction order with respect to ethylene partial pressure, the linear alpha olefin (LAO) isomer distribution, the product linearity, and the product selectivity from ethylene oligomerization over a heterogeneous cobalt oxide supported on carbon catalyst have been discussed in Chapters 2 and 3. An analytical solution for a rate expression was also developed with two assumptions: 1. the rate determining step is the

propagation of adsorbed olefins with gaseous ethylene and 2. the propagation rate constant is independent of the olefin chain length. Under these assumptions, the rate expression is consistent with the catalyst surface being highly covered by olefins. It will be desirable to develop rigorous kinetic modelling to show how the propagation rate constant varies or stays relatively constant as the olefin chain length increases. In addition, this kinetic modelling will be able to assess the assumption of the rate determining step being the propagation of adsorbed olefins with gaseous ethylene as well as how the catalyst surface is covered with olefins. One of the main challenges for developing kinetic modelling for this reaction is obtaining the binding energy values for the olefins. As the olefin chain length increases, the number of isomers also increases which makes it more difficult to obtain the binding energy values for those isomers. In addition, the binding energy value also depends on the cobalt phase as well as its orientation. DFT calculations will be necessary to obtain these values.

5.2.3 Investigation of catalyst supports for cobalt catalysts for olefin oligomerization

In this dissertation, activated carbon Norit Darco MRX was used as the carbon support for cobalt for ethylene oligomerization. We have shown in Chapter 4 that the surface functional groups of the carbon support influence the activity and the selectivity of the cobalt catalyst during the oligomerization. The environment of cobalt can also influence the activity of the catalyst. We have studied ethylene oligomerization over cobalt oxide supported on activated carbon Darco BG1 with more impurities (e.g., Al, Ca, Fe, and Mg) than the MRX carbon, and the oligomerization activity of this catalyst was only one sixth of the activity with the MRX carbon. It is unclear which impurities and how the impurities lower the activity of the catalyst. *In situ* and *operando* catalyst characterizations including *operando* X-ray absorption spectroscopy (XAS) will be useful to

understand what condition the cobalt catalyst is the most active, the most stable, and the most selective to linear and alpha olefins. In addition, acid wash treatment of the BG1 carbon to remove the impurities with subsequent high temperature treatment to remove the surface functional groups will be useful for comparison as the catalyst support for cobalt with the MRX catalyst support for cobalt for ethylene oligomerization.

The effect of different carbon morphologies as well as different catalyst supports than carbon can be investigated for future research directions. In this dissertation, only activated carbon supports with 3D structures were studied as the catalyst supports. We have also tried to oligomerize ethylene with a cobalt supported on Vulcan XC 72 (carbon black) at the reaction temperature of 200 °C with the catalyst pretreated at 230 °C in argon. This carbon black has a 0D structure and more than 99 mol% carbon.[4,5] Surprisingly, the activity of this catalyst was one order of magnitude lower than the activity of the cobalt oxide supported on MRX high-temperature-treated carbon despite lower levels of impurities. This result suggests that the activity of a heterogeneous cobalt supported on carbon catalyst is also influenced by the structure of the carbon. A cobalt supported on silica (Davisil 646) catalyst was also studied for ethylene oligomerization at the reaction temperature of 200 °C. The catalyst was initially pretreated at 450 °C in H_2 with the purpose of reducing the cobalt oxide to cobalt metal because cobalt metal is the more active phase when being supported on carbon. Surprisingly, the cobalt supported silica catalyst had three orders of magnitude lower activity than the cobalt metal supported on MRX high-temperature-treated carbon. This result also suggests that the activity of the heterogeneous cobalt catalyst depends on catalyst support. *In situ* and *operando* catalyst characterizations of these cobalt catalysts will be beneficial to understand how the catalyst supports influence the activity and the selectivity of the heterogeneous cobalt catalysts for olefin oligomerization.

5.2.4 Catalyst regeneration of heterogeneous cobalt catalysts for ethylene oligomerization

In Chapter 3, we have shown that the cobalt metal supported on carbon catalyst deactivated during the 36 h reaction at 200 °C and caused a pressure built up afterwards due to polyethylene formation. It may be desirable to regenerate the catalyst as well as remove the polyethylene from the catalyst bed and the line after the reaction. Toluene is an option for this catalyst regeneration because we were able to remove the liquid oligomers as well as a fraction of polyethylene from the spent catalysts for XPS analyses.

5.3 References

1. X. Li, X. Yang, J. Zhang, Y. Huang and B. Liu, In situ/operando techniques for characterization of single-atom catalysts, *ACS Catal.*, 2019, **9**, 2521-2531.
2. L. Lukashuk, N. Yigit, R. Rameshan, E. Kolar, D. Teschner, M. Hävecker, A. Knop-Gericke, R. Schlögl, K. Föttinger and G. Rupprechter, Operando insights into CO oxidation on cobalt oxide catalysts by NAP-XPS, FTIR, and XRD, *ACS Catal.*, 2018, **8**, 8630-8641.
3. I. K. van Ravenhorst, A. S. Hoffman, C. Vogt, A. Boubnov, N. Patra, R. Oord, C. Akatay, F. Meirer, S. R. Bare and B. M. Weckhuysen, On the Cobalt Carbide Formation in a Co/TiO2 Fischer–Tropsch Synthesis Catalyst as Studied by High-Pressure, Long-Term *Operando* X-ray Absorption and Diffraction, *ACS Catal.*, 2021, **11**, 2956-2967.
4. I. C. Gerber and P. Serp, A theory/experience description of support effects in carbon-supported catalysts, *Chem. Rev.*, 2020, **120**, 1250-1349.
5. P. U. Karanjkar, S. P. Burt, X. Chen, K. J. Barnett, M. R. Ball, M. D. Kumbhalkar, X. Wang, J. B. Miller, I. Hermans, J. A. Dumesic and G. W. Huber, Effect of carbon supports on RhRe bifunctional catalysts for selective hydrogenolysis of tetrahydropyran-2-methanol, *Catal. Sci. Technol.*, 2016, **6**, 7841-7851.